TÉCNICO LISBOA

Seakeeping optimization of a fast displacement catamaran on the basis of strip-theory codes

Filipe de Carvalho Ribeiro Belga

Thesis to obtain the Master of Science Degree in

Naval Architecture and Marine Engineering

Supervisor(s): Prof. Manuel Filipe Simões Franco Ventura
Prof. Serge Sutulo

Examination Committee

Chairperson: Prof. Carlos António Pancada Guedes Soares
Supervisor: Prof. Serge Sutulo
Member of the Committee: Prof. Shan Wang

December 2017

This page was intentionally left blank.

Acknowledgments

First and foremost, I would like to thank professors Manuel Ventura and Sergey Sutulo for the opportunity of studying this particular research topic that covers the fields of hydrodynamics, seakeeping in particular, and ship design which are much of my interest. I would also like to thank for their continuous support and guidance during the making of this dissertation.

To professor Carlos Guedes Soares for the availability, encouragement and help provided, particularly during my Erasmus semester.

To professors Sérgio Ribeiro e Silva and José Alberto Falcão de Campos for the unconditional guidance, encouragement and advice provided throughout my time as student, not only within academic contexts but for my personal extracurricular projects as well.

To professors José Miguel Rodrigues and Roberto Vettor for the vital help with strip theory and wave statistics, having contributed immensely to the successful completion of this dissertation.

To professor Nuno Fonseca for having provided the experimental results of the model testing of the catamaran.

To Mr. Heinrich Söding for the support and guidance with respect to PDStrip.

To DAMEN Shipyards for having kindly provided the catamaran model used as parent model in the optimization procedure. I would like to thank Katerina Xepapa and Joana Grilo in particular for the assistance and the genuine efforts put into the achievement of my goals.

To all my friends, for their immense support both in and out of the academic context and, above all, for their priceless friendship which kept me sane during the most stressful periods.

Last but not least, I would like to thank my family, my parents and sisters, for the continuous support, patience, trust and sacrifices during this last tiring year.

This page was intentionally left blank.

Resumo

Neste trabalho foi optimizado o comportamento de um catamarã rápido em ondas de proa (casco de deslocamento) para transporte de tripulação a operar numa hipotética plataforma *offshore* na bacía do Altentejo, em Portugal. Com o objectivo de avaliar a precisão da teoria das faixas no cálculo dos movimentos de arfagem e cabeceio de catamarãs de alta velocidade (negligenciando a interacção entre cascos para ondas de proa), foi realizado um estudo comparativo entre três programas computacionais: PDStrip, um programa com código-fonte aberto, uma aplicação desenvolvida internamente no CENTEC no Técnico Lisboa (IST) e o *software* comercial Maxsurf. Estes códigos foram aplicados a um catamarã e um mono-casco rápidos, para os quais estão disponíveis dados experimentais em tanques de ensaio. Os resutados indicaram o PDStrip (com correções para painel de popa) como sendo a ferramenta numérica mais adequada para a rotina de optimização desenvolvida. O valor RMS (raiz média quadrada) das acelerações verticais na proa e o índice MSI (Motions Sickness Incidence) foram selecionados como funções objectivo a minimizar. Movimentos relativos de grande amplitude (e.g., *slamming*, *green water*) não foram considerados neste estudo, mesmo que possam ocorrer. De forma a incluir um estudo preliminar do arranjo geral do catamarã, as dimensões e posição da zona de passageiros no convés principal foram optimizados com base na minimização do valor médio de MSI ao longo do seu comprimento. Critérios de estabilidade do High Speed Craft (HSC) Code foram aplicados, tendo sido também imposto um critério de resistência máxima ao avanço, calculada com base num método empírico que estima os efeitos de interferência hidrodinâmica. O coeficiente de resistência de onda foi calculado com a teoria do corpo esbelto. Distâncias entre cascos, S/LWL, no intervalo entre 0.2 a 0.4 foram consideradas nos cálculos de estabilidade, resistência e MSI. O método de Lackenby foi utilizado para gerar variações de um modelo mãe. Combinações de *LCB* e C_b foram impostas, variando ambos os parâmetros num intervalo de +-10%. Finalmente, o catamarã óptimo foi estudado em termos de operabilidade a duas velocidades distintas, considerando critérios impostos pelo HSC Code e pela DNV-GL sob a forma de acelerações médias de um centésimo das maiores acelerações medidas.

Palavras-chave: catamarã, teoria das faixas, PDStrip, optimização do comportamento em ondas, acelerações RMS, índice de MSI, bacía do Alentejo, índice de operabilidade

This page was intentionally left blank.

Abstract

The present work optimizes the seakeeping performance of a displacement catamaran in head seas to operate as a fast crew supplier for an offshore platform at the Alentejo basin, Portugal. In order to assess the accuracy in predicting heave and pitch motions of fast displacement catamarans (assuming negligible interaction between demi-hulls in head seas), three codes based on the ordinary strip-method were compared: the open-source code PDStrip, an in-house code earlier developed at CENTEC in Técnico Lisboa (IST) and the commercial software Maxsurf. The codes were applied to a fast catamaran and a fast mono-hull, for which experimental data from model testing were available. Results indicated PDStrip (with transom terms) as the most suited to be used in the optimization procedure. The RMS vertical acceleration responses at the bow and the average Motion Sickness Incidence (MSI) at the passenger area were selected as objective functions to minimize. Extreme effects such as slamming and green water were neglected, even though they might occur. As an attempt to include a preliminary design of the general arrangement, the dimensions and position of the passenger area on deck were set in order to minimize motion sickness. Stability criteria from the High Speed Craft (HSC) Code were applied, as well as a constraint on the maximum total ship resistance, computed with empirical formulae that estimate the hull interference components. Slender-body theory was used to calculate wave resistance. The effects of horizontal clearance ratios S/LWL between 0.2 and 0.4 were studied with respect to resistance, stability and MSI. The method of Lackenby was used to generate hull variations from a parent model, for which combinations of *LCB* and C_b were imposed, varied within the range of +-10%. Finally, an operability assessment of the optimized catamaran operating at two different speeds was carried out based on limiting seakeeping criteria imposed by the HSC Code and DNV-GL in terms of the average 1% highest accelerations.

Keywords: catamaran, strip theory, PDStrip, seakeeping optimization, RMS accelerations, motion sickness, Alentejo basin, operability index

This page was intentionally left blank.

Contents

List of Tables

List of Figures

Nomenclature

Constants

ρ	Density of salt water
g	Acceleration of gravity

Ship dimensions and hull coefficients

Δ	Ship displacement
∇	Underwater hull volume
BOA	Breadth overall
BWL	Breadth at the waterline
DWL	Design waterline/draft (same as *T*)
D	Depth
LCB	Longitudinal centre of buoyancy
LCG	Longitudinal centre of gravity
LOA	Length overall
LPP	Length between perpendiculars
LWL	Length of the waterline
VCG	Vertical centre of gravity (same as *KG*)
S	Horizontal clearance (distance between the centrelines of the demi-hulls)
S/LWL	Horizontal clearance ratio
C_b	Block coefficient
C_m	Midship section coefficent
C_p	Prismatic coefficient
C_{wp}	Waterplane coefficient

Reference frames

ξ, η, ζ Inertial reference frame of the ship

x, y, z Reference frame used to denote remote locations along the deck

Ship motions

β Wave heading

ω_0 Circular wave frequency

ω_e Circular frequency of encounter

V Vessel speed

ξ_a Wave amplitude

ξ_j Amplitude of the harmonic motion

ξ_z Absolute vertical displacement at a remote location

a_z Absolute vertical acceleration at a remote location

A_{jk} Generalized added mass matrix

B_{jk} Generalized damping coefficient matrix

C_{jk} Generalized restoring coefficient matrix

f_e Frequency of encounter

F_n Froude number

F_j^E Exciting force/moment

j, k Directions of motion, $j, k = 1, ..., 6$

k_0 Wave number

M_{jk} Generalized mass matrix

Short term responses

$H_{1/3}$ Significant wave height (same as H_s)

m_{iz} Spectral moments ($i = 0, 2, 4$)

RMS_{az} RMS vertical acceleration responses

RMS_{vz} RMS vertical velocity responses

RMS_z RMS vertical displacement responses

S_z Ship vertical displacement responses upon S_ξ

S_ξ Idealized wave spectrum

S_{az} Ship vertical acceleration responses upon S_ξ

T_p Peak period

Miscellaneous

C_w Wave resistance coefficient

GZ Righting lever (same as stability curve)

R_T Total ship resistance

This page was intentionally left blank.

Glossary

CFD	Computational Fluid Dynamics
HSC	High Speed Craft
MSI	Motion Sickness Incidence
RAO	Response Amplitude Operator
RMS	Root Mean Square
SWATH	Small Waterplane Area Twin Hull

This page was intentionally left blank.

Chapter 1

Introduction

1.1 Motivation

The ever increasing rate of energy consumption and its high dependency on fossil fuels is, nowadays, a major concern not only among the scientific community (researchers, engineers) but for politicians as well, who tend to encourage environmental friendly policies to counteract the problem and even for ordinary people who seem to be increasingly interested in such matters.

Despite the clear improvements for a modern life provided by fossil energy, its misuse contributed to serious environmental problems. The overall pollution levels, particularly airborne as a by-product of the industry at heavily populated areas, have never been higher. Also, despite the more sceptic opinions, it is generally agreed that the quick rate of climate changes is a real concern that will deeply affect the human population, particularly the generations to come.

Adding to this, global economies slowly came to realize that keeping the production rate constant was going to be impossible since fossil fuels are non-renewable resources. This forced the energy sector to renovate, focusing on the development of cleaner and even renewable alternatives and the improvement of industrial processes to increase efficiency. Maintaining this direction is vital in order to limit the most devastating effects of pollution, including ceasing the production of greenhouse gases and decreasing any other kind of harmful emissions. In fact, the growth of solutions for alternative energy sources seems to show no sign of slowing down.

However, given the current energy needs, the reality is that we continue to depend on fossil fuels. To further illustrate this idea, it is interesting to note that the peak of traditional oil extraction, i.e. onshore reservoirs, was reached in 2012 and that in 2013 4 million wells had been drilled, 81% located at geopolitically unstable countries (Carvalho, 2016). Driven by the developments in technology, the increasing know-how of the industry and the economical situation at the time, operators eventually ventured off to offshore sites. Despite the big investments on prospecting, drilling and control/maintenance, as well as the tight restrictions imposed by the harsh marine environment, energy companies continuously seek sources at increasing pace and depth in order to follow the energy demand. It is then clear that, for now,

the investment on the oil and gas industry should not be withdrawn.

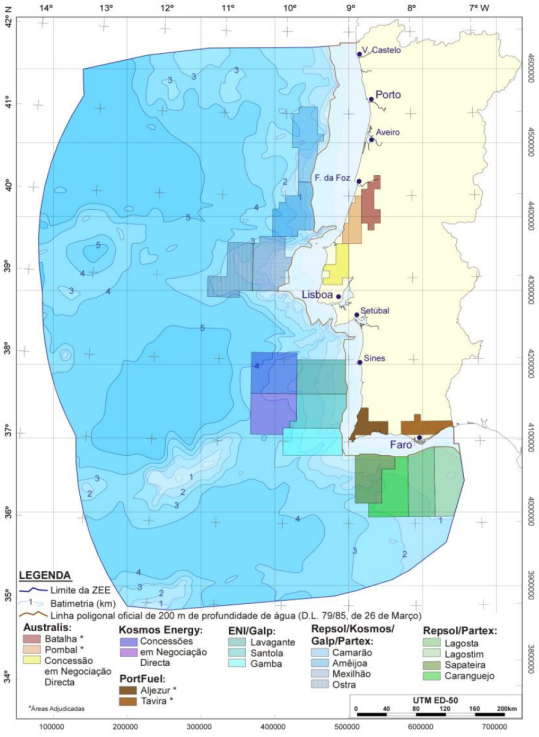

Figure 1.1: Map of the concession areas in Portugal (source: [43])

In Portugal, there has been a lot of speculation regarding the existence of economically viable reservoirs. ”More than half of the Exclusive Economic Zone (EEZ) has potential for hydrocarbon exploration” stated José Miguel Martins from ENMC (Entidade Nacional para o Mercado de Combustíveis) at a conference in 2015, adding that despite the increasing research (between 2007 and 2013, oil companies spent over 260 million euros on prospection), a lot more work is still to be done ([86], [21]). Nevertheless, as seen in Figure 1.1, several companies already hold concession rights over Portuguese basins to perform prospection studies. Carvalho (2016) conceptualized a potential deep offshore hydrocarbon field located 50 Km off the coast, at the Alentejo Basin. This basin comprises 3 concession areas managed by Galp (30%) and Eni (70%) that sum up to 9100 Km^2: Lavagante, Santola and Gamba. This work laid the ideal foundation for a solid case study to be developed for this dissertation. Within this scenario, there are many interesting subjects worth developing from the point of view of a naval architect, one of which relates with the need of supplying crew, namely workers, inspectors, engineers or even specific cargo to an offshore platform at a given rate (daily, weekly, etc.). At this point we are left with a vital task: the selection of the appropriate vessel to perform this mission. Such craft should be fast, efficient and safe, even when facing harsh sea states, as it might be the case at an offshore location.

Multi-hulls, in particular catamarans, take advantage of a high transverse stability, reduced roll and large deck areas to carry more cargo over narrower hulls without carrying ballast. As a result, their shallow drafts and small hydrodynamic resistance allow them to be designed for high speeds. Together with a high provision of non-sinkability and increased seaworthiness, it is assured an effective application of

catamarans as high-speed crafts for the transport of passengers. In fact, the bulk of all the ferry fleet in operation consists of catamarans - 70% in 2014 ([41]). Furthermore, a quick look onto the world fleet of crew supply vessels operating offshore allow us to conclude that catamarans are a suited choice.

All in all, the problem that motivated this dissertation can be summarised as follows: design of a fast crew supplier catamaran for an offshore platform operating at the Alentejo basin. However, as it will be discussed further ahead, this description of the problem is far from being complete.

1.2 Topic overview and objectives

Nowadays, ship design considers a ship as a complex system integrating a series of subsystems. In fact, it comprises its complete life cycle, from the design itself, whether it is conceptual, preliminary, contractual or detailed, to the construction, operation (including maintenance and repairs) and scrapping phases. Mathematically, each of these stages represents a non-linear optimization problem of certain objective functions in the presence of constraints imposed by the stake holders. This dissertation focused solely on the preliminary design stage, often intended to fill a gap between the initial concept and the contract phase, being particularly important when the level of conceptualization lacks detail for a solid feasibility evaluation, as is the case. In this regard, the selection of the main dimensions and the development of the hull form appeared as the most immediate concerns, for which there were two solutions: either resort to estimate methods based on statistical regressions with data compiled from existing designs to generate a ship model or use a parent hull suited for the intended mission and optimize it according to specific figures of merit, while imposing constraints of any sort. For this dissertation, it was chosen the later approach, for which a parent model kindly provided by DAMEN Shipyards was used. The model referred to a 30 meters passenger catamaran with a service speed of 25 knots.

As for high speed vessels, the requirement to operate well at high speeds, often in adverse weather conditions, is paramount. Thus, the main emphasis was put into improving the seakeeping performance of the DAMEN catamaran. In fact, high accelerations can significantly decrease the operability level of such vessels not only in terms of structural damage but because they can jeopardize safety and welfare onboard as well, which seemed particularly important considering that the catamaran was going to operate as a crew supply vessel. Therefore, the minimization of response accelerations and seasickness of passengers was prioritized. Extreme effects such as slamming an green water have been neglected, even though they might occur. Although there are quite powerful methods available for predicting seakeeping behaviour, namely CFD solvers, the fact that the chosen tool was to be embedded into an optimization procedure was an important limitation. Strip theories, despite the limited range of application (slow speeds, slender hulls, small motion amplitudes, inviscid fluid assumptions), require low computational power and provide fast calculations, which seemed ideal for the proposed work. With respect to the type of motions to study, considering the higher transverse stability of double-hulled vessels, it seemed reasonable to assume that the most critical situations come from heave and pitch motions upon head seas. Therefore, these were the main focus. Furthermore, the strip theory codes the author found avail-

able are not particularly suited to predict motions of catamarans. Thus, an assumption about negligible interaction between demi-hulls was exploited, which is acceptable in head and following seas.

For the purpose of selecting a strip-theory code to be used in the optimization procedure, a benchmarking study was carried out, a work that comprised the entire first part of this dissertation. Three software packages based on the ordinary strip-method (Salvesen et al., 1970) were considered: PDStrip, a public-domain code developed by Söding and Bertram (2009); an in-house code earlier developed at CENTEC (Centre for Marine Technology and Ocean Engineering) in Técnico Lisboa (IST) (linear version of Fonseca and Guedes Soares (1998), hereinafter referred to Fonseca, and the commercially available software Maxsurf, for which the module Motions was used (Bentley Systems, Incorporated, 2013a). Their numerical predictions were compared with model tests of a catamaran [63] and the fast mono-hull Model 5 [15]. The goal was to assess not only the accuracy in computing heave and pitch motions of catamarans but their capacity to do it at high speeds.

Throughout the second half of the dissertation, PDStrip, with transom terms, was used as seakeeping tool to optimize the DAMEN catamaran operating at 25 knots as a fast crew supplier used in the transport of 12 passengers to an offshore platform at the Alentejo basin, for which the work of Costa et al. (2001) was used to simulate the seastates at the location. The RMS vertical acceleration responses at the bow and the average Motion Sickness Incidence (MSI) for 65 minutes of exposure ([87], [34]) at the passenger area were selected as objective functions to minimize. Both were assessed considering the most probable seastate. In this regard, as an attempt to include a preliminary design of the general arrangement, the dimensions and position of the passenger area on deck were optimized in order to maintain the average motion sickness at a minimum level. Furthermore, stability criteria from the High Speed Craft (HSC) code [73] was applied, as well as a constraint on the maximum allowed total ship resistance. The wave resistance was computed with slender-body theory and the method of Jamaluddin et al. (2013) was used to calculate total resistance, including the hull interference components. Both criteria enabled a study of the effects of the horizontal clearance, S. Additionally, although S has not been directly included into seakeeping calculations, it was taken into account when computing the average MSI at the passenger area. This has been accomplished by defining a relationship between the length of the passenger area and its width (the later being a function of the horizontal clearance), for a given minimum allowed area, estimated based on a database of similar vessels resorting to regression analysis.

In order to quickly generate a large number of hull variations from the parent model, the well known method of Lackenby was used to impose combinations of *LCB* and C_b, varied within the range of +-10%, while maintaining the main dimensions of the underwater hull geometry, namely, *LWL*, *BWL* and displacement. The limits of the parametric transformation were subject of analysis.

In terms of software, MATLAB was used as the engine of the optimization procedure, controlling PDStrip to carry the seakeeping calculations ([119]), Maxsurf Modeler ([9]) to process the hull models and perform the parametric transformations, Maxsurf Resistance ([8]) to compute the wave resistance and Max-

surf Stability the stability calculations ([10]) - see Figure 1.2. For a more complete overview of the optimization routine refer to the synthesis model of Figure 4.11.

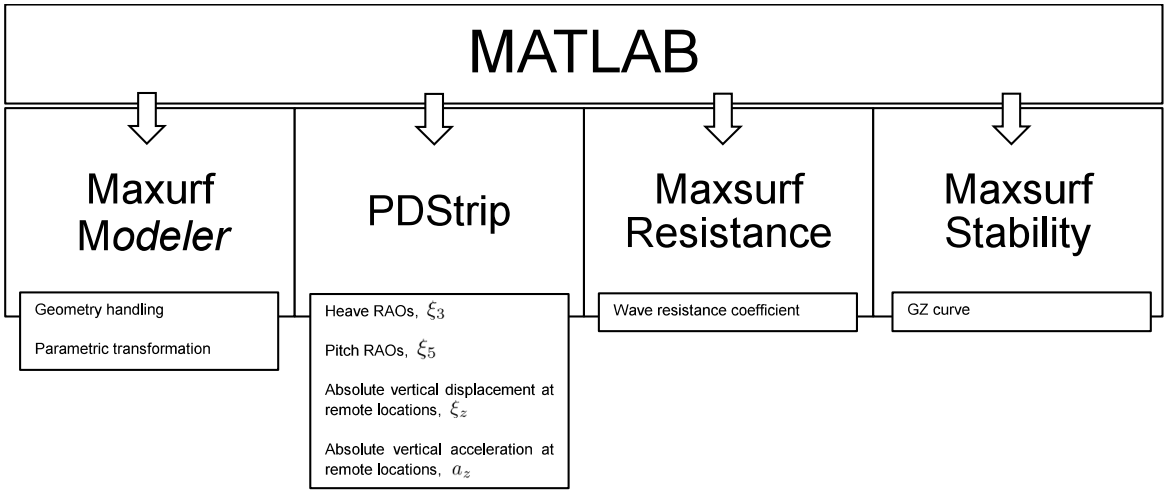

Figure 1.2: Tools used to perform the optimization procedure

The effects of *LCB* and C_b on the RMS vertical acceleration responses at the bow, the average Motion Sickness Incidence (MSI) at the passenger area and total ship resistance were studied. In addition, relationships have been established between variations of C_{wp} and *BWL*/*DWL* and the resulting heave and pitch motions. The influence of the seastates on RMS accelerations and motion sickness, as well as the effects of horizontal clearance on resistance, stability and motion sickness have been evaluated.

Finally, the operability index of the optimum catamaran for two different speeds (service and 90% of maximum speed) was estimated based on limiting seakeeping criteria imposed by the High Speed Craft (HSC) code and DNV-GL in terms of the average 1% highest accelerations.

1.3 Structure of the dissertation

This dissertation will be divided in 5 chapters. The first one is an introductory chapter, presenting the motivations that led to the development of this dissertation and an overview of the scope of the work, including the intended objectives. The second chapter reviews the state of the art with respect to the existing methods to predict ship motions and their inclusion into optimization procedures. Then, chapters 3 and 4 cover the two main subjects explored in this dissertation. As mentioned above, the first (Chapter 3) addresses the benchmarking study of three strip theory codes and the selection of the most suited one to predict heave and pitch motions of high-speed catamarans in head seas based on comparisons with experimental data, including an overview of their individual formulations and assumptions. Chapter 4 covers the optimization of a catamaran operating as a fast crew supplier used in the transport of 12 passengers to an offshore platform located 50 Km off the coast of Sines at the Alentejo basin, in Portugal. This chapter includes a description of the parent model used and the seastates in which it will operate. The method to generate hull variations, the selection of the objective functions and constraints are here

addressed as well. The optimization results are then presented, including a few considerations regarding the effects of the hull shape coefficients on motions and the influence of the seastates and the distance between demi-hulls both on the objective functions and the imposed constraints. Finally an operability assessment of the optimum hull form is carried out based on limiting seakeeping criteria imposed by the classification societies. Due to the extension of chapters 3 and 4, both include a final section that summarises the most significant conclusions. Finally, Chapter 5 presents the overall achievements of the work presented here as well as suggestions from the author regarding topics that are worth further developing.

Chapter 2

State of the art

2.1 Seakeeping simulation methods and strip theories

As it is defended by Salvesen et al. (1970), the performance of a vessel in a realistic seaway should be the ultimate criteria for the design of any hull. Predicting ship motions and dynamic loads is, however, a very complex problem. As a consequence, these calculations were mostly neglected from the design procedures up until the 1950's. Instead, laboratory experiments with ship models would be performed. However, besides being expensive and time consuming - not feasible to evaluate individual designs -, reliable tools to relate the behaviour of the model with the behaviour of the vessel in the chaotic ocean environment were unavailable by that time. Inspired by the field of electromagnetic communications, Pierson and St Denis (1953) showed that spectral analysis could be the solution for this problem. The superposition principle was applied and it was hypothesized that the responses of a ship to irregular waves could be the sum of the responses to regular waves of all frequencies. Their work was a clear landmark in the seakeeping area and brought to light the importance of developing theoretical and numerical methods to predict wave responses.

Several seakeeping theories have been developed with relative success throughout the years. The 2-D harmonic flow solution of Ursell (1949) for the heaving motion of a half-immersed circular cylinder and the generalisation to arbitrary shapes using conformal mapping techniques was a major breakthrough towards the development of a consistent theory of ship motions. These results were later applied in the form of frequency domain strip theories, of which the work of Korvin-Kroukovsky and Jacobs (1957) is an outstanding example. Their strip theory for heave and pitch motions in head waves became the first ship motion theory suitable for numerical computations with adequate accuracy for engineering purposes. Numerous modifications and extensions came afterwards, e.g., [76], [92], [117], but the work of Salvesen et al. (1970) is seen today as one of the most significant contributions to the seakeeping field, being considered a standard reference and one of the most cited strip theories. These basically simplify the complex, fully non-linear ship motions into two sets of coupled linear differential equations: one for heave and pitch and the other for horizontal plane motions, i.e. sway, yaw and roll. The hydrodynamic coefficients are calculated for each cross section of the ship resorting to conformal mapping techniques

or 2-D panel methods and integrated to obtain the final global forces. Comparisons with experimental data throughout the years tend to show a satisfactory agreement for heave and pitch motions and for vertical and horizontal wave-induced loads, while for horizontal motions (sway, yaw, roll) the accuracy of strip theories is far more uncertain ([26]). Basic assumptions for such theories are potential flow, slenderness of the hull and linearity of the hydrodynamic forces, which implies that, in principle, the results are only valid for relatively small amplitude motions.

Often, for large ships, motions can be adequately described by linear theory. Still, some effects translate into considerable non-linear forces and thus, must be considered. This includes large amplitude motions which can induce impact between the ship and the sea surface, a phenomenon that can not be described linearly and might result into adverse stresses, and the case of smaller ships or ships with prominent hull flare shapes ([47]). In order to account for these non-linear effects, time domain solutions are used rather than formulations in the frequency domain. If the motions are strictly sinusoidal in time and the non-linear effects are not excessively strong, the equations of motion are solved in the time domain while the hydrodynamic forces are represented by frequency dependent coefficients. Otherwise, the hydrodynamic problem is solved in the time domain together with the equations of motions. Some early work following this approach includes Finkelstein (1957) and Stoker (1957), who used it to study water waves, Cummins (1962), who pioneered its application to the unsteady ship motion problem and Ogilvie and Tuck (1969), who related the time domain motion equations with the frequency domain equations via Fourier analysis. Later, Fonseca and Guedes Soares (1994) applied a time domain strip theory to solve the formulation proposed by Cummins (1962). Their description of the seakeeping problem was developed to study heave and pitch motions and vertical loads of ships in regular waves considering non-linear hydrostatic forces. The results were found close to the frequency domain solution. With Fonseca and Guedes Soares (1998), the authors further refined the previous work to include non-linear Froude-Krylov forces which, together with the hydrostatic forces, dominate the non-linear effects ([53]). Comparisons between numerical and experimental results for a containership advancing in regular and irregular waves showed that, for relatively slow ships, the method was appropriate for engineering applications, being capable of representing the main non-linearities, thus standing as a clear improvement to the linear solution ([49], [52], [51], [54]). With the goal of studying the limits of the method in terms of ship speed, the authors tested it with a fast mono-hull, $F_n = 0.4$, having compared numerical results with experimental data ([85], [53]). Results showed that the method represents well vertical ship responses for low and moderate speeds but over predicts motions and structural loads as the speed increases. Davis and Holloway (2003) and Holloway and Davis (2006) stand as other publications that refer a time domain strip theory used to predict ship motions of fast ($F_n = 0.6 - 0.9$), slender vessels in head seas, validating it with model testing for conventional hulls suitable for catamarans, SWATH hull forms and hulls suitable for high-speed mono-hulls.

Generally speaking, strip theories assume that the advance velocity of the vessel is small because they do not properly account for the interaction between the steady wave system of the advancing ship and the oscillatory effects of ship motions ([115]). With the intent of adding speed related effects into the hy-

drodynamic problem, 2 1/2-D strip theories were developed, an approach which lies between standard 2-D strip theories and 3-D panel methods. The main difference for a typical strip theory is that, although the formulation is still based on the 2-D Laplace equation, the free surface condition is solved in 3-D. A few examples include Faltinsen et al. (1991), Hermundstad et al. (1999) and Holloway and Davis (2006). Despite this, by using strip theories, several important effects are still being neglected, namely, 3-D phenomenon related with the interaction between ship sections, a proper account for the effect of the advance speed on the ship motions, the computation of the hydrodynamic coefficients at low frequencies, etc. ([89], [26]). At the same time, the account for viscous flows and large amplitude ship motions, which motivated the development of time domain theories, continues to be a problem. To overcome these limitations, there was an increasing focus on 3-D panel methods, mainly via Rankine sources or Green function, both in time and frequency domain, after the 1980's, driven by the breakthroughs in computer sciences ([5], [33], [6], [12], [32], [80], [89], [38], [120]).

Nowadays, researchers are interested in even more complex, far more powerful, methods that allow to more accurately predict the seakeeping behaviour and resistance of a wide variety of vessels, including multi-hulls. The development of CFD solvers, particularly turbulence models like Reynolds Averaged Navier-Stokes (RANS), stand as the state of the art in seakeeping ([112], [130], [23], [24], [90], [26], [122]). Because instead of being added in post-processing, all the previously mentioned effects are implicitly included in the flow equations that are to be solved, the potential for simulating unsteady flows and ship motions is huge. So far, such methods applied to problems associated with steady resistance and propulsion in calm water have achieved high accuracy. As for seakeeping, results are promising and continuously improving ([26]). However, the computational effort required to simulate such problems is still extremely high for a wide number of practical applications, particularly at early stages of the design process. Therefore, it still is useful and meaningful to resort to less demanding tools, namely strip theories, of which the work of Datta et al. (2013), Rajendran et al. (2015) and Rajendran et al. (2016) are recent examples.

2.2 Strip theories and catamarans

During the 1970's, the application of strip theories was expanded to multi-hulls, particularly SWATH vessels. Clear examples of that development are Ohkusu and Takaki (1971), Lee et al. (1973) and Hadler et al. (1974). Lee et al. (1973) studied heave and pitch motions of a SWATH in head seas and found that the analytical prediction overestimated the response amplitude at the resonance encounter frequencies. These discrepancies were associated with an inadequate account for two different effects: viscosity and the 3-D hydrodynamic interaction between the two hulls, i.e. interference effect, especially at higher speeds. Regarding the viscosity problem, while the damping mechanism of ship motions is being controlled by the wave making effect, the viscous damping can be neglected. However, for the case of a heaving SWATH, due to the vorticity generated by the flow separation along the struts, the viscous damping gains significance and has to be considered ([83], [82], [20]). Such conclusions motivated

the development of strip theories for twin-hulled vessels and Lee and Curphey (1977) showed that the effects of viscous damping on the motions of a SWATH hull could be predicted by combining strip theory with a cross-flow approach. This idea was later adopted by several authors, including Chan (1993) and Schellin and Rathje (1995). Centeno and Guedes Soares (1999), Centeno et al. (2000), Centeno et al. (2001) and Triunfante Martins et al. (2004) extended the method to conventional catamaran hull forms. Despite this, viscous effects are generally considered unimportant to the heaving and pitching of catamarans, an idea which is supported by numerical results ([109], [65], [64]). More recently, Castiglione et al. (2011) investigated the seakeeping behaviour of a catamaran resorting to ShipX (VERES), that includes a 2 1/2-D strip theory, and compared the results against CFD and experimental data. Despite the fairly good agreements, it became clear that strip theory over estimates the catamaran motions.

In any case, considering the advantages of strip theories in terms of low computational effort, making them ideal for optimization procedures, particularly during early design stages and within academic contexts, it seems clear that there still is room for improvement regarding its use to predict the motions of catamarans. Despite the limited application range, weather in terms of speed (for which 2 1/2-D strip theories are an alternative), weather due to its inability to properly account for the hull interaction, such theories continue to be subject of investigation.

2.3 Embedding seakeeping analysis into design procedures

Up until the late 1980's, despite a good volume of research on embedding systematic seakeeping analysis into the design procedures, the conclusions didn't bear substantial developments ([110], [81]). The bulk of the work would actually focus on ship resistance as hydrodynamic parameter to optimize, of which is example Salvesen et al. (1985). The reality is that the resistance problem is, without question, a vital aspect of any ship design. In light of this, a great amount of investigation has been continuously presented throughout the years, all of which aimed for the development of optimization procedures that addressed this problem in early stages of the design ([98], [97], [84], [18], [42], [19], [22], [88], [13], [127], [1], [128]).

The development of high-speed vessels and its use to transport passengers raised awareness for the importance of including early seakeeping analysis in the design and optimization procedures in order to increase wellness and comfort onboard. In the early 1990's, Hearn et al. (1990, 1991) developed a procedure aimed to assess the sensitivity of certain seakeeping characteristics upon the change of the main particulars, for which a numerical tool based on strip-theory was used to perform the seakeeping calculations. A destroyer was used as case study. This work, based on systematic variations, resulted in a series of design charts that were intended to aid the designers in modifying hull forms. Still, as pointed out a few years later by Sarioz (1993), "(...) it is not possible to produce generalised design guidelines which are applicable to all ships, ranging from small high-speed vessels to giant low speed bulk carriers", being now clear that the seakeeping characteristics are influenced quite differently by changes in the hull form parameters depending on the type of vessel. In light of this, by applying non-linear optimisation

techniques to the problem of seakeeping design, Hearn et al. (1992) expanded the range of designs covered by the previous model. The new results were applied to design a trawler and a general cargo vessel.

Around the same time, as part of a Greek research project, Papanikolaou (1990), Nowacki and Papanikolaou (1990) and Papanikolaou et al. (1991) focused on the preliminary design and computer-aided optimization of a high-speed SWATH car-passenger ferry and developed a model that pushed the boundaries of ship design optimization. Starting from a pre-existing design, it was developed a three stage techno-ecnonomical optimizer which included: a parametric economical evaluation that had Net Present Value (NPV) and Required Freight Rate (RFR) as measures of merit; a global hydrodynamic optimizer based on Hilleary's tangent search method to generate the main dimensions, proportions and form parameters of the vessel and a local hydrodynamic optimizer relying on Lagrange's multiplier method dedicated to the refinement of the wetted hull form. The minimization of the calm water resistance with respect to least power requirement and the improvement of the seakeeping performance, while avoiding resonances in roll/pitch/heave, were the main focus in terms of hydrodynamics. This work was further developed during the following years and broadened to include any fast displacement catamaran design. Modules for the generation of hull forms and to handle the obtained design, including preparation of common naval architecture drawings were embed into the overall optimization procedure. Papanikolaou et al. (1996) presented a research paper that focused solely on the hydrodynamic module. To deal with the seakeeping problem, quasi 2-D (strip or slender body theory approach) and 3-D panel methods were used.

Kukner and Sarioz (1995) proposed a forward/inverse methodology applied to high speed hull forms, in particular a speed patrol vessel, and developed realistic seakeeping criteria to investigate the possibility of improving existing designs. Such criteria included minimizing heave/pitch peak RAOs and accelerations, as well as preventing extreme effects such as slamming and deck wetness. The authors used calm water resistance as constraint in the procedure. Systematic series were generated from the parent hull resorting to the method of Lackenby by varying *LPP* and *B/T* ratio, both by ± 10 %, *LCB* (± 2 %) and block coefficient C_b (± 5 %). The resulting models were analysed using a non-linear direct search technique associated with a 2-D strip theory based software to assess the seakeeping performance.

Purvin (2003) studied the design of a slender, semi-displacement catamaran with variable horizontal clearance ratios and its influence upon both the heave/pitch responses and the calm water resistance. The analysis was carried out in SWAN-2 (Ship Wave Analysis), a time domain Rankine panel method developed in MIT (Massachusetts Institute of Technology, Cambridge, Massachusetts, USA). Around the same period, Maisonneuve et al. (2003) implemented the procedures developed during FANTASTIC, a 3 years research program focused on the improvement of design methodologies of ship hull shapes, into the optimization of a fast mono-hull. The authors used Esteco SpA's ModeFRONTIER as optimization environment, FRIENDSHIP-Modeler for the parametric modelling of the hull and a multi-objective genetic algorithm (MOGA). The main goal was to identify the main particulars, which were varied by about ± 10 %, that minimized the calm water resistance while maximizing the seakeeping capabilities of the

vessel, measured in terms of comfort of the passengers via Motion Sickness Incidence (MSI) index. The displacement and the transverse metacentric height were used as constraints. The standard linear strip theory software SOAP (Seakeeping Operability Analysis Program) developed by Esteco SpA was used to carry the seakeeping calculations while the resistance predictions were performed using WARP (Wave Resistance Program), a linear potential flow code developed by CETENA. Similar work has been done by Vernengo et al. (2009) and Biliotti et al. (2011).

In association with the US Navy, Rollings (2003) presented a seakeeping analysis of small displacement high-speed vessels using SHIPMO, a strip theory based software developed by MARIN (Maritime Research Institute Netherlands, Wageningen, The Netherlands). Several hulls derived from the Series 64 models were generated as combinations of four different parameters: *B/T* ratio, $\Delta/\left(0.01\mathit{LPP}\right)^3$ which is a payload indicator and C_b. The author considered several operational conditions and the seakeeping performance was ranked based on Bales Estimator, a specific index that accounts with the waterplane area coefficient C_{wp}, the draft to length ratio *T/LPP* and the prismatic coefficient C_p. Still in the Navy sector, Dudson and Rambech (2003) performed the seakeeping optimization of a fast catamaran designed for the US Navy as a Littoral Surface Craft, while maintaining the good resistance characteristics of the design upon a specific operational scenario. The seakeeping analysis was carried out resorting to the strip theory based code ShipX (VERES), developed by Marintek, accompanied by model testing. The main objective was to minimize roll/heave/pitch response RAOs as well as their RMS values.

Grigoropoulos (2004) proposed a methodology for hull form optimization in calm and rough water applied to two case studies: a conventional reefer and a naval destroyer. The method was based on an initial optimization of a parent hull form in terms of seakeeping (minimization of the sum of the peak values of vertical acceleration and relative motion near the ship bow in head seas) and the improvement of the resulting optimum hull form for calm water resistance. Hull variants were obtained by applying the method of Lackenby and manipulating both the main dimensions and form parameters C_{wp}, *LCF*, C_b, *LCB*, C_m and KB. The seakeeping calculations were carried out in a classic linear strip theory method while for resistance the panel code SWAN-2 (Ship Wave Analysis) was used. Grigoropoulos and Chalkias (2010) presented a development of the previous work in which the hull forms were optimized via wash waves (calm water) and selected dynamic responses (rough water). This time the methodology was implemented in the optimization of a planning hull form and a fast displacement ferry. The hull variations were generated parametrically using FRIENDSHIP-Modeler and evaluated using evolutionary strategies for a dual-objective optimization.

Kapsenberg (2005) presented a method to find a hull form that satisfies a set of seakeeping requirements associated with the minimization of vertical motions and accelerations. The procedure starts with a parent hull of a frigate characterized by polynomials that define the beam on the waterline, the draft and the sectional area as a function of the length. An optimization routine resorting to Lewis transforms is then used to vary the hull form until the vertical accelerations and relative bow motion are minimum. The seakeeping analysis is performed by a linear strip theory software with forward speed corrections as developed by Delft University of Technology.

Resorting to Simulation-Based Design (SBD) ([17]), Campana et al. (2006) presented the fundamentals for hydrodynamic shape optimization, including strategies to reduce the computational effort, techniques for mesh manipulation and methodologies for verification and validation of results, applied to a US Navy surface combatant. The objective function was the minimization of total resistance (bare hull) and the heave/pitch peak RAOs were set as constraints. Two RANS solvers, CFDSHIP-Iowa and MGShip, were used to study the total resistance, wake and free surface waves, while the seakeeping assessment was carried out in SMP (Ship Motion Program), a strip theory based code.

As previously said, the wellness and comfort are, especially for passenger ships, two very important aspects. From this perspective, Sariöz and Narli (2005) investigated the effect of seakeeping criteria on the performance of passenger vessels. Such criteria included Motion Sickness Incidence (MSI), Motion-Induced Interruptions (MII) and an habitability index, for which RMS (Root Mean Square) accelerations were computed. The authors remarked on the influence of the level of limiting value selected as the seakeeping criteria on the estimated seakeeping performance of a passenger vessel. Furthermore, in Cepowski (2010) studied the influence of changes in the form coefficients, centre of buoyancy and centre of waterplane on the seakeeping behaviour of passenger-car ferries. For every ship variant sailing in the assumed operational conditions, the following seakeeping parameters were calculated: maximum significant roll amplitudes, maximum significant amplitude of vertical/lateral accelerations and maximum Motion Sickness Incidence (MSI). These results allowed the author to develop design guidelines based on regression functions. Regarding Motion Sickness Incidence (MSI), Cepowski (2012) later discussed the influence of the environmental conditions on sea sickness and presented several indexes that measure it, including MSI. In fact, the use of this index as a parameter to minimize in an optimization procedure is not new (e.g. Maisonneuve et al., 2003). It is, nonetheless, a common approach. Scamardella and Piscopo (2014), for instance, proposed a new index as the parameter to be minimized in a single-objective seakeeping optimization of a passenger ship, the Overall Motion Sickness Incidence (OMSI), defined as the mean Motion Sickness Incidence (MSI) on the ship main deck. The authors' proposal stands as an alternative to the more classic optimization techniques, where seakeeping performances are optimized simply by minimizing the peak values of heave/pitch RAOs. Parametric modelling via Lackenby method was used to generate several hull forms derived from the NPL systematic series by varying *LCB*, C_b and C_p and by using bare hull resistance and trim as constraints. Two operating scenarios were considered in the procedures. The authors suggested that the proposed method can also be applied to Motion Induced Interruptions (MII) and included into multi-objective optimization procedures. Later, Piscopo and Scamardella (2015) applied the developed OMSI to optimize a wave piercing high-speed catamaran.

Bagheri et al. (2014) presented a study in which it is used a Genetic Algorithm (GA) combined with a linear strip theory code for minimizing the peak value of vertical displacement of the ship bow. The new hull forms were generated from Series 60 and Wigley hulls by changing the main dimensions (length, breadth, draft by ± 10 $\%$) as well as the hull offsets by ± 3 $\%$. The main constraint of the optimization procedure was constant displacement.

Later, Vernengo et al. (2015) optimized a semi-SWATH passenger ferry in terms of seakeeping and

resistance at different speeds resorting to a multi-objective global convergence genetic algorithm. The hull model was generated parametrically and a 3D linear Rankine sources panel method was used to compute the total resistance and peak vertical accelerations at the main deck in regular head seas, both to be minimized. Still in this framework, the work of Vernengo and Bruzzone (2016) is worth mentioning.

Based on a SBD approach, Ang et al. (2015) integrates a geometry modification technique - Free Form Deformation (FFD) - with advance optimization and evaluation algorithms - Genetic Algorithm (GA) -, in order to improve the efficiency and the hydrodynamic performance of offshore vessels. The goal was to reduce the total resistance while optimizing the seakeeping performance by minimizing the roll peak RAO, for which a CFD code and strip theory were used, respectively.

2.4 Summary

As it can be acknowledged, plenty of research has been developed on the assessment and optimization of the seakeeping behaviour of vessels as a result of the widespread development of high-speed crafts and its use to transport passengers. In fact, the present demands of the industry, which commonly resort to catamarans for this purpose, reinforce the relevance of the subject.

Despite the continuous development of more advanced and accurate tools to predict motions, strip theories remain a meaningful research topic due to the low computational power required and the fast calculations provided, even considering their limited range of applications (slow speeds, slender hulls, small motion amplitudes, inviscid fluid assumptions). They are particularly useful within academic contexts, during early design stages and for inclusion into optimization procedures.

Chapter 3

Benchmarking study of strip-theory codes to predict heave and pitch motions of fast displacement catamarans in head seas

As the operational requirements become more demanding in terms of safety, comfort and efficiency (both economic and energetic), the urgency for vessels with exceptional seakeeping capabilities increase. At the same time, the challenges created by the growth of sea exploration scatter, leading to the need and development of new designs and solutions that often materialize in the form of faster and bigger vessels with unconventional shapes (e.g., offshore industry). There are several dynamic problems that affect the behaviour of a ship on wavy seas, namely, wave induced movements that increase ship resistance and reduce propeller efficiency, affecting the economic viability of the project. Also, relative motions of extreme amplitudes between the ship and the waves that lead to structural damage (slamming, deck equipment damage due to water boarding or even engine and propeller shaft overload caused by the propeller coming out of the water) and causes passengers to lose the capacity of standing, causing discomfort and jeopardizing the overall safety of the ship. Finally, excessive accelerations, which not only overload the equipment and the cargo but can cause sea sickness on the crew and passengers as well. Acknowledging the consequences of these problems and minimizing them is extremely important in order to guarantee that the vessel will be able to fulfill its mission. Thus, the importance of seakeeping optimization in an early stage of the design process, i.e. right during preliminary design. In any case, the scope of the work of this dissertation neglects extreme effects such as slamming, focusing solely on absolute motions and accelerations.

A seakeeping analysis involves two distinct problems: the hydrodynamics between the hull structure and the waves and the representation of the stochastic characteristics associated with the considered

seaway. Throughout this chapter, the first problem will be solved resorting to a classic strip theory formulation (Salvesen et al., 1970). Despite the development of powerful methods, namely CFD solvers, strip theories continue to be a meaningful research subject. Watanabe and Guedes Soares (1999) underlines that although linear strip theory has been established several years ago as an adequate tool for the assessment of ship motions and wave-induced loads during early stages of design, it is known to have some limitations. These include low ship speed, the absence of 3-D effects and not properly accounting for viscous flows nor large amplitude motions. In any case, the low computational power required together with the ability to provide quick results make them ideal to be used during early design stages and within academic contexts. For the same reasons, strip theory codes are highly suited to be included into optimization procedures.

In fact, the objective of this dissertation was the seakeeping optimization of a fast displacement catamaran to operate as a crew supply vessel (Chapter 4), motivating the use of strip-theory as numerical method to predict ship motions. This led to a benchmarking study to assess the capacity of three different codes (PDStrip, Fonseca and Maxsurf Motions) to accurately predict heave and pitch motions of catamarans in head seas. The goal was to select one of them to include into the automated optimization procedure. As previously said, the reason to focus solely on heave and pitch motions had to do with the fact that they represent the most critical situations for a fast catamaran when compared with rolling motions, given the higher transverse stability. Furthermore, an assumption about negligible interaction between demi-hulls, acceptable in head and following seas, was exploited since the codes used in the benchmarking study did not include such considerations. In any case, it is clear that narrowing this study to wave headings with the same direction of the forward ship motion is a rather simplistic way of looking into the problem (particularly from the perspective of seakeeping optimization). However, it is the only approach that allows resorting to those three codes to make plausible motion predictions of catamarans. Using them to assess the seakeeping behaviour, for instance, in beam seas, would compromise the assumption of negligible hull interaction and, consequently, the obtained results.

3.1 Background Theory

The potential flow formulation around a ship hull advancing in wavy seas and oscillating lays the foundation for strip methods. It is assumed that the fluid is incompressible, inviscid and irrotational since the problem depends largely on gravitational forces, even though in some cases viscous effects must also be considered. In any case, for heave and pitch motions, which is the main focus of this dissertation, the effect of viscous forces can be neglected without significant losses in accuracy [109]. Within these assumptions, the velocity field $\vec{V} = (u, v, w)$ can be represented as a scalar Φ, the velocity potential, that satisfies the continuity equation, $\vec{V} = \vec{\nabla}\Phi$, leading to the well known Laplace equation $\vec{\nabla}^2\Phi = 0$. The Laplace equation has many solutions and thus, the uniqueness of the solution will depend on the definition of appropriate boundary conditions for the entire fluid domain. Furthermore, the solution of the exact boundary value problem is far too complex. Therefore, it needs to be simplified in order to remove the

non-linearities and the 3-D interactions between steady and unsteady flows. This results in restrictions on the slenderness of the vessel, its advance speed and the amplitude/frequency of oscillation. Different combinations of restrictions result in different seakeeping formulations and this is where strip theories come in. Throughout this chapter, only the main governing equations will be presented. However, the lecture notes of Fonseca (2009) present a thorough review of the complete hydrodynamic problem formulation within ideal fluid assumptions including the derivation of the boundary value problem and its linearization, a reading the author encourages for a better understanding of the topic.

3.1.1 Governing equations

Although several reference frames are generally defined for seakeeping calculations, for the purpose of evaluating motion results, only the inertial coordinate system is needed in which motions are periodic. Let (ξ, η, ζ) be fixed with respect to the mean position of the ship and in steady translation with the forward velocity with ζ vertically upwards through the centre of gravity, ξ in the direction of forward motion and the origin at the undisturbed free surface as seen in Figure 3.1.

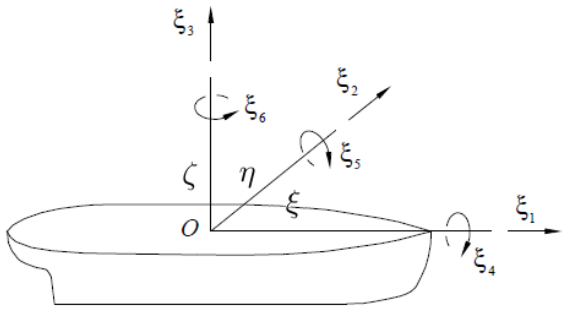

Figure 3.1: General coordinate system and conventions ([46], adapted)

The motions of a ship have six degrees of freedom: three translations and three rotations. The translations on the (ξ, η, ζ) directions consist on surge, sway and heave and are represented by ξ_1, ξ_2 and ξ_3 as seen in Figure 3.1. The rotations in respect to those same axis are roll, pitch and yaw, respectively, ξ_4, ξ_5 and ξ_6. From hereinafter, except when noted, this subscript indicial notation will be used to denote the ship displacements in a six degrees of freedom system.

Generally speaking, the equations of motion result from the equilibrium between external forces, hydrodynamic in this case, and the inertial forces associated to the mass that defines the ship. The hydrodynamic forces result from pressure integration over the wetted surface of the hull. The integration of Bernoulli equation results into two force components, one associated with the dynamic pressure and the other with the hydrostatic pressure, i.e., hydrostatic forces. By splitting the dynamic term into independent components, the exciting force and the radiation force emerge. The former is associated with the incident wave field pressure and the perturbation of that field due to the presence of the ship (diffraction phenomenon). The radiation force is a result of the problem where the ship, advancing with a certain speed, is forced to oscillate on the absence of incident waves. The combination of all these

contributions results in equation (3.1).

$$F_j^E + F_j^R + F_j^B = F_j^M, \quad j = 1, ..., 6 \tag{3.1}$$

, where F_j^M represents the inertial forces, F_j^E the exciting forces, F_j^R radiation forces and F_j^B the restoring forces that result from combining the hydrostatic forces with the ship weight. The subscript j denotes the direction of motion: $j = 1, 2, 3$ the force components in the x, y, z directions and $j = 4, 5, 6$ the moment components about those same axes. Under the assumptions that the responses are linear and harmonic, the six linear coupled differential equations of motion can be written, using subscript notation, as in equation (3.2) as function of frequency/speed dependent coefficients.

$$\sum_{k=1}^{6} \left[(M_{jk} + A_{jk}) \ddot{\xi}_k + B_{jk}\dot{\xi}_k + C_{jk}\xi_k \right] = \left|F_j^E\right| e^{i\omega_e t} \quad j = 1, ..., 6 \tag{3.2}$$

, where M_{jk} are the components of the generalized mass matrix of the ship, A_{jk} and B_{jk} are the added mass and damping coefficients corresponding to the real and imaginary parts of the radiation force/moment, C_{jk} are the hydrostatic restoring coefficients and $\left|F_j^E\right|$ are the complex amplitudes of the exciting force/moment $F_j^E = \left|F_j^E\right| e^{i\omega t}$. The frequency of encounter ω_e is the same as the frequency of the response and relates to the wave frequency ω_0 by the following expression:

$$\omega_e = \omega_0 - k_0 U \cos\beta \tag{3.3}$$

, where $k_0 = \omega_0^2/g$ is the wave number and β is defined as the ship heading relative to the waves, for which the convention used here assumes $\beta = 180°$ for head seas. Finally, for a ship with lateral symmetry and a slender hull form, the derived equations for coupled heave and pitch motion follow from equation (3.2) and are presented here in matrix form:

$$\begin{bmatrix} \Delta + A_{33} & A_{35} \\ A_{53} & I_{55} + A_{55} \end{bmatrix} \begin{Bmatrix} \ddot{\xi}_3 \\ \ddot{\xi}_5 \end{Bmatrix} + \begin{bmatrix} B_{33} & B_{35} \\ B_{53} & B_{55} \end{bmatrix} \begin{Bmatrix} \dot{\xi}_3 \\ \dot{\xi}_5 \end{Bmatrix} + \begin{bmatrix} C_{33} & C_{35} \\ C_{53} & C_{55} \end{bmatrix} \begin{Bmatrix} \xi_3 \\ \xi_5 \end{Bmatrix} = \begin{Bmatrix} \left|F_3^E\right| \\ \left|F_5^E\right| \end{Bmatrix} e^{i\omega_e t} \tag{3.4}$$

where Δ represents the total mass of the ship and I_{55} is the moment of inertia in the 5$^{\text{th}}$ mode. The solutions of the second order linear differential equations (3.4) are harmonic:

$$\xi_j(\omega_e) = \Re\{\xi_j^A e^{i\omega_e t}\} = \xi_j^a \cos(\omega_e t - \theta_j), \quad j = 3, 5 \tag{3.5}$$

, where ξ_j^A is the complex amplitude of the harmonic motion, ξ_j^a is the real amplitude and θ_j the phase angle that represents the delay of the response.

3.1.2 Global hydrodynamic coefficients

As stated before, with the goal of maintaining an adequate simulation time for practical applications while ensuring a good level of accuracy, strip theory was selected as tool for seakeeping analysis to be

embedded into an optimization procedure. The main goal of strip theory is to provide a simple, straight forward and quick method to compute the motions of a vessel upon a wavy seaway. Despite being a complex 3-D problem, the hull-waves interaction that induces hydrodynamic forces causing the vessel to oscillate can be simplified. Initially proposed by Korvin-Kroukovsky and Jacobs (1957) for heave and pitch motions, the main goal of strip theories is to approximate this 3-D phenomena to a set of 2-D, simpler, problems. The vessel is "sliced" into a finite number of cross sections, or strips, and the sectional forces represented in terms of derived or experimentally obtained coefficients. Later, Salvesen et al. (1970) further refined the work of Korvin-Kroukovsky and Jacobs (1957) to correct some of the original terms and broadened it to include sway, roll, and yaw motions, as well as wave induced vertical and horizontal shear forces, bending moments, and torsional moments, a contribution seen today as quintessential in strip theory. For the remaining part of this chapter, the derived global hydrodynamic coefficients for heave and pitch motions are going to be presented following the formulation of the ordinary strip-method of Salvesen et al. (1970). The hydrodynamic coefficients are computed for each 2-D strip by solving the linearised boundary value problem at the corresponding cross section. The global coefficients result from the integration of the sectional coefficients along the ship length. Again, only the main results will be shown here but, for further reading, the author advises the lecture notes of Fonseca (2009) or the work of Salvesen et al. (1970) itself.

Radiation forces The complex amplitude of the radiation force/moment due to heave and pitch coupled motions is given by:

$$F_j^R = \sum_{k=3,5} \xi_k \left(\omega_e^2 A_{jk} - i\omega_e B_{jk}\right), \quad j = 3, 5 \tag{3.6}$$

The added-mass and damping coefficients A_{jk} and B_{jk} are shown in Table 3.1. Note that if the ship has a transom stern, Salvesen et al. (1970) proposes additional terms that supposedly improve motion predictions.

Table 3.1: Added mass and damping coefficients for heave/pitch coupled motions [109]

	Original	Transom corrections
A_{33}	$\int_L a_{33} d\xi$	$-\frac{U}{\omega_e^2} b_{33}^{tr}$
B_{33}	$\int_L b_{33} d\xi$	$+U a_{33}^{tr}$
A_{35}	$-\int_L \xi a_{33} d\xi - \frac{U}{\omega_e^2} B_{33}^0$	$+\frac{U}{\omega_e^2} x_{tr} b_{33}^{tr} - \frac{U^2}{\omega_e^2} a_{33}^{tr}$
B_{35}	$-\int_L \xi b_{33} d\xi + U A_{33}^0$	$-U x_{tr} a_{33}^{tr} - \frac{U^2}{\omega_e^2} b_{33}^{tr}$
A_{53}	$-\int_L \xi a_{33} d\xi + \frac{U}{\omega_e^2} B_{33}^0$	$+\frac{U}{\omega_e^2} x_{tr} b_{33}^{tr}$
B_{53}	$-\int_L \xi b_{33} d\xi - U A_{33}^0$	$-U x_{tr} a_{33}^{tr}$
A_{55}	$\int_L \xi^2 a_{33} d\xi + \frac{U^2}{\omega_e^2} A_{33}^0$	$-\frac{U}{\omega_e^2} x_{tr}^2 b_{33}^{tr} + \frac{U^2}{\omega_e^2} x_{tr} a_{33}^{tr}$
B_{55}	$\int_L \xi^2 b_{33} d\xi + \frac{U^2}{\omega_e^2} B_{33}^0$	$+U x_{tr}^2 a_{33}^{tr} + \frac{U^2}{\omega_e^2} x_{tr} b_{33}^{tr}$

Here, all the integrals are over the length of the ship and U is the forward speed of the ship. a_{33} and b_{33} represent the sectional added mass and damping coefficients for heave (ζ direction). Depending on the method used to compute the 2-D radiation potential for forced harmonic motions that determines a_{33} and b_{33}, different results with different accuracies can be obtained. A_{33}^0 and B_{33}^0 refer to the speed

independent components of A_{33} and B_{33}. x_{tr} is the $\xi-$coordinate of the aftermost cross section of the ship and a_{33}^{tr} and b_{33}^{tr} are the added mass and damping coefficients evaluated at that section.

Exciting forces As stated before, the exciting forces and moments are associated with two phenomena. The field of incident waves, a contribution commonly referred to as Froude-Krylov forces, and the perturbation of that field due to the presence of the ship, which is at the origin of the diffraction forces. Bearing this in mind, for heave and pitch motions, the amplitude of the exciting force and moment is given in Table 3.2 including corrections for ships with transom sterns.

Table 3.2: Heave exciting force and pitch exciting moment [109]

	Original	Transom corrections
F_3^E	$\rho\xi_a \int_L \left(f_3^D + f_3^K\right) d\xi$	$+\rho\xi_a \frac{U}{i\omega_e} f_3^{Dtr}$
F_5^E	$-\rho\xi_a \int_L \left[\xi \left(f_3^D + f_3^K\right) + \frac{U}{i\omega_e} f_3^D\right] d\xi$	$-\rho\xi_a \frac{U}{i\omega_e} x_{tr} f_3^{Dtr}$

Again, all the integrals are over the length of the ship and U is its the forward speed. f_3^K and f_3^D represent the sectional Froude-Krylov and diffraction forces, respectively, in the vertical direction ($\zeta-$ axis) for unit amplitude incident waves. Regarding the former component, the classical theory of linear gravity-waves defines, within deep water assumptions, the potential of a progressive incident wave with an arbitrary direction, which makes f_3^K easy to compute by evaluating it at the mean wetted cross section. Alternatively, it can be computed at each time step, an approach commonly followed by time domain formulations. As for f_3^D, as an alternative to the direct determination of the 2-D diffraction potential, Green theorem is usually applied in order to solve it as function of the 2-D radiation potential ([46], [109]). Finally, f_3^{Dtr} is the diffraction force evaluated at the aftermost section at x_{tr}. ξ_a represents the wave amplitude and ρ is the fluid density.

Restoring forces The restoring forces result from equating the hydrostatic forces with the ship weight and follow directly from hydrostatic considerations. Time domain formulations usually evaluate them at the instantaneous wetted surface, which creates a dependency on time/frequency and forward speed. On the other hand, frequency domain formulations assess them at the mean position of the wetted surface, being the approach followed here.

$$F_j^B = -\sum_{k=3,5} C_{jk}\xi_k, \quad j = 3,5 \tag{3.7}$$

, where the coefficients C_{jk} are given by:

$$\begin{aligned} C_{33} &= \rho g A_{wp} \\ C_{35} &= C_{53} = -\rho g M_{yy} \\ C_{55} &= \rho g \nabla G M_L \end{aligned} \tag{3.8}$$

, where ∇ is the static underwater hull volume, A_{wp} is the static waterplane area, M_{yy} is the first area

moment of the static waterplane and GM_L the longitudinal metacentric height.

3.2 Overview of Fonseca, PDStrip and MaxMotions

As stated before, with the goal of maintaining an adequate simulation time for practical applications while ensuring a good level of accuracy, strip theory was selected as method for seakeeping analysis to be embedded into an optimization procedure of a high-speed catamaran. This motivated the comparison of three different available codes: Fonseca, PDStrip and MaxMotions (see Table 3.3). Despite a few non-linear considerations by PDStrip, all the codes are linear and the computations are carried out in the frequency domain, following in a general sense the formulation presented in the previous section. It is also important to underline the fact that none of the codes included in the benchmarking study consider the double-hulled configuration of the vessel and thus, an assumption of negligible hull interaction was exploited. Table 3.4 presents the main features and limitations of each code and Table 3.6 overviews the reference frames used. Further ahead, a more detailed description of each code is presented.

Table 3.3: Strip theory codes used in the benchmarking study

Code, Version	Acronym	Type	Developer	Reference
Unknown	Fonseca	Frequency domain	Nuno Fonseca (CENTEC)	Fonseca and Guedes Soares* (1998)
PDStrip, rev. 32	PDStrip	Frequency domain	Heinrich Söding	Söding and Bertram (2009)
Maxsurf Motions, V20	MaxMotions	Frequency domain	Bentley Systems	Bentley Systems, Incorporated (2013a)

* Linear version

Table 3.4: Main features of the codes

Features	Fonseca	PDStrip	MaxMotions
Non-linear motions	No	No	No
Non-linear transverse drag forces	No	Yes	No
Transom terms	No	Yes (optional)	Yes (optional)
Maximum number of strips/cross sections	40	100	200
Minimum number of equally spaced cross sections (recommended)	21	30-40	15-30
Maximum number of offset points per cross section	20	100	15 (mapping terms)
Minimum number of offset points per half cross section (recommended)	8-10	10	3 (mapping terms)
Cross sections defined with equal number of offset points/mapping terms	Yes	No	Yes
Offset points approximately equally distant along cross section	Yes	Yes	-
Maximum number of wavelengths used for motion results	30	200	500
User defined wavelength range	yes	yes	no
Relative computational speed with highest Fonseca settings (except wavelengths)	high	medium high	very low

Table 3.5: Methods applied by the codes to compute the 2-D radiation potential

Code	Method	Reference
Fonseca	Frank close-fit source distribution method	Frank (1967)
PDStrip	Patch method	Söding (1993)[1]
MaxMotions	Multi-parameter conformal mapping	Bentley Systems, Incorporated (2013a)[2]

[1] Alternatively refer to [119], [11]

[2] It follows the solution of [125] for a heaving unit circle, applied to a hull shape via multi-parameter conformal mapping

Table 3.6: Coordinate systems used by the codes

	Code	Coordinate Origin	+ x-axis	+ y-axis	+ z-axis
Geometry Data	Fonseca	fwdPP, centerplane, DWL	aft	port	upwards
	PDStrip	amidships, centerplane, baseline	forward	port	upwards
	MaxMotions	non applicable	forward	starboard	upwards
Inputs	Fonseca	amidships, centerplane, DWL	forward	port	upwards
	PDStrip	amidships, centerplane, baseline	forward	port	upwards
	MaxMotions	amidships, centerplane, baseline	forward	starboard	upwards
Motion Results	Fonseca	LCG, centerplane, baseline	forward	port	upwards
	PDStrip	amidships, centerplane, baseline	forward	starboard	downwards
	MaxMotions	LCG, centerplane, baseline	forward	starboard	upwards

Fonseca is a frequency domain strip-theory code developed at CENTEC (Centre for Marine Technology and Ocean Engineering) in Técnico Lisboa (IST), corresponding to the linear version of the time-domain method of Fonseca and Guedes Soares (1998). Although there is a substantial number of research papers validating the results of the non-linear version of the code, showing good accuracy in predicting motions and loads of relatively slow ships ([49], [52], [51], [54]), the linear version Fonseca lacks documentation and validation but it essentially follows the formulation of Salvesen et al. (1970) presented in the previous section (without transom terms in the equations). The numerical solution for the 2-D radiation potential in forced harmonic motions, which allows to determine the sectional added masses, damping coefficients and diffraction force, is obtained via Frank close-fit method [56].

MaxMotions is a seakeeping module of the commercially available software Maxsurf [7]. Again, the code follows the ordinary-strip method [109]. Motions can be computed both with and without transom corrections. The 2-D solution for the potential is obtained via multi-parameter conformal mapping. Reasonable accuracy has been achieved in terms of seakeeping predictions for a wide range of vessel types. Such results can be found in the appendices of the manual [7] or in independent publications such as Ghassemi et al. (2015). The main advantage of using Maxsurf Motions is the user friendly interface and the possibility of integration into optimization procedures via automation (VBA's). The speed of the analyses is, however, quite slow, particularly as the number of cross sections and analysed frequencies increase.

PDStrip is a public domain strip method based code written in FORTRAN developed by Söding and Bertram (2009). The resulting code computes the seakeeping of ships, including sailing vessels, and other floating bodies. The method applies the already cited publication of Söding (1969) to compute ship motions (essentially the same results as Salvesen et al., citeyearSalvesen1970). Despite considering mainly linear responses, it takes into account a few non-linear effects that will be briefly discussed in due course. As stated a few years ago by Palladino et al. (2006), the validation of PDStrip continues to be work in progress. Although it has been used by many researchers for a wide variety of purposes including manoeuvring simulations [116], [115], analysis of wave-induced dynamic effects on sailing yachts [16], computation of drift forces on offshore wind farm installation vessels [3] or even integrated into a global design tool [107], a thorough work of comparison with both experimental results and other seakeeping codes is still to be done [95], [59].

Recalling Table 3.6, note that the inertial reference frame (ξ, η, ζ) is, according to Söding and Bertram (2009), positioned at amidships, rather than at the centre of gravity. The method computes added mass and damping coefficients slightly different than what has been shown in Table 3.1 but the results are essentially the same. Considering only the heave and pitch contribution, the added mass and damping coefficients are given by equations (3.9).

$$\begin{aligned}
[A] &= \Re\left\{\int_L \begin{bmatrix} 0 & 1 \\ 0 & -\xi \end{bmatrix} \left(-i\omega_e + U\frac{\mathrm{d}}{\mathrm{d}\xi}\right)\left(a_{33} - \frac{ib_{33}}{\omega_e}\right)\begin{bmatrix} 0 & 0 \\ i\omega_e & i\omega_e\xi - U \end{bmatrix} d\xi\right\} \\
[B] &= \Im\left\{\int_L \begin{bmatrix} 0 & 1 \\ 0 & -\xi \end{bmatrix} \left(-i\omega_e + U\frac{\mathrm{d}}{\mathrm{d}\xi}\right)\left(a_{33} - \frac{ib_{33}}{\omega_e}\right)\begin{bmatrix} 0 & 0 \\ i\omega_e & i\omega_e\xi - U \end{bmatrix} d\xi\right\}
\end{aligned} \tag{3.9}$$

Again, the integrals are along the ship length. The reason for the different formulation has to do with the way the transom corrections, associated with the term $\mathrm{d}/\mathrm{d}\xi$, are included in the code. For the same reason, the heave exciting force and the pitch exciting moment are presented with a different formulation - equations (3.10) -, rather than as stated in Table 3.2. In any case, only linear considerations have been taken into account, meaning that the sectional Froude-Krylov force is evaluated at the mean wetted cross section, similarly to Fonseca and MaxMotions.

$$\begin{aligned}
F_3^E &= \rho\xi_a \int_L \left(f_3^D + f_3^K + i\frac{U}{\omega_e}\frac{\mathrm{d}f_3^D}{\mathrm{d}\xi}\right) d\xi \\
F_5^E &= -\rho\xi_a \int_L \xi\left(f_3^D + f_3^K + i\frac{U}{\omega_e}\frac{\mathrm{d}f_3^D}{\mathrm{d}\xi}\right) d\xi
\end{aligned} \tag{3.10}$$

Furthermore, the method accounts for two extra contributions to the hull forces (radiation and excitation) when compared with the standard procedure [109]: a longitudinal force associated with the surging motion and a transverse non-linear drag force. Starting with the contribution of the longitudinal force on the radiation forces, the hydrodynamic added mass in surge is computed using an empirical formula described by equation (3.11).

$$a_{11} = \frac{\Delta}{\pi\sqrt{\frac{\rho LPP^3}{\Delta}} - 14} \tag{3.11}$$

, where Δ is the vessel displacement, *LPP* the length between perpendiculars and ρ the fluid density. This yields the generalized longitudinal force acting on the ship, which coupled with the global hull motions originates an additional contribution to the hydrodynamic coefficients. Still, considering only heave and pitch motions, the longitudinal force will only contribute to the added mass coefficient A_{55} :

$$\delta A_{55} = \omega_e^2 a_{11} z_0^2 \tag{3.12}$$

, where δA_{55} denotes the additional contribution to A_{55} and z_0 refers to the waterline level. Considering now the contribution of the longitudinal force to the exciting forces, the diffraction part is considered negligible. Thus, only the Froude-Krylov part is taken into account. Again, considering only heave and pitch motions, the longitudinal force will contribute to the pitch exciting moment.

$$\delta F_5^K = \int_L z_\xi p \frac{dA}{d\xi} d\xi + z_{\xi_{tr}} p_{tr} A_{tr} \tag{3.13}$$

, where δF_5^K denotes the additional contribution to the Froude Krylov moment F_5^K, p refers to the pressure calculated at the centre of each cross section $(\xi, 0, z_\xi)$, A is the corresponding immersed area and the index tr denotes values evaluated at the transom stern. Therefore, the term $z_{\xi_{tr}} p_{tr} A_{tr}$ vanishes if the transom corrections are to be neglected from the calculations. As usual, the integral is evaluated along the ship length. It follows that at the centre of a cross section, the pressure is given by:

$$p = -\rho g e^{-k_0(z_\xi + T)} \xi_a e^{-ik_0 \cos\beta} \tag{3.14}$$

, where ξ_a is the wave amplitude and T refers to the mean draft of the ship cross section.

The second contribution to the hull forces is a transverse non-linear drag force that depends quadratically on the transverse velocity at each cross section. The drag force at a cross section in $\zeta-$ direction is:

$$f_z = \frac{\rho}{2}\sqrt{v_y^2 + v_z^2} v_z B C_z \tag{3.15}$$

, where B is the section beam, C_z is the resistance coefficients of the cross section for vertical flow, $\sqrt{v_y^2 + v_z^2}$ is the absolute value of the transverse velocity and v_y, v_z its components in the horizontal and vertical directions, respectively. Furthermore, v_y and v_z can be interpreted as relative velocities between the water (w) and the ship sections (u), setting:

$$\begin{aligned} v_y &= w_y - u_y \\ v_z &= w_z - u_z \end{aligned} \tag{3.16}$$

Due to the non-linear force components f_z, the absolute transverse velocity is taken as an equivalent linearised velocity, constant in time, that depends on the complex amplitude of v_y and v_z - equation

(3.17). The sectional drag force can then be re-written as in equation (3.18).

$$\overline{v} = \frac{8}{3\pi}\sqrt{|v_y|^2 + |v_z|^2} \tag{3.17}$$

$$f_z = \frac{\rho}{2}\overline{v}\,(w_z - u_z)\,BC_z \tag{3.18}$$

It follows that the two transverse velocity components u_y, u_z depend on ship motions ξ_j as in equation (3.19) and the water velocity components w_y, w_z depend on the wave amplitude ξ_a as in (3.20).

$$\begin{aligned} u_y &= i\omega_e\xi_2 - \xi_6\,(U - i\omega_e\xi) \\ u_z &= i\omega_e\xi_3 + \xi_5\,(U - i\omega_e\xi) \end{aligned} \tag{3.19}$$

$$\begin{aligned} w_y &= \omega_0\xi_a e^{-ik_0\xi\cos\beta - k_0 T}\sin\beta \\ w_z &= i\omega_0\xi_a e^{-ik_0\xi\cos\beta - k_0 T} \end{aligned} \tag{3.20}$$

Logically, ship motions are not known *a priori*. Thus, the process of computing the transverse drag forces is iterative. Finally, in the equations above, the terms involving u_y, u_z contribute to the radiation forces while the terms involving w_y, w_z contribute to the exciting forces. Again, considering heave and pitch motions, this leads, respectively, to the following equations:

$$\begin{aligned} \delta[A] &= \Re\left\{-\frac{\rho}{2}\int_L \overline{v}\begin{bmatrix} i\omega_e BC_z & UBC_z - i\omega_e\xi BC_z \\ -i\omega_e\xi BC_z & -U\xi BC_z + i\omega_e\xi^2 BC_z \end{bmatrix} d\xi\right\} \\ \delta[B] &= \Im\left\{-\frac{\rho}{2}\int_L \overline{v}\begin{bmatrix} i\omega_e BC_z & UBC_z - i\omega_e\xi BC_z \\ -i\omega_e\xi BC_z & -U\xi BC_z + i\omega_e\xi^2 BC_z \end{bmatrix} d\xi\right\} \end{aligned} \tag{3.21}$$

$$\begin{aligned} \delta F_3^E &= \frac{\rho}{2\xi_a}\int_L \overline{v} w_z BC_z\xi \\ \delta F_5^E &= -\frac{\rho}{2\xi_a}\int_L \overline{v}\xi w_z BC_z d\xi \end{aligned} \tag{3.22}$$

Again, all integrals are along the ship length and δ refers to variations to the original radiation forces and exciting forces.

Regarding the restoring coefficients, they are effectively computed has stated in equation (3.8), considering the mean position of the wetted surface. However, as a result of programming decisions from the developers, PDStrip computes the first area moment of the static waterplane with respect to the midship section, resulting in different coefficients for C_{35} and C_{53}. Furthermore, there is an addition in C_{53} if transom terms are to be included in the calculations:

$$\delta C_{53} = z^{tr} A^{tr} \tag{3.23}$$

, where z_{tr} is the $z-$coordinate of the centroid of the area of wetted transom A^{tr}.

Finally, the numerical solution for the sectional radiation potential, described in Söding (1993) (alterna-

tively [11], [119]), follows a patch method that approximates the potential as a superposition of point sources. The cross section contour is defined by offset points and for each segment between adjacent offset points, one source is generated near the midpoint. The difference for a traditional panel method is that the integral of the boundary conditions along each segment is used (i.e. desingularized Rankine point sources), rather than satisfying the boundary conditions right at the collocation point in the middle of each segment. According to the author this is a more accurate method of predicting sectional forces.

3.3 Verification and validation with model tests of a catamaran and a fast mono-hull

The seakeeping tools described earlier are here used to compute the heave and pitch motions of two different hulls in head seas and the results validated against experimental data. As explained before, this situation is critical for high speed catamarans, being the main concern of this dissertation.

Both tested models were taken from literature. The first is a catamaran from Guedes Soares et al. (1999) tested at the model basin of CEHIPAR (Canal de Experiencias Hidrodinámicas de El Pardo) in Madrid, Spain. The tests were carried out at four Froude numbers ranging between 0 and 0.6 with a model of a passenger ferry catamaran designed to operate in sea-environment. Such results will be used to draw some conclusions regarding the possibility of determining the seakeeping characteristics of catamarans based on the numerical analysis of the corresponding demi-hull.

Table 3.7: Main characteristics of the tested models and corresponding full scale ships

	Catamaran, demi-hull (full-scale)	Catamaran, whole (model)	Model5 (full-scale)	Model5 (model)
Scale	1	1:10	1	1:10
LOA [m]	43.52	4.35	51.25	5.13
LPP [m]	43	4.3	50	5
LWL [m]	43	4.3	50	5
BOA, cat [m]	-	1.14	-	-
BWL [m]	2.7	0.27	5.83	0.58
D [m]	4.55	0.45	4	0.4
T [m]	1.354	0.14	1.57	0.157
Δ [Kg]	91945	183.89	183697	183.70
∇ [m^3]	89.705	0.1794	179.22	0.179
Horizontal clearance (S) [m]	-	0.86	-	-
LCB [m]	-3.37	-0.337	-3.17	-0.317
VCG [m]	3.71	0.371	1.69	0.169
C_b [-]	0.571	0.571	0.396	0.396
C_p [-]	0.702	0.702	0.626	0.626
Roll radius of gyration [%BOA]	43.3	43.3	40	40
Pitch radius of gyration [%LPP]	26.7	26.7	25	25
Tested Froude numbers	0, 0.2, 0.4, 0.6	0, 0.2, 0.4, 0.6	0.57, 1.14	0.57, 1.14

Another important aspect of this dissertation is speed. In fact, since the catamaran to be designed will operate at high speed, the range of Froude numbers covered by Guedes Soares et al. (1999) seemed insufficient. Furthermore, data from model testing of high speed catamarans was not found, which shows that this could be an under developed research topic. Therefore, test results from a high speed mono-hull

were used instead. This leads us to Model5 from Blok and Beukelman (1984), a mono-hull generated by a systematic series developed by the authors and tested at MARIN (Maritime Research Institute) in Wageningen, The Netherlands at Froude numbers 0.57 and 1.14. These results can be found, perhaps in a more accessible way, in Arribas and Fernandez (2006). An important note to mention is that contrary to the catamaran case, where the author of this dissertation had access to the corresponding full scale 3-D model, with Model 5 that was not the case. In fact, the geometry had to be taken from Arribas and Fernandez (2006) in pdf format, a meticulous work that might have affected the numerical results.

The main characteristics of both tested models and the corresponding full scale ships used for the numerical analysis can be found in Table 3.7. Figures 3.2(a) and 3.2(b) show their underwater hull body lines.

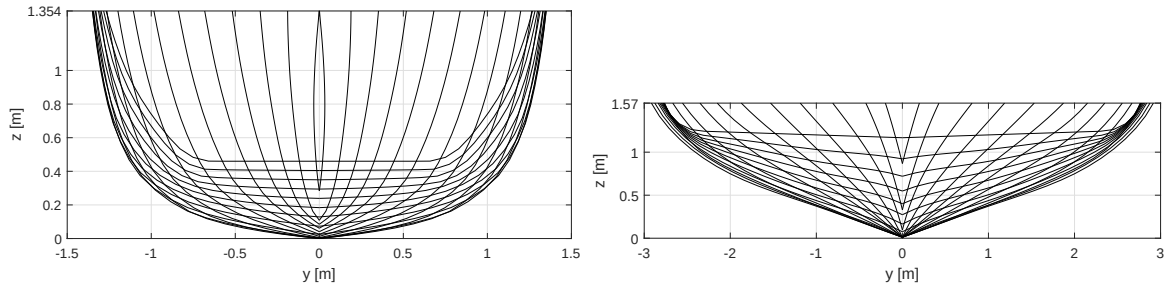

(a) Catamaran demi-hull [63] (b) Model5 [15]

Figure 3.2: Underwater body lines of the full scale ships

Next, the transfer functions of the heave and pitch motions are presented in a non-dimensional way. Heave Response Amplitude Operators (RAOs) have been divided by the wave amplitude (ξ_a) while the pitch RAOs by the wave slope ($k_0\xi_a$). These motion amplitudes are plotted versus wave frequency and each graph corresponds to a different Froude number. Results for the catamaran case can be seen in Figure 3.4 for heave and Figure 3.5 for pitch, while for Model 5 one should refer to Figure 3.3 for heave and Figure 3.6 for pitch. In each plot the numerical results can be compared with the corresponding data from model testing.

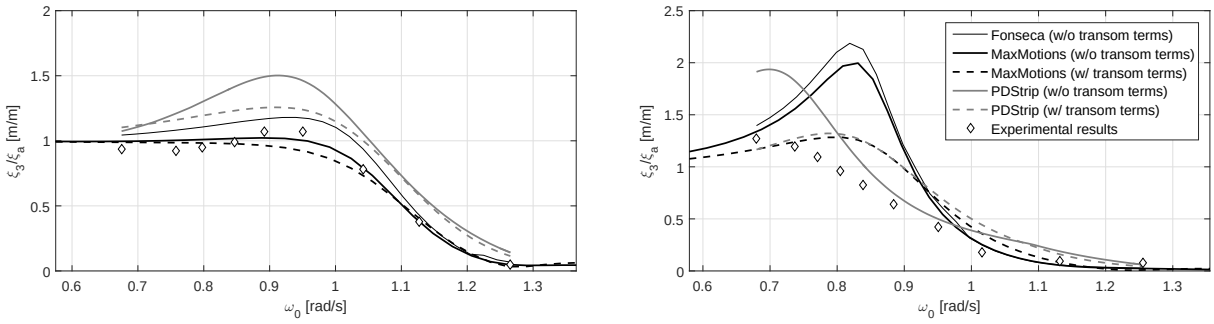

(a) Fn = 0.57 (b) Fn = 1.14

Figure 3.3: Heave RAOs as function of the wave frequency, Model5

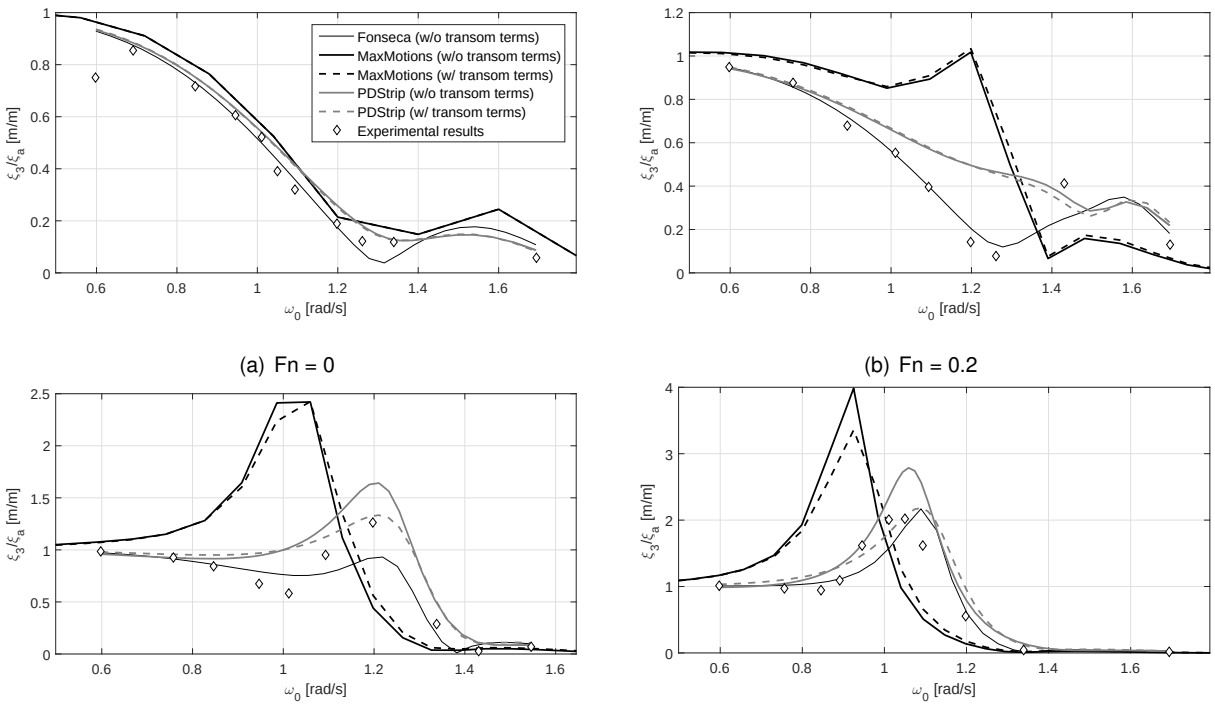

(a) Fn = 0

(b) Fn = 0.2

(c) Fn = 0.4

(d) Fn = 0.6

Figure 3.4: Heave RAOs as function of the wave frequency, Catamaran

The first conclusion to be taken from the analysis is that with increasing vessel speed, the accuracy in predicting heave and pitch motions with strip theory decreases. In Figures 3.7 and 3.8, which plot the absolute differences between numerical and experimental results at different Froude numbers, this effect is particularly well illustrated. As stated before, this is a known limitation of strip theories and a general principle that must be taken into account. For higher Froude numbers, heave and pitch response peaks are generally overestimated.

Given the nature of the coefficients of the equation of motion (refer to Tables 3.1 and 3.2 and to equations 3.8), transom terms have no effect at zero speed. Such terms are only meaningful as the ship starts moving. However, since PDStrip considers speed-independent transom corrections for the restoring coefficient C_{53} as shown in equation (3.23) and for the Froude-Krylov force as in (3.13), there is at $F_n = 0$ a small visible difference between its predictions both in Heave, Figure 3.4(a), and in Pitch, Figure 3.5(a). This seems to be adverse for pitching motion. With Maxsurf, this difference does not exist. In any case, at zero speed, Fonseca seems to make the most accurate predictions. PDStrip, without transom terms in particular, also performs reasonably well.

As the speed increases, it is visible that the inclusion of transom terms tends to damp the system. At higher speeds ($F_n = 0.6, 1.14$) this effect appears to be advantageous both for heave and pitch motions as Figures 3.7 and 3.8 indicate. Adding to this, at $F_n = 0.2$, heave predictions seem to have been adversely affected by the inclusion of transom terms in the equations. At $F_n = 0.4$, the opposite happened. At $F_n = 0.57$, the inclusion of transom terms improve the heave predictions of PDStrip but

that is not the case with Maxsurf Motions. Regarding pitch RAOs, at $F_n = 0.2, 0.4$, the prediction of Maxsurf Motions improve with the inclusion of transom terms while with PDStrip this decreases accuracy. Finally, at $F_n = 0.57$, the inclusion of transom terms generally makes pitch predictions worse. In Table 3.8, these conclusions have been summarised based on the results of Figures 3.7 and 3.8.

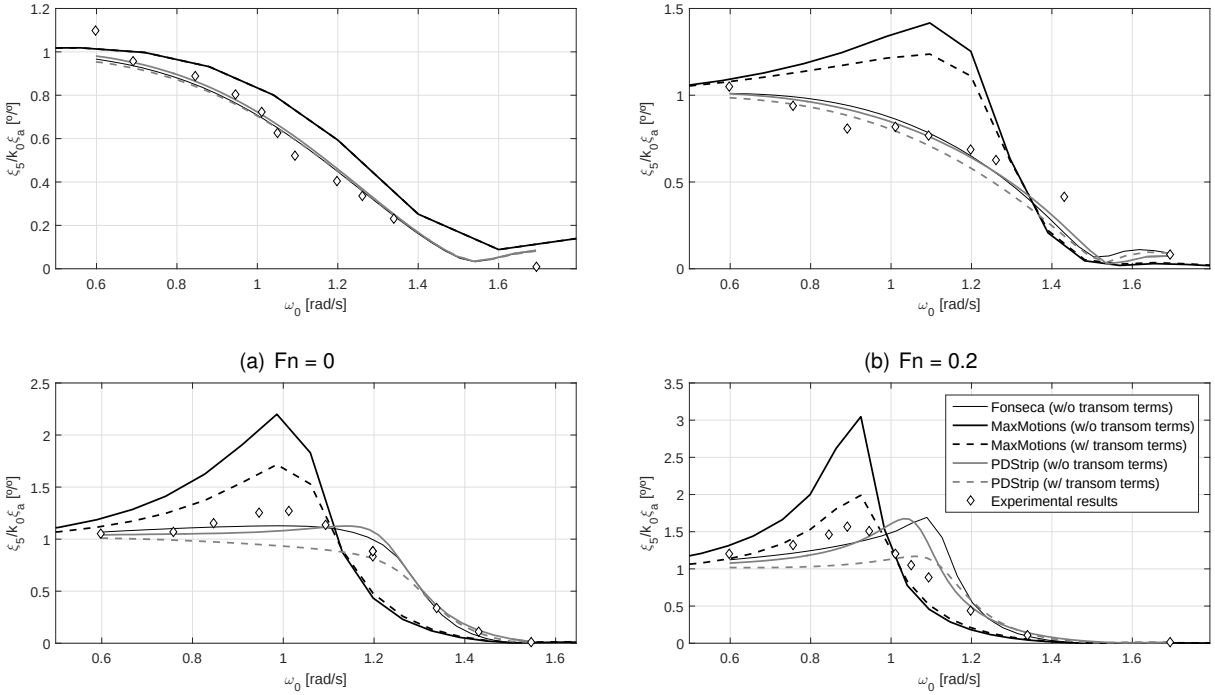

(a) Fn = 0 (b) Fn = 0.2

(c) Fn = 0.4 (d) Fn = 0.6

Figure 3.5: Pitch RAOs as function of the wave frequency, Catamaran

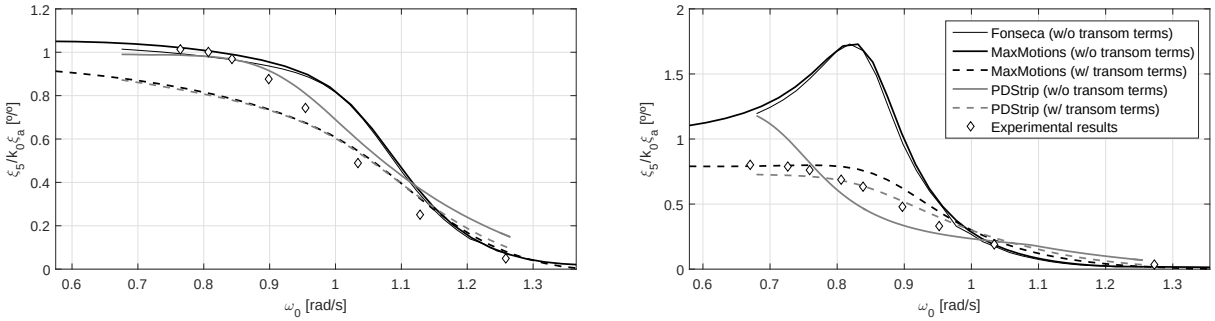

(a) Fn = 0.57 (b) Fn = 1.14

Figure 3.6: Pitch RAOs as function of the wave frequency, Model5

It seems clear that at higher Froude numbers, the inclusion of transom terms is beneficial. It is interesting to note that the non-linear version of Fonseca (Fonseca and Guedes Soares, 1998) has been mainly used to predict motions and wave loads of slower large displacement vessels (e.g., containerships) and, in fact, neglects transom terms. The conclusions of Marón et al. (2004) and Fonseca and Guedes Soares (2004c), where that code was applied to a fast mono-hull, showed precisely that at

Table 3.8: Improvement of the motion predictions with the inclusion of transom terms in the equations

F_n	Maxsurf Motions		PDStrip	
	Heave	Pitch	Heave	Pitch
0	-	-	slightly	no
0.2	no	yes	no	no
0.4	yes	yes	yes	no
0.57	no	no	yes	no
0.6	yes	yes	yes	yes
1.14	yes	yes	yes	yes

higher Froude numbers its accuracy decreases significantly. This seems to indicate that if the transom terms are neglected the range of applications should focus on slower vessels and Fonseca (linear version), which also excludes such terms, is more suited for lower Froude numbers.

For the case of the catamaran, when analysing resonance peaks, it is important to note that, as pointed out by Guedes Soares et al. (1999), it is possible that they might not have been accurately captured by the experiments because of the frequency separation between experimental points. In any case, it becomes quite obvious that for speeds greater than zero, the heave resonance peaks of the catamaran are poorly predicted by Maxsurf Motions, regardless of the inclusion of transom terms, as observed in Figure 3.4. In fact, the overall results for heaving motions are not promising. However, the pitch results seem better (Figure 3.5), particularly for very short and very long waves. Still, near the resonance peak, the motions are clearly overestimated, an effect that is attenuated with the inclusion of transom terms. Nevertheless, when compared with the remaining codes, Maxsurf Motions seems to be the one that better predicts the pitch resonance frequencies at $F_n = 0.4, 0.6$, particularly at 0.6 where, overall, with the inclusion of transom terms the best results are obtained. In the case of Model 5, predictions with Maxsurf Motions at $F_n = 0.57$ are reasonably accurate for very short and very long waves both for heave and pitch, although there is a clear loss in accuracy when predicting pith motions with transom terms. As Figure 3.3 shows, the heave resonance peak is underestimated, although better results are obtained without transom terms. For the pitch case, not using transom terms overestimates motions at the middle range frequencies. In any case, Maxsurf Motions predicts heaving motions at $F_n = 0.57$ with the highest accuracy, without transom terms in particular. At the highest Froude number, heaving motions are largely overestimated, while for the pitch case pretty good results are obtained with the inclusion of transom terms. Without them, a big discrepancy with the experimental results is observed.

Apart from the pitch motion at Froude number 0.6, both Fonseca and PDStrip predict the catamaran motions with greater success. Fonseca, in particular, computes heave and pitch motions quite well, as observed in Figure 3.7(a), including the frequency at which resonance occurs. Figures 3.4 and 3.5 show that at lower Froude numbers, the best results are obtained with Fonseca. This is particularly obvious for $F_n = 0.2$. Still, for $F_n = 0.4$ the heave resonance peak is underestimated and PDStrip with transom terms presents the best prediction. At $F_n = 0.6$ the resonance frequency is a bit overestimated both by Fonseca and PDStrip. With transom terms, PDStrip is able to predict the resonance peak as accurately as Fonseca. For pitching motions, at $F_n = 0.4$, both Fonseca and PDStrip fail to compute resonance peak and frequency, although Fonseca gives the overall best results due to the good agreement at the

low and high end frequency spectrum. At Froude number 0.6 the resonance pitch frequency as predicted by Fonseca and PDStrip appears to be too large, although the peak value seems to be correct (without transom terms in the case of PDStrip). In the case of Model 5, Fonseca consistently overstimates heave and pitch motions at both speeds. The same happends with PDStrip, although at $F_n = 1.14$ the use of transom terms improves a lot the results, particularly for pitch motion. At $F_n = 0.57$ not using transom terms works better, as PDStrip without them overestimates heave resonance peak and underestimates almost the entire frequency spectrum of pitch motions.

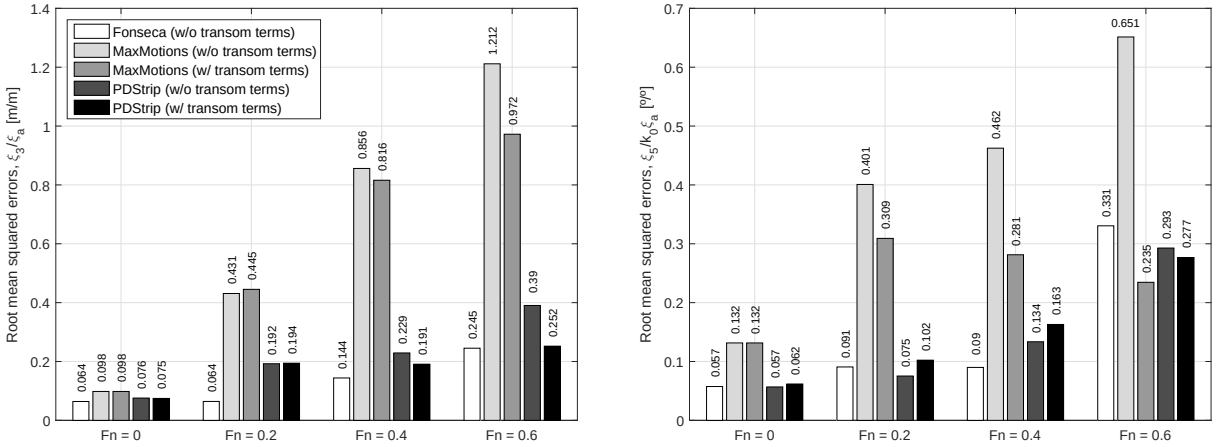

(a) Heave RAOs (b) Pitch RAOs

Figure 3.7: Root mean squared absolute differences between numerical and experimental results, Catamaran

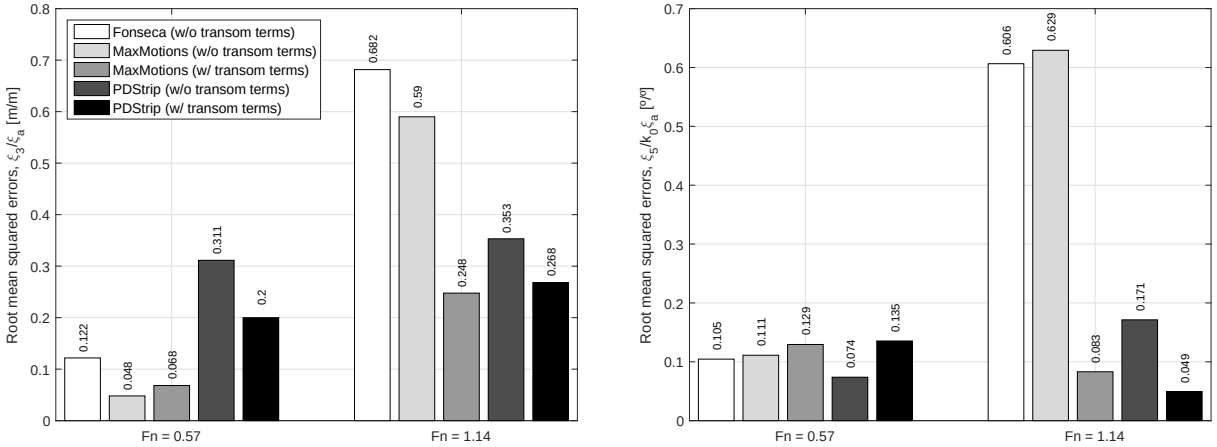

(a) Heave RAOs (b) Pitch RAOs

Figure 3.8: Root mean squared absolute differences between numerical and experimental results, Model5

Figures 3.7 and 3.8 summarise the absolute difference (in the same units as the RAOs) between the numerical results obtained with each code and the experimental data, averaged over all measured frequencies. In order to average these results, the square root of the average squared differences was

used. Since the errors are squared before they are averaged, a relatively higher weight is given to larger errors. This is beneficial for this study where big deviations from the experimental results are particularly undesirable. Adding to this, in Appendix A.1 for the catamaran and B.1 for Model 5 these errores can be found, discretized for each experimental frequency.

Finally, in Appendix A.2 the numerical results for the global coefficients of the coupled heave and pitch equations as function of the wave frequency can be found for the catamaran case. Similarly, Appendix B.2 presents the same results for Model 5. These results are compiled into groups of two tables (one for each equation of the motion equation (3.4)), each group corresponding to a different Froude number. This work, despite time-consuming, served the purpose of investigating in depth the real mathematical causes of the divergences between predictions of each code. However, given the scope of the work of the present dissertation and the limited time to accomplish it, this investigation was put on hold, standing now as suggestion for future work.

3.4 Summary

It has been shown that, as expected, the accuracy level in predicting heave and pitch motions with strip theories decreases with speed. At higher Froude numbers ($F_n = 0.6, 1.14$) this effect seems to be mitigated by including transom terms in the equations. In these cases PDStrip (with transom terms) performs quite well. For $F_n = 0, 0.2, 0.4, 0.57$, not using transom terms is a better option. In general, Fonseca seems to be the most suited choice for $F_n = 0, 0.2, 0.4$, while at Froude number 0.57 both Maxsurf Motions or PDStrip work well. Table 3.9 summarises these conclusions.

Table 3.9: Most appropriate code to predict heave and pitch motions at different Froude numbers

F_n	Heave	Pitch
0	Fonseca[1]	Fonseca
0.2	Fonseca	PDStrip (w/o transom terms)
0.4	Fonseca[2]	Fonseca[5]
0.57	MaxMotions (w/o transom terms)	PDStrip (w/o transom terms)
0.6	Fonseca[3]	MaxMotions (w/ transom terms)
1.14	MaxMotions (w/ transom terms)[4]	PDStrip (w/ transom terms)

[1] Differences between the codes are negligible
[2] Resonance peak more accurately predicted with PDStrip (w/ transom terms)
[3] Similar results with PDStrip (w/ transom terms). Resonance frequency overestimated with both methods.
[4] Similar results with PDStrip (w/ transom terms). Amplitudes at the middle frequency range poorly estimated with both methods.
[5] Resonance frequency more accurately predicted with MaxMotions

Unfortunately, no direct relation was found between the accuracy of computations and the vessel configuration. Still, given the order of magnitude of the differences between numerical and experimental results for the case of Model 5 when compared to the catamaran (see Figures 3.7 and 3.8), it seems that these strip theory codes perform better with mono-hulls, as expected. Although the contribution of the viscous damping is only recognized significant for the rolling motions of mono-hulls, there were attempts to improve agreement with experimental data for catamarans by introducing additional viscous forces also in heave and pitch motions ([82], [28], [27], [29] or [124]). Although this does not seem

very likely for normal displacement vessels, a direct comparison between possible viscous and potential contributions can be performed in the future. In any case, as seen in the previous figures, considering the known limitations of the presented methods, PDStrip with transom terms should perform reasonably well with heaving/pitching catamarans being capable of determining the resonance peak, both in terms of frequency and amplitude, with sufficient accuracy, particularly at higher speeds. This is an important aspect because the catamaran that will be optimized in the next chapter operates at $F_n \approx 0.77$. In addition, it is worth mentioning the following characteristics of the code (refer to Table 3.4 for more information):

1. Provides fast seakeeping calculations, an imperative feature considering that the code was to be embedded into an optimizer;
2. It is compiled into an executable file with separate input text files where the analysis parameters and geometry are set. Once gain, this was quite convenient since the code was to be included into an optimization procedure, where a minimum level of automation is required;
3. Allows a large number of ship sections and offset points for geometry discretization, which improves accuracy during seakeeping computations;
4. Allows a large number of wavelengths within a wide range to be used for motion results, which is advantageous for a proper definition of the complete frequency range;
5. It is an open source fortran code, which allows the code to be edited or improved if necessary, a convenient characteristic bearing future work in mind.

As a final note, it is important to point out some difficulties the author faced when working with the codes and to leave a few comments on the available documentation. Staring with Fonseca, a remark on the support documentation must be made. Several papers have been published that reference the use of a time domain strip-theory code developed at CENTEC to predict ship motions ([47], [48], [53]). However, the frequency-domain formulation of the code used here, does not appear to be mentioned anywhere. This presented a problem for the author since there was no way to be sure about the actual method that was being used. Adding to this, the documentation (unofficial) about the structure of input file [55] was a bit ambiguous regarding the adopted reference frame. Finally, it is worth mentioning the self explanatory nature of the output files.

Regarding PDStrip, its support documentation [119] is very detailed, including a thorough description of the input files. However, the output files were completely unintelligible, which ended up forcing the time-consuming task of looking into the source code in order to process the results. This aspect of PDStrip have already been mentioned by authors like Palladino et al. (2006) who faced the same type of problems. On top of that, the code had to be modified so that the needed results were displayed. In summary, working with PDStrip proved to be extremely laborious.

Finally, it is worth mentioning that Maxsurf Motions interface is in fact very user-friendly. However, the software was accessed via automation (resorting to VBA). This allowed to run multiple analyses with

different vessel speeds and considering different methods (e.g. with and without transom terms), without having the need to define new inputs after each run (it is important to remember that the analyses with Maxsurf Motions can become quite lengthy). One of the problems that came up had to do with the lack of an automation manual for this module of Maxsurf. It was verified that some of the units of the inputs used to set the seakeeping analysis within the automation environment differ from the ones displayed at the software interface, which caused a few initial mistakes. In terms of support documentation, the Motions Manual [7] is in reality quite complete. Still, it is important to note that some of the software results, weather in terms of RAOs or intermediate hydrodynamic coefficients, are not presented as stated in the manual, mostly because they are non-dimentionalized in a slightly different way. This has to do with the fact that some of the theoretical references are direct transcriptions of standard publications [109] and little care has been put into updating the formulations to what is actually being displayed.

Chapter 4

Seakeeping optimization of a fast crew supplier catamaran to operate at the Alentejo basin

Any optimization procedure in ship design starts by clearly defining the problem to address, i.e. what is the objective of the optimization? Which function or functions of merit should be selected? Which constraints to impose? How to generate hull variations and evaluate them? Also, how to select the best solution out of many feasible ones on the basis of a criterion, or rather, a set of criteria? This includes setting a mathematical model with certain objective functions in the presence of constraints imposed by the stake holders. Generally, by means of an initial inquiry, specific requirements are set, namely the type of vessel, type of cargo, required service speed, route, classification society or flag, upon which the design is optimized weather in terms of construction cost, carrying capacity, Required Freight Rate (RFR), safety, comfort, environmental impact, hull resistance, among many others.

Generally speaking, the hull must provide an adequate capacity to carry a given payload at a required speed in a defined sea state while fulfilling statuary requirements such as stability, structural strength or freeboard [81]. Adding to this, economic requirements usually limit the vessel proportions. However, it was decided that for the scope of this work, the main dimensions were going to be kept constant.

In the case of a high speed vessel, the requirement to operate well at high speeds, often in adverse weather conditions, is paramount. As it is defended by Salvesen et al. (1970), the performance of a vessel in a realistic seaway should be the ultimate criteria for the design of any hull. In fact, it is known that high accelerations can significantly decrease the operability level of such vessels. This is particularly critical if the mission includes transporting passengers which are susceptible to seasickness. The welfare onboard must then be maximized. In any case, the scope of the work of this dissertation neglects extreme effects such as slamming and green water, even though they might occur.

In terms of motions, the vessel was constrained to heave and pitch, which is consistent with the fact

that double-hulled vessels have higher transverse stability and thus, heave and pitch motions present a more critical situation. Also, it was assumed that it would only encounter head seas as a result of an assumption about negligible interaction between the hulls of the catamaran (acceptable for head and following seas). In fact, this effect becomes very significant for other wave headings, namely beam seas. However, since PDStrip, the code selected as seakeeping tool during the first part of this dissertation (Chapter 3), neglects that phenomenon, assessing the seakeeping performance of the catamaran upon a larger range of wave directions would compromise the results. In any case, it is important to keep in mind that, as a result of the random nature of the sea, the seakeeping optimization performed in this dissertation has its limitations.

Throughout this chapter, the optimization of catamaran operating as a fast crew supplier for an offshore platform at the Alentejo basin will be presented. First, the parent model used to generate new hull forms is described, followed by the characterization of the seastates that the vessel will have to face. Then, the optimization problem is presented with a discusion about the method used to generate hull variations and the selection of the objective functions and constraints. The main tool used to develop the optimizer was MATLAB together with PDStrip for seakeeping calculations, accessed via system command and the Maxsurf modules (via VBAs): Modeler, Resistance and Stability.

4.1 Parent model characteristics

At this early stage of the basic design, there is no sufficient data to proceed with any accurate computations. One must go one of two ways: either resort to estimate methods based on statistical regressions with data compiled from existing designs to generate a ship model or use a parent hull suited for the intended mission and optimize it according to specific figures of merit, while imposing constraints of any sort. For this dissertation, it was chosen to follow the later approach.

(a) 2610 Model

(b) Topaz Zenith Model

Figure 4.1: Typical designs of a fast crew supplier catamaran

In order to guarantee a certain degree of realism, the author contacted DAMEN SHIPYARDS, a Dutch company with a long history of ship design and ship building, who were kind enough to provide the Maxsurf model of a 30 m catamaran that is effectively used in the industry. However, the provided model

corresponded in fact to a passenger ferry (operating at a service speed of 25 knots achieving a maximum of 30 knots), which differed from the operational profile proposed for this dissertation. Despite this, because its main dimensions and speeds did not deviate too much from the ones of publicly available supply vessels, of which the 2610 and the Topaz Zenith of Figure 4.1 are examples, the author decided to use it as parent hull nonetheless (note that the vessel speeds were maintained). The main characteristics of the vessel are summarised in Table 4.1. Note that given the lack of information in terms of weight distribution, values for KG and *LCG* had to be assumed. Regarding the vertical centre of gravity, KG, it was fixed at 1.5 meters from the baseline. *LCG* was imposed at the same position as the longitudinal centre of buoyancy which, in principle, should not affect the seakeeping characteristics of the vessel significantly [81].

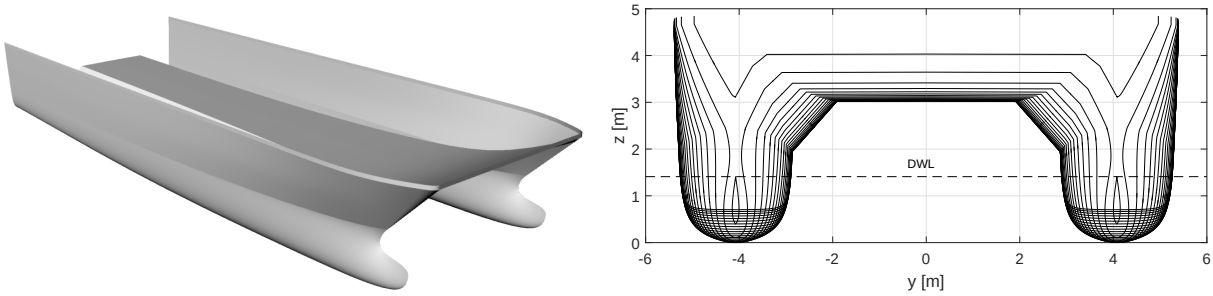

(a) Rendered model in Rhinoceros

(b) Hull body lines

Figure 4.2: Overview of the parent model by DAMEN

Table 4.1: Main characteristics of the parent model by DAMEN

V service [kn]	25 (F_n = 0.77)
V maximum [kn]	30
t voyage, 50 km [min]	65
LOA [m]	30
LPP [m]	28.389
LWL [m]	28.386
Horizontal clearance (S) [m]	8.152
S/LWL	0.2872
BOA [m]	10.772
LOA/BOA	2.785
BWL, demi-hull [m]	2.361
D [m]	4.675
T (DWL) [m]	1.41
Δ [t]	112.600
LCB = LCG [m]	-0.926
KG [m]	1.5
C_b [-]	0.581
C_p [-]	0.776

In order to assess the rules under which the vessel will have to abide, the High Speed Craft (HSC) code defines in *Chapter 1 General Comments and Requirements, 1.4 Definitions, 1.4.29* a high-speed craft as a "craft capable of maximum speed, in knots, equal or exceeding $7.192\nabla^{0.166}$". For the case of the DAMEN parent hull, this minimum speed gives 15.742 knots. Considering the maximum speed of 30 knots, it has been proven that it is indeed obliged to fulfil the requirements of the HSC code. At this point is important to asses the number of passengers to carry. A regression study was performed with this in-

tent, resorting to a database of fast crew supplier catamarans developed by the author. Figure 4.3 shows the number of passengers as function of LOA/BOA ratio. Note that only vessels up to approximately 30 metre in length were displayed.

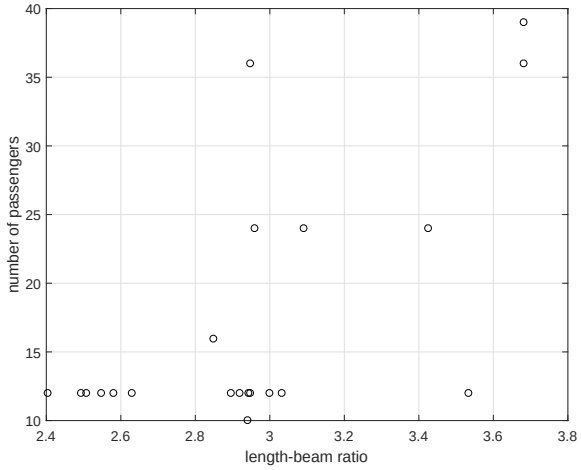

Figure 4.3: Number of passengers as function of LOA/BOA ratio

Despite some deviations, there is a clear trend to carry exactly 12 passengers. It is interesting to note that according to the HSC code, a vessel is only classed as a passenger craft, for which the rules impose tighter requirements, if it carries more than 12 passengers (HSC code [73], *Chapter 1 General Comments and Requirements, 1.4 Definitions, 1.4.47*). Therefore, it was decided to fix the number of passengers to 12, which classes the catamaran to optimize as a cargo craft (HSC code [73], *Chapter 1 General Comments and Requirements, 1.4 Definitions, 1.4.10*).

4.2 Description of the seastates at the Alentejo basin

As stated earlier, the vessel will operate at the Alentejo basin, transporting crew and cargo between shore and an oil platform located 50 km from Sines. Figure 4.5 shows a detailed view of the map of concessions in Portugal (Figure 1.1), highlighting the location of the hypothetical hydrocarbon field proposed by Carvalho (2016).

The discretization of the wave regime along the Portuguese coast has been done by Costa et al. (2001). The authors present the results of a long term program of data collecting, initiated in 1979 by Instituto Hidrográfico (IT) with the support of several Portuguese institutions. The wave measurements from Sines station were gathered between 1988 and 2000 and will be used here to characterize the environment where the catamaran will operate. However, it is important to note that in reality Sines station is located near the coast, where water depths do not exceed the 200 m line (refer to Figure 1.1). Therefore, its measurements do not translate the sea environment at the site of interest. Unfortunately, this was the information the author found available and thus, it was still used with the purpose of representing the sea spectrum at the Alentejo basin.

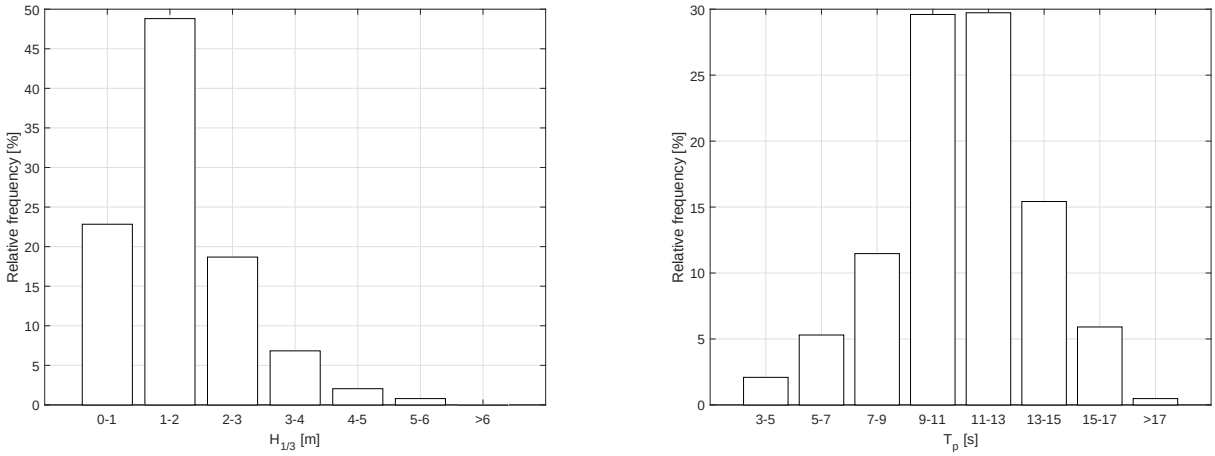

(a) Frequency of significant wave heights

(b) Frequency of peak periods

Figure 4.4: Ocean wave data for the Alentejo basin, measured at Sines station between 1988-2000 [35]

Table 4.2: Scatter diagram [%] for the Alentejo basin, measured at Sines station between 1988-2000 [35]

$H_{1/3}$	T_p [s]								
[m]	3-5	5-7	7-9	9-11	11-13	13-15	15-17	>17	
0-1	0.480	1.210	2.620	6.760	6.790	3.520	1.350	0.110	*22.840*
1-2	1.020	2.590	5.600	14.450	14.510	7.530	2.880	0.230	*48.810*
2-3	0.390	0.990	2.140	5.530	5.550	2.880	1.100	0.090	*18.670*
3-4	0.140	0.360	0.780	2.020	2.030	1.050	0.400	0.030	*6.810*
4-5	0.040	0.110	0.240	0.610	0.610	0.320	0.120	0.010	*2.060*
5-6	0.020	0.040	0.090	0.240	0.240	0.120	0.050	0.000	*0.800*
	2.090	*5.300*	*11.470*	*29.610*	*29.730*	*15.420*	*5.900*	*0.470*	*100%*

In order to describe an idealized wave frequency spectrum $S_\zeta(\omega_0)$, researchers have proposed several formulations that dependent on different parameters using data collected by observation stations and satellite data in various regions - parametric wave spectra. The JONSWAP spectrum, developed by the Joint North Sea Wave Project, has been used extensively in the offshore industry and thus, it was applied for the present work. The formulation presented here [46], depends on the significant wave height, $H_{1/3}$, and peak period, T_p, data that has been previously shown.

$$S_\zeta(\omega_0) = \frac{\alpha}{\omega_0^5} e^{-1.25\left(\frac{\omega_p}{\omega_0}\right)^4} \gamma^{e^{-\frac{1}{2\sigma^2}\left(\frac{\omega_0}{\omega_p}-1\right)^2}} \tag{4.1}$$

where,

$$\omega_p = \frac{2\pi}{T_p} \tag{4.2}$$

$$\alpha = 5\pi^4 (1 - 0.287 \log\gamma) \frac{H_{1/3}^2}{T_p^4} \tag{4.3}$$

$$\gamma\,(\text{peak enhancement factor}) = \begin{cases} 5, & \text{if} \quad T_p \leq 3.6\sqrt{H_{1/3}} \\ e^{5.75-1.15\left(\frac{T_p}{\sqrt{H_{1/3}}}\right)}, & \text{if} \quad 3.6\sqrt{H_{1/3}} < T_p \leq 5\sqrt{H_{1/3}} \\ 1, & \text{if} \quad T_p > 5\sqrt{H_{1/3}} \end{cases} \tag{4.4}$$

$$\sigma\,(\text{step function}) = \begin{cases} 0.07, & \text{if} \quad \omega_0 \leq \omega_p \\ 0.09, & \text{if} \quad \omega_0 > \omega_p \end{cases} \tag{4.5}$$

As an example of the resultant wave spectra, Figure 4.6 plots $S_\zeta\,(\omega_0)$ for all possible peak periods considering the most probable significant wave height range according to the scatter diagram of Table 4.2. Note that the calculations were made using the mean value of each class of $H_{1/3}$ and T_p, even though the results display the class intervals. Figure 4.6 indicates that the variance spectrum tend to increase with wave (peak) period, as expected. However, it seems that for the range of $T_p = 3 - 5$ seconds the results go against this trend, presenting higher variances than expected. This has to do with the influence of the peak enhancement factor on the wave spectrum and, in particular, the JONSWAP formulation followed here. As it can be seen from equation (4.4), for lower periods, the use of $\gamma = 5$ increases the results quite significantly.

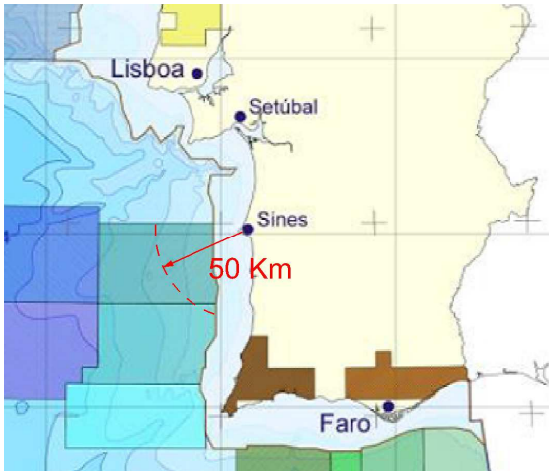

Figure 4.5: Location of the hydrocarbon field proposed by Carvalho, 2016 (source: [43], adapted)

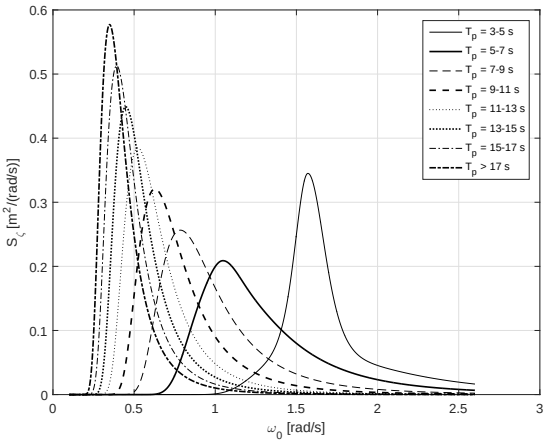

Figure 4.6: Wave spectra at the Alentejo basin as function of the wave frequency for $H_{1/3} = 1 - 2$ m

4.3 Overview of the optimization problem

At this point, the problem to address seems to be fully described: seakeeping optimization of a 30 m catamaran to operate as a fast crew supplier of an offshore platform at the Alentejo basin. Also, it was considered that the vessel was operating at service speed. However, which method will be used to obtain different hull forms? Also, when referring to seakeeping, there are several aspects that are worthy considering. What should be the objective function? Minimizing peak RAOs? Absolute vertical displacements? Accelerations? Or is it more logical to assess the seaworthiness of the vessel considering the

seaway in which it will operate and the resulting responses? In addition, which constraints should be applied? Such questions will be discussed during this chapter.

4.3.1 Generation of hull variations

In order to generate new hull forms from the parent model, the linear distortion method of Lackenby (parametric transformation) was used by varying the block coefficient (C_b) and the longitudinal centre of buoyancy (LCB) systematically via Maxsurf Modeler [9]. These variables were selected simply because they serve quite effectively the purpose of quickly generating a large number of hull variations. Also, the work of Kukner and Sarioz (1995), Rollings (2003), Grigoropoulos (2004), Cepowski (2010), Scamardella and Piscopo (2014), Piscopo and Scamardella (2015), among others, has shown that the seakeeping performance is clearly affected by changing such parameters.

The range of C_b and *LCB* values to study was set to +-10% of the original values, i.e. the ones of the parent hull. Figure 4.7 shows all the combinations used to generate new hull forms. The number of hulls to generate was set so that 15 different values of C_b and *LCB* were being used, which gives 225 different models including the parent one. Note that the Lackenby method maintains the main dimensions of the underwater hull geometry, i.e., displacement (Δ), waterline length (*LWL*) and maximum beam at the waterline (*BWL*), while the shape coefficients C_p, C_{wp} and C_m are free to vary together with the design waterline (*DWL*) that adjusts itself with respect to the displacement. This means that both the length overall (*LOA*) and beam overall (*BOA*) might suffer some changes. Another important aspect to point out is the fact that some (*LCB*, C_b) combinations might generate hull geometries that are not valid, which will be assessed further ahead. Finally, regarding the horizontal clearance S, although it has been considered in this optimization procedure, the author didn't find a feasible way to directly include it in the generation of new hull forms.

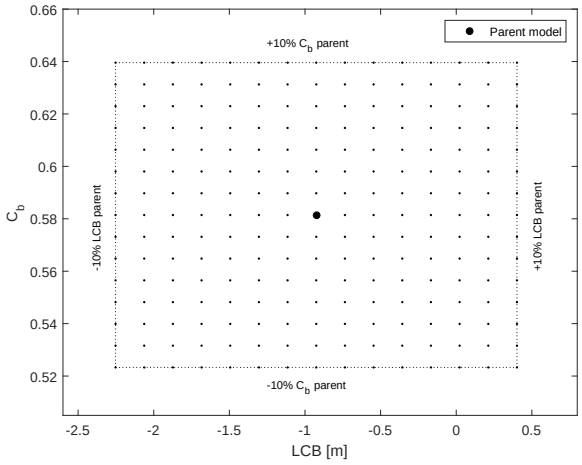

Figure 4.7: Combinations of parameters used to generate hull variations and the +-10% boundaries

4.3.2 Selection of the objective functions

4.3.2.1 RMS vertical acceleration responses

As stated earlier, assessing the performance of a high-speed craft in a realistic seaway is paramount. From this perspective, high accelerations are critical, known to significantly affect the operability level of such vessels. To express the ship-fixed coordinates of the remote locations, a new reference frame (x, y, z) is here defined as the inertial reference frame (ξ, η, ζ) shifted along ξ to the aft perpendicular of the vessel. Note that PDStrip, the tool used here for the seakeeping computations, positions (longitudinally) the inertial reference frame at the midship section and not at the centre of gravity (refer to Chapter 3.1 Background Theory). Following this notation, the absolute vertical displacement ξ_z at a remote location on the vessel (x, y, z) is given by equation (4.6), assuming the motions are small. It is important to note that rolling motions are being neglecting, i.e., heave and pitch motions do not vary with y.

$$\xi_z(x, \omega) = \Re\{\left[\xi_3^A(\omega) - x\xi_5^A(\omega)\right] e^{i\omega t}\} \tag{4.6}$$

, where ξ_j^A with $j = 3, 5$ is the complex amplitude of the harmonic heaving and pitch motions, respectively. Let now $\omega = \omega_e$, in order to account to the relative speed between the ship (U) and the encountering head waves ($\beta = 180°$). A sea spectrum $S_\zeta(\omega_e)$ is computed as follows:

$$S_\zeta(\omega_e) = \frac{S_\zeta(\omega_0)}{1 - \frac{2\omega_0 U}{g}} \tag{4.7}$$

Once $\xi_z(x, \omega_e)$ have been computed by PDStrip, ship vertical responses S_z upon a given sea spectrum $S_\zeta(\omega_e)$ can be calculated according to equation (4.8). This is a true assumption if the ship responses are linear and both the responses and the wave spectra are Gaussian processes.

$$S_z(x, \omega_e) = |\xi_z(x, \omega_e)|^2 S_\zeta(\omega_e) \tag{4.8}$$

At this point is it useful to point out a few statistical properties of the ship responses. In particular, defining the spectral moments associated with the vertical responses m_{0z}, m_{2z} and m_{4z}.

$$m_{0z} = \int_{\omega_e} S_z(x, \omega_e)\, d\omega_e \tag{4.9}$$

$$m_{2z} = \int_{\omega_e} \omega_e^2 S_z(x, \omega_e)\, d\omega_e \tag{4.10}$$

$$m_{4z} = \int_{\omega_e} \omega_e^4 S_z(x, \omega_e)\, d\omega_e \tag{4.11}$$

Finally, in order to obtain frequency independent responses, it is possible to resort to these spectral moments to define Root Mean Squared (RMS) displacements, RMS_z, velocities, RMS_{v_z}, and accelerations, RMS_{a_z}. RMS values are considered good statistical measures since they provide useful and immediate (although inevitably less detailed) information, without the need to consider the whole range of frequencies.

$$RMS_z = \sqrt{m_{0z}} \tag{4.12}$$

$$RMS_{v_z} = \sqrt{m_{2z}} \tag{4.13}$$

$$RMS_{a_z} = \sqrt{m_{4z}} \tag{4.14}$$

This leads us to the main objective function selected for this optimization problem, the minimization of maximum RMS_{a_z} value on deck, given the most probable seastate the vessel would have to face sailing at service speed. Logically, this should correspond to a location at the forward extremity of the vessel, i.e., $x = LOA$, where accelerations are known to be more severe (this can be proved simply by looking into the equation (4.6)). However, given that the length overall of the generated models might not be exactly the same (see Chapter 4.3.1), the author was forced to fix a remote location near the bow to measure RMS accelerations. The selected point was set at $x = 28.5$ m, approximately at the same vertical of the length of waterline, which should be the same for all models.

4.3.2.2 Motion Sickness Incidence (MSI)

In addition to RMS vertical acceleration responses, since the mission of the catamaran includes transporting crew between shore and an offshore location, the welfare onboard had to be considered as well. To asses motion sickness, the Motion Sickness Incidence (MSI) index was computed. The MSI index derives from the mathematical model proposed by O'Hanlon and McCauley (1973) to assess the percentage of passengers who vomit after 2 hours of exposure to a certain motion. The experiments were carried out on over 500 seated subjects with their heads against a backrest and eyes opened inside a closed cabin oscillating vertically. McCauley et al. (1976) re-analysed the original work and proposed a time dependent model . This approach was more suited for this work since the actual voyage duration of the catamaran is known (see Figure 4.8). Here, the formulation described in Colwell (1989) is presented and deppends on the average RMS vertical acceleration $|RMS_{a_z}|$ and the average peak frequency (between maxima or minima) of the vertical motions of the ship $|f_e|$.

$$MSI\% = 100\Phi\left(z_a\right)\Phi\left(z_t\right) \tag{4.15}$$

, where $\Phi\left(z\right)$ is the standard normal distribution function.

$$\Phi\left(z\right) = \frac{1}{\sqrt{2\pi}} e^{-\frac{z^2}{2}} \tag{4.16}$$

$$z_a = 2.128 \log_{10}\left(\frac{|RMS_{a_z}|}{g}\right) - 9.277 \log_{10}|f_e| - 5.809\left(\log_{10}|f_e|\right)^2 - 1.851 \tag{4.17}$$

$$z_t = 1.134 z_a + 1.989 \log_{10} t - 2.904 \tag{4.18}$$

$$|RMS_{a_z}| = 0.798 RMS_{a_z} \tag{4.19}$$

$$|f_e| = \frac{1}{2\pi}\frac{RMS_{a_z}}{RMS_{v_z}} \tag{4.20}$$

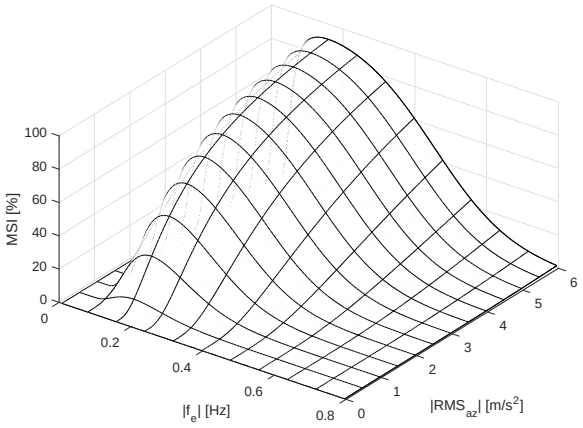

Figure 4.8: MSI model as proposed by [87], considering $t = 65$ min

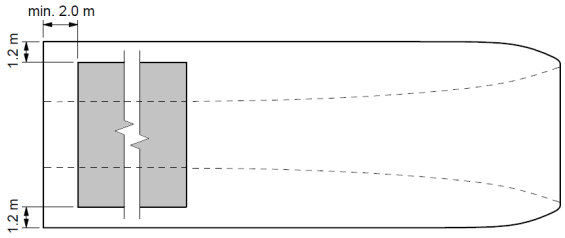

Figure 4.9: Position on deck of the passenger area (in grey) with respect to the ship sides and the aft perpendicular

The MSI was then computed at multiple locations at the area reserved to carry the passengers/crew. Note that the term passenger area used here does not correspond to the whole superstructure. Given the small number of passengers that the vessel will carry and the duration of the voyage, there is no need to have accommodations onboard and thus, in this area we can only find an area for seats, a bathroom and eventually a small galley. As an attempt to include a preliminary study of the general arrangement into the optimization process, the passenger area was positioned on deck so that the average MSI was minimum. For this purpose, it was decided to fix its position with respect to the ship sides (1.20 m) and assume a minimum distance of 2 m to the aft edge of the vessel as illustrated in Figure 4.9. Adding to this, it was necessary to estimate the minimum area needed, as function of the number of passengers, Figure 4.10. Once again, a database of similar vessels was used to perform this study.

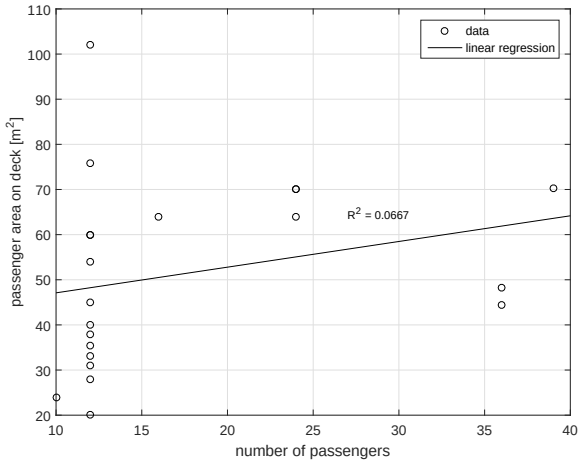

Figure 4.10: Area designated for passengers as function of the number of passengers

Given the high dispersion of the presented data, the regression shows a quite small coefficient of deter-

mination, $R^2 = 0.0667$. For the same number of passengers it seems that there are a large number of ways to layout the general arrangement of the vessel, some solutions giving more space to passengers than others. Other reason could have to do with different voyage times, the larger ones demanding the existence of an additional division for accommodations or even larger galleys for extra comfort. In any case, the area of $48.240\ m^2$ obtained with the regression line for 12 passengers seemed reasonable.

Coming back to Figure 4.9, it becomes now clear that for a constant passenger area with fixed width, the length will change for different horizontal clearances S. Bearing this in mind, for a given S, the passenger area is positioned on deck in order to minimize the average motion sickness. This was the solution the author found in order to consider the double-hulled configuration of the vessel in the seakeeping calculations, which leads us to the second criteria to select the optimum hull: the one with minimum average MSI at the passenger area, once again, considering the most probable seastate the vessel will have to face sailing at service speed. In principle this objective should not be incompatible with the minimization of RMS_{a_z} at $x = 28.5$ m. For this purpose the following range of horizontal clearance ratios was studied: $S/\text{LWL} = 0.2 - 0.4$.

4.3.3 Constraints

Once the objective functions have been established, the constraints of the optimization must be set. The first has to do with total hull resistance and the second with stability requirements imposed by the HSC code.

4.3.3.1 Total ship resistance criteria

The first selected criteria postulates that a feasible solution, or hull in this case, cannot require more engine power than the parent vessel at the same speed (in service condition). In order words, the upper bound in terms of total hull resistance is imposed by the DAMEN catamaran. As it will become clearer further ahead, for this criteria, when referring to the resistance of the parent model, it is implied the use of the original horizontal clearance.

The resistance of catamarans has always been a hot topic of research but the accuracy in predicting it continues to be one of the major design challenges in naval architecture. In fact, despite the amount of research in the area, there still is a high degree of uncertainty when predicting the calm water resistance of catamarans, especially at high Froude numbers, due to the inadequacy of the experimental data obtained so far [106]. Similarly to the case of the mono-hull, there are two components that contribute for the total resistance of a catamaran, namely, viscous resistance and wave-making resistance. Sahoo et al. (2007) states that the wave resistance of catamarans continues to be the one that stimulates more research, since viscous resistance has been computed resorting to the ITTC-1957 line (friction component) plus a form factor, methodology that has been generally accepted. In fact, the same author defends that form factor seems to be the least researched aspect. Another important investigation area of the resistance of catamarans relates to the so called interference component. Due to the presence

of a second hull, each resistance component must be multiplied by an interference factor that may either come from a viscous or wave origin [75]. The viscous interference is caused by the asymmetric flow around the demi-hulls and affects both the boundary layer formation and the longitudinal vortices development. The wave interference is associated with an interaction of the wave systems. This whole interference phenomenon is particularly affected by the lack of experimental validity. It wasn't until Insel and Molland (1992) that the first article applicable to high-speed catamarans was published, meaning Froude numbers greater than 0.5. The authors investigated into the calm water resistance of high-speed displacement and semi-displacement catamarans with symmetrical hulls and proposed an equation for the total resistance that accounted for both the viscous and wave interference effects. Research on this topic has been continuously carried out around the world ([106], [105], [77]).

The method used here to compute the resistance of catamarans follows the description of Jamaluddin et al. (2013). The authors further developed the pioneering work of Insel and Molland (1992) and generated an empirical formulae to calculate the interference of the ship resistance components dependent on the horizontal clearance ratio S/LWL - equations (4.23) and (4.24). S refers here to the distance between the centrelines of the demi-hulls. The total resistance of a catamaran begins by calculating the total resistance coefficient, C_T, of the demi-hull along with the interference coefficients.

$$C_T = (1 + \beta k)\, C_f + \tau C_w \tag{4.21}$$

, where $(1 + \beta k)\, C_f$ translates the viscous resistance component and C_w the wave-making resistance, which will be calculated with slender-body theory by the resistance package of Maxsurf [8]. β and τ represent the respective interference factors. $(1 + \beta k)$ is known as viscous form factor and C_f is the coefficient of friction resistance, obtained by the well known skin friction formula ITTC-1957 as function of Reynolds number Re.

$$C_f = \frac{0.075}{\left(\log_{10} Re - 2\right)^2} \tag{4.22}$$

$$(1 + \beta k) = 3.03 \left(LWL/\nabla^{1/3}\right)^{-0.40} + 0.016\, (S/LWL)^{-0.65} \tag{4.23}$$

$$\begin{aligned}
\tau &= 0.068\, (S/LWL)^{-1.38}, \quad \text{at} \quad F_n = 0.19 \\
\tau &= 0.359\, (S/LWL)^{-0.87}, \quad \text{at} \quad F_n = 0.28 \\
\tau &= 0.574\, (S/LWL)^{-0.33}, \quad \text{at} \quad F_n = 0.37 \\
\tau &= 0.790\, (S/LWL)^{-0.14}, \quad \text{at} \quad F_n = 0.47 \\
\tau &= 0.504\, (S/LWL)^{-0.31}, \quad \text{at} \quad F_n = 0.56 \\
\tau &= 0.501\, (S/LWL)^{-0.18}, \quad \text{at} \quad F_n = 0.65
\end{aligned} \tag{4.24}$$

Finally the total resistance force of the catamaran is calculated with equation (4.25), considering the total (doubled) wetted surface area, *WSA*.

$$R_T = \frac{1}{2}\rho \times V^2 \times WSA \times C_T \tag{4.25}$$

, where ρ is the fluid density and V the ship speed. As stated before, it was considered the range

$S/\text{LWL} = 0.2 - 0.4$.

4.3.3.2 Intact stability criteria

At this early stage of the preliminary design, there is no information about hull compartments and tanks. Therefore, for the scope of the work of this dissertation, only intact stability has been considered. Also, it is assumed that the catamaran is operating in displacement mode. The HSC code [73], defines in *Chapter 1 General Comments and Requirements, 1.4 Definitions, 1.4.22* displacement mode as "the regime, whether at rest or in motion, where the weight of the craft is fully or predominantly supported by hydrostatic forces". Within this assumption and considering the vessel a cargo craft, the intact stability requirements are set in HSC code [73], *Chapter 2 Buoyancy, Stability and Subdivision, 2.3 Intact Stability in the Displacement Mode*.

Adding to this, information about the geometry of superstructure, which would impose requirements in terms of heeling due to wind, and the conditions of high-speed turning is also limited. Therefore, the criteria applied here only concerns stability curves in terms of righting lever GZ. According to HSC code [73], *Annex 7 Stability of Multi-hull Craft, 1 Stability Criteria in the Intact Condition, 1.1 Area under GZ curve*, the area A_1 under GZ curve up to an angle q shall be at least:

$$A_1 = 0.055 \times 30^\circ/\theta \quad (m.rad) \tag{4.26}$$

, where θ is the smaller of the following angles: the downflooding angle; the angle at which the maximum GZ occurs or 30°. Furthermore, in *Annex 7 Stability of Multi-hull Craft, 1 Stability Criteria in the Intact Condition, 1.2 Maximum GZ* it is stated that the maximum GZ value shall occur at an angle of at least 10°.

Note that, for the reasons stated before, the downflooding angle in criteria 1.1 has been neglected. Also, it is important to mention a few aspects regarding the stability analysis of the generated hull variations. This analysis was carried out with Maxsurf Stability [10]. Note that, for the same model, the GZ curve will change with horizontal clearance S. However, contrary to the assessment of motion sickness and resistance, where the effect of changing S was evaluated during the post processing of the results from the respective software, for stability, the horizontal clearance must be set in the model itself prior to the analysis with Maxsurf. This means that all the generated hull variations would have to be modelled individually with different S values, which is obviously not feasible. For this reason only $S/\text{LWL} = 0.2872$ was considered in stability calculations. The consequences of selecting a optimum hull with a different horizontal clearance will be evaluated further ahead.

4.4 Synthesis model

All in all, the main problem addressed in this dissertation can be summarized as follows:

Optimization of fast crew supplier catamaran sailing at 25 kn to operate at an offshore platform at 50

km off the coast of Sines at the Alentejo basin by minimizing the RMS vertical acceleration response at the bow and the average motion sickness incidence at the passenger area, considering resistance and stability criteria.

Figure 4.11 represents the MATLAB procedure that automatically generates hull variations and evaluates them in terms of seakeeping, resistance and stability, including the numerical tools used for that purpose.

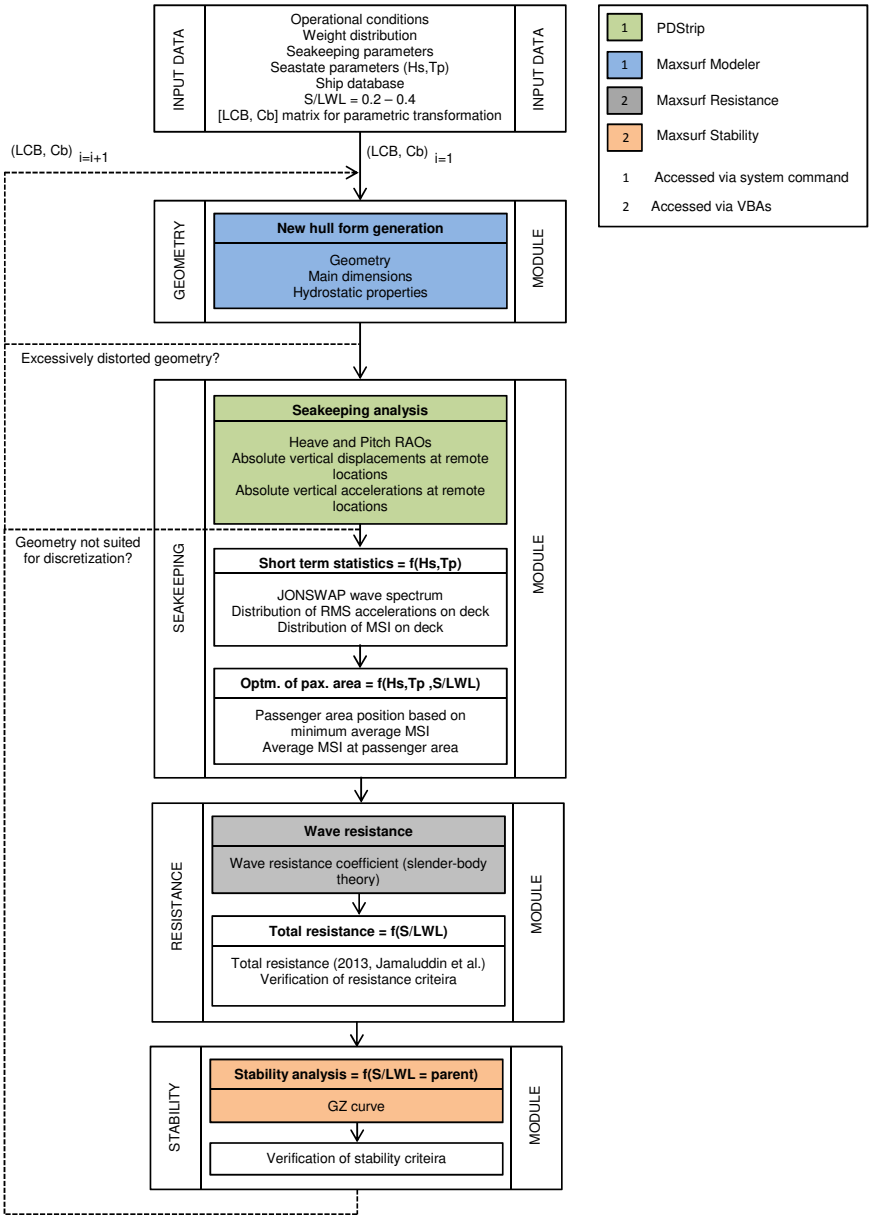

Figure 4.11: Flowchart of the MATLAB procedure that generates hull variations from the parent model and evaluates them in terms of seakeeping, resistance and stability

4.5 Optimization results

4.5.1 Limits of parametric transformation of the hull geometry

The parametric transformation of Lackenby basically involves shifting the hull ordinates fore and aft until the required parameter specifications, *LCB* and C_b in this case, are met without changing the section shapes (unless scaling them) and the main dimensions of the vessel. The main advantage of this method is that it keeps the fairness of the hull during the process, which in reality limits the degree of geometric variation. In practice, what Maxsurf Modeler, used here to perform this task, does is that it attempts to find a faired geometrical solution that satisfies the required *LCB* and C_b. If there is none, the software automatically searches for the nearest (*LCB*, C_b) pair and repeats the process. Nevertheless, this does not mean that all found solutions are suitable for numerical analysis. Bearing this in mind, Figure 4.12(a) displays all the numerically valid models that were obtained. Figures 4.12(b) and 4.12(c) show the resulting shape parameters, namely C_p and C_{wp} which, as previously said, where allowed to change during the parametric transformation. By definition, it can be observed a clear linear relationship between block and prismatic coefficients, where the slope of the curve is in fact the midship coefficient $C_m = C_b/C_p$.

As stated before, although 224 combinations of (*LCB*, C_b) have been used to generate hull variations from the parent model, not all resulting geometries were valid. The comparison of Figures 4.12(a) with 4.7 shows that around 15% of the models have been neglected. In fact, only 190 geometries were suited for numerical analysis, discounting the parent hull. The first criteria to evaluate this suitability checks if the geometry is excessively distorted. This verification is carried out in MATLAB when importing the geometry from Maxsurf Modeler. The second criteria is related with the capacity of PDStrip to discretize the resulting ship sections.

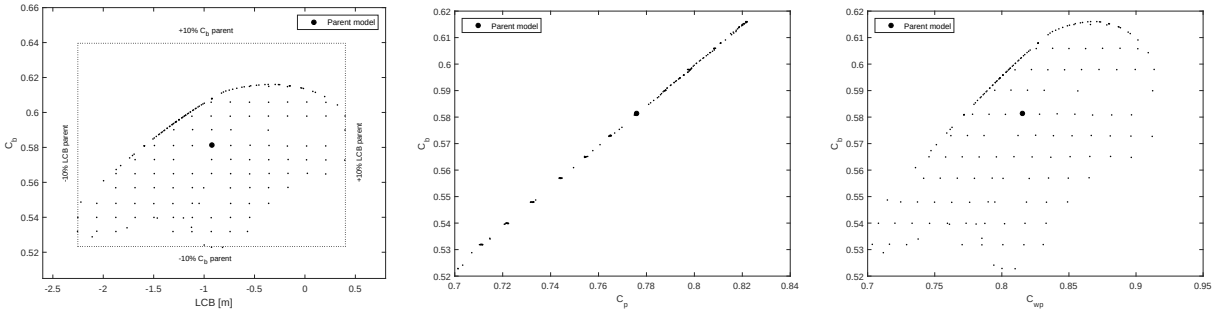

(a) (*LCB*, C_b) combinations that generated numerically valid models, including the original +-10% boundaries

(b) Resulting prismatic coefficients

(c) Resulting waterplane coefficient

Figure 4.12: Overview of the numerically valid models generated from (*LCB*, C_b) combinations

Another important aspect to point out relates with ship models that, although being suited for numerical analysis, have been generated with a (*LCB*, C_b) pair seemingly shifted with respect to the original 15x15 matrix of Figure 4.7. The reason for this was discussed in the first paragraph of this chapter and has to do

with the iterative nature of the method that searches for the nearest set of parameters with which a faired hull is obtained. In fact, it is possible to observe the formation of a well defined boundary resembling a parabola concave downwards in Figure 4.12(a). The region bellow it, bounded by the +-10% *LCB* boundaries, identifies quite clearly the limits of variation of block coefficient and longitudinal centre of buoyancy, outside of which there are no feasible hull solutions. This indicates that the +10% boundaries were overestimated. In fact, in terms of block coefficient, to perform variations over +6% is not possible. Obviously, these conclusions are particular to the parent model that is being used.

4.5.2 Seakeeping results

To present the seakeeping results the author resorted to colour plots. The idea was to facilitate the visualisation of the gradient of the acceleration and motion sickness incidence as functions of *LCB* (measured with respect to *LPP*/2) and C_b, each pair representing a different model. By doing so one can directly visualise the effect such parameters have on those functions and effectively determine the hull for which they are minimum. Also, the matrix type distribution of *LCB* and C_b is quite convenient since it allows to study seakeeping trends of the variation of only one parameter (neglecting the very small variations pointed out before). As pointed out earlier, the operating conditions considered here refer to the most probable sea state and a service speed of 25 knots.

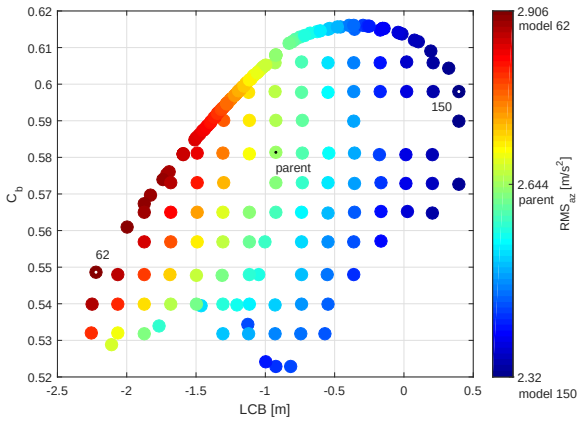

Figure 4.13: RMS vertical acceleration response at $x = 28.5$ m ($\approx$ *LWL*) considering the most probable seastate at V_s = 25 knots ($H_{1/3}$ = 1-2 m, T_p = 11-13 s, prob = 14.51%) as function of (*LCB*, C_b)

The analysis of the previous figure indicates that for the same block coefficient, an increase of the longitudinal centre of buoyance to an aft position will improve vertical plane seakeeping performance, evaluated here in RMS accelerations. Regarding C_b, it seems that models with smaller values experience lower accelerations. However, the influence of block coefficient appears to be less significant, particularly for higher values of *LCB*. In any case, given that the remaining shape parameters vary (recall Figure 4.12), it is not possible to be certain regarding the influence of block coefficient. This conclusions are in agreement with the work of several authors ([81], [60], [113] and [100]). Adding to this, model 150 seems to have the best seakeeping qualities, showing significant improvements when compared to the parent

model (around 12.3% less RMS vertical acceleration responses).

Next, the motion sickness results will be presented for two different horizontal clearances (refer to Chapter 4.3.2.2 for the assumed considerations). It is important to stress the fact that for this optimization procedure, the most probable seastate was considered. This is particularly important for motion sickness because the positioning of the passenger area, where it is being measured, will mathematically change depending on the seastate. However, for obvious reasons, it had to be fixed. In the next chapter, when presenting the final results for the optimum hull, the effects of the seastates on the position optimization of the passenger area will be discussed.

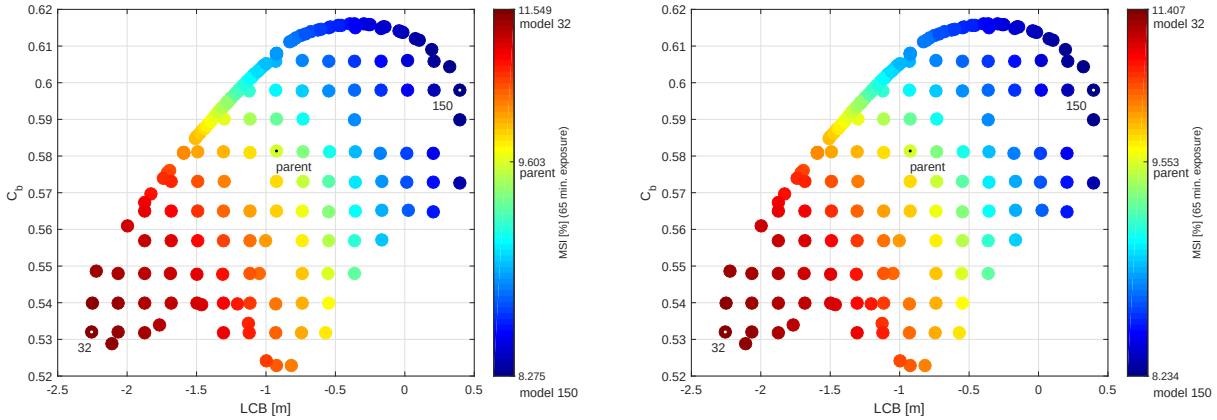

(a) $S/LWL = 0.2872$ (parent horizontal clearance) (b) $S/LWL = 0.4$

Figure 4.14: Average MSI at passenger area considering the most probable seastate at V_s = 25 knots ($H_{1/3}$ = 1-2 m, T_p = 11-13 s, prob = 14.51%) as function of (*LCB*, C_b)

Improvements in terms of motion sickness have been achieved by shifting the longitudinal centre of buoyancy forward (for constant C_b values). Since there is a direct dependency on RMS accelerations, which benefit significantly by increasing *LCB*, this was an expected result. In fact, a quick analysis of the MSI model of Figure 4.8 shows that, for a given frequency, MSI increases asymptotically with RMS_{a_z}. On the other hand, the effect of decreasing C_b was quite surprising. It has been shown that reducing the block coefficient lowers RMS accelerations, although not as effectively as moving *LCB* forward. In any case, the same effect would be expected on motion sickness. However, Figure 4.14 indicates that decreasing the block coefficient actually contributes for higher incidences. Again, as *LCB* increases this effect is less significant but it is noticeable nonetheless. The reason for this has to do with the average peak frequencies of ship motions $|f_e| = RMS_{a_z}/RMS_{v_z}/2\pi$. In fact, frequency plays a very interesting role in the MSI model. Figure 4.8 indicates that for a given value of acceleration, the incidence of motion sickness increases up to frequencies of about 0.16 Hz. In fact, even moderate accelerations should be avoided near that frequency region, as they produce the highest MSI values. Beyond 0.16 Hz motion sickness starts to decrease, until it reaches zero incidence. As pointed out by O'Hanlon and McCauley (1973), humans can apparently tolerate higher accelerations at higher frequencies without experiencing the same tendency towards motion sickness. Note that this frequency region of 0.16 Hz is characteristic

of this particular model that considers 65 minutes of exposure. Coming back to the MSI results, it was found that all generated hull forms experience average peak frequencies between $0.35 - 0.37$ Hz, a range that is indeed captured by the descending part of the MSI model, beyond 0.16 Hz. Again, within this region, for the same acceleration levels, decreasing $|f_e|$ enhances MSI. Adding to this, given the relation between RMS accelerations and average peak frequencies, lowering RMS_{a_z} decreases $|f_e|$ as well (within $0.35 - 0.37$ Hz). Thus, for constant *LCB* values, since lowering C_b is not a very effective way of improving seakeeping performance, i.e., RMS_{a_z} decreases slightly, the resulting reduction of $|f_e|$ leads to a higher incidence of motion sickness in that specific region of the model.

In any case, model 150 proves once more to be the most suited in terms of seakeeping, regardless of the horizontal clearance, which leads us to another discussion. It is clear that as the horizontal clearance increases, the width of the passenger area increases as well due to the constraints imposed in Chapter 4.3.2.2. Thus, for the same area, the length of the passenger area becomes smaller. Since it has been considered that heave and pitch motions do not vary with the y coordinate, a smaller length of passenger area means that the passengers can be positioned at locations along the deck where the motion sickness is, in average, smaller. This explains the differences from Figure 4.14(a) to Figure 4.14(b) and why MSI is lower with furthest hulls. In any case, it seems that even for large differences in terms of horizontal clearance, the effects on motion sickness are not very significant (gains of the order of 0.01% in absolute MSI difference). Adding to this, by observing the previous figures, one can conclude that the gradient of the motion sickness as function of *LCB* and C_b is pretty much constant. This means, for instance, that around 1.3% less people will get seasick when exposed to heave and pitch motions if they sail in model 150 when compared with the parent hull, regardless of the horizontal clearance.

4.5.3 Resistance and stability results

Following the strategy adopted in the previous chapter, Figure 4.16 shows colour plots to quickly illustrate the effects of the shape parameters in total hull resistance. In addition, these figures include information regarding ship models that did not satisfy the resistance criteria postulated in Chapter 4.3.3.1. These have been marked with a black X.

Results show that the interference effect between the hulls of the catamaran is indeed quite predominant from the point of view of hull resistance. Substantial savings in terms of required power can be achieved by manipulating the horizontal clearance. Considering the service speed of 25 knots, from Figure 4.15(a) to 4.15(b), the parent hull can benefit from requiring less 239.420 kW of effective power. In any case, it is important to bear in mind that this saving in terms of resistance carry additional constructions costs, which must be considering in any engineering problem. Figure 4.16 suggests trends that are incompatible with seakeeping optimization. For the same block coefficient, increasing *LCB* is disadvantageous for total resistance, as is decreasing block coefficient for constant *LCB*. As a result, hull geometries with minimum resistance appear in regions of the figure that do not favour seakeeping (Figures 4.13

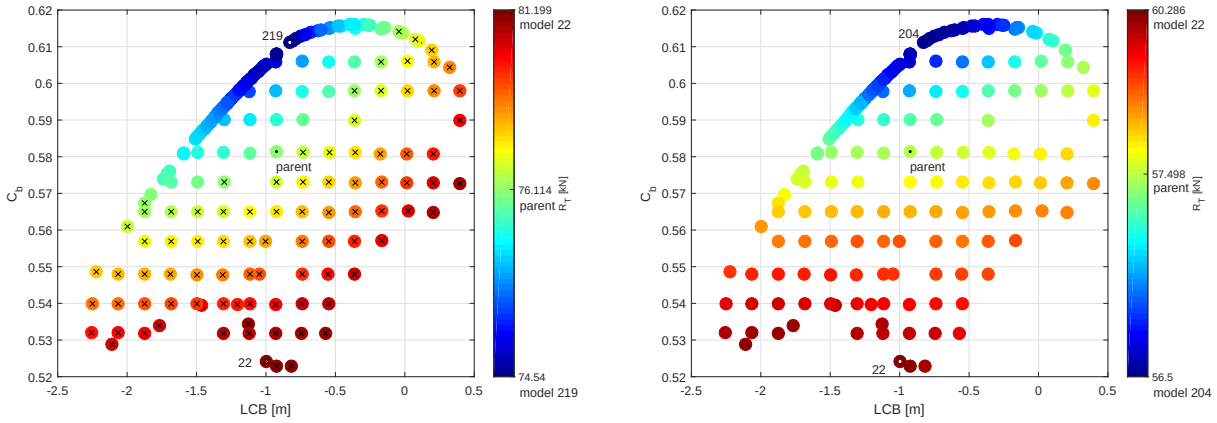

(a) $S/LWL = 0.2872$ (parent horizontal clearance) (b) $S/LWL = 0.4$

Figure 4.15: Total hull resistance at V_s = 25 knots as function of (*LCB*, C_b) with models that fail to satisfy the resistance criteria marked with a black X

and 4.14). As it can be seen in Figure 4.15(a), the total resistance of the parent hull is 76.114 kN. Any model with $R_T > 76.114$ kN does not satisfy the resistance criteria. Figure 4.16 shows the percentage of models that fulfil this requirement for a given horizontal clearance. It seems that for $S/LWL \leq 0.28$ there are no feasible solutions while for $S/LWL \geq 0.308$ all models satisfy the requirement. When compared to the parent horizontal clearance, these limiting situations represent minus 20 cm and plus 78 cm of deck width, respectively. Regarding stability assessment, as duly noted in Chapter 4.3.3.2, the author was forced to stick to the parent horizontal clearance, with which all models satisfied the imposed criteria in terms of minimum heeling angle of maximum GZ and minimum area under GZ curve. In Chapter 4.7.3, the stability results of the optimum hull form will be shown, together with an assessment of the consequences of selecting different horizontal clearance from the perspective of stability.

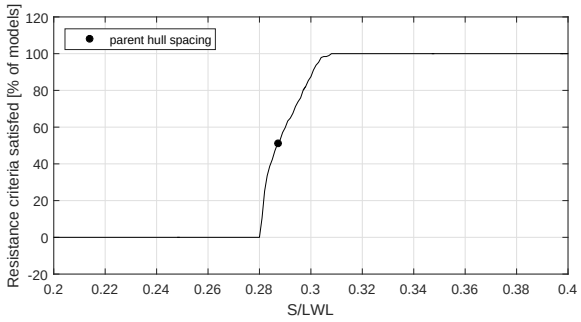

Figure 4.16: Percentage of models that satisfy the resistance criteria as function of the horizontal clearance

4.6 Selection of the optimum hull

Next, in Figure 4.17, are presented all generated models that satisfy the resistance and stability criteria, although, as stated before, stability ended up not limiting the number of possible solutions.

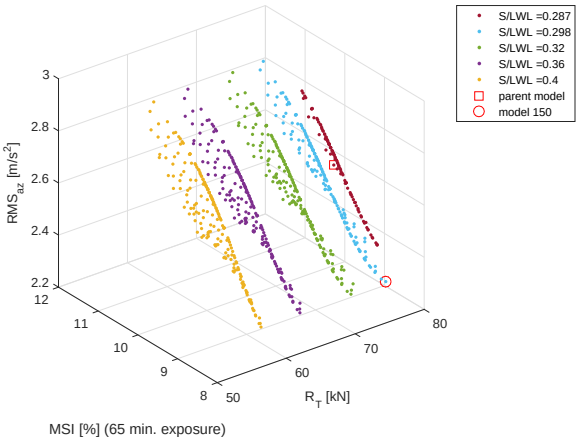

(a) 3-D representation of the family of possible solutions

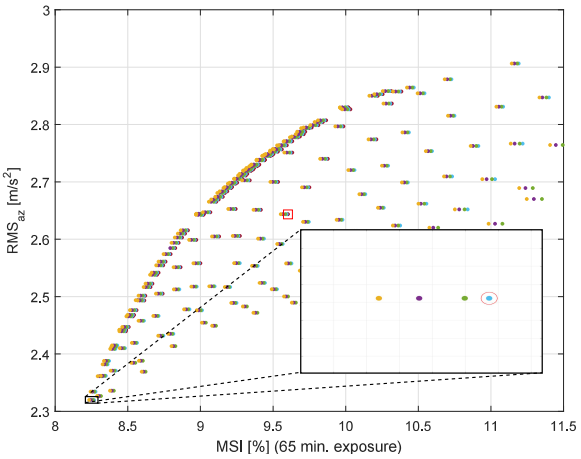

(b) Maximum RMS vertical acceleration response on deck as function of the average MSI at passenger area with detail view of the optimum region

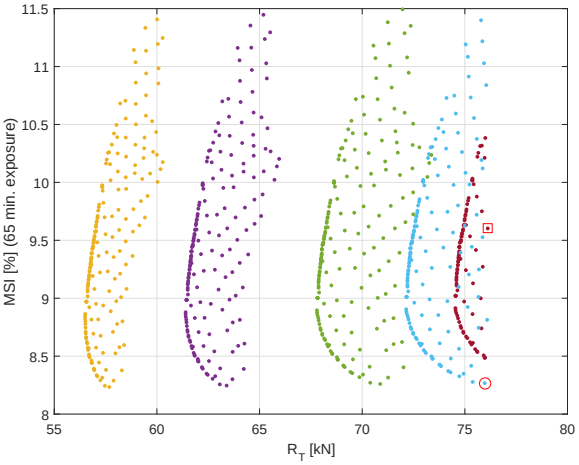

(c) Average MSI at passenger area as function of total hull resistance

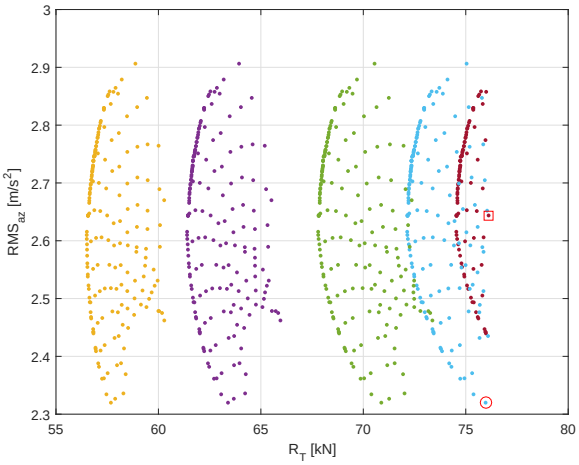

(d) Maximum RMS vertical acceleration response on deck as function of total hull resistance

Figure 4.17: Family of possible solutions considering the most probable seastate at V$_s$ = 25 knots ($H_{1/3}$ = 1-2 m, T_p = 11-13 s, prob = 14.51%) with optimum hull model circled in red

Even though the objective functions only concern the minimization of RMS_{az} and MSI, a third axis with R_T was included. This provides information about the horizontal clearance, which in reality generate complete new sets of possible solutions, each assigned to a different colour. At the end of previous chapter (Figure 4.16), it has been shown that the percentage of models that satisfy the resistance criteria decreases as the the horizontal clearance becomes smaller. In fact, models with $S/LWL \leq 0.28$ are automatically excluded. Furthermore, results showed that the minimum horizontal clearance that captures the optimum region is $S/LWL = 0.298$. This region will be further discussed next but it refers to the minimum RMS acceleration value within the whole family of possible solutions (see Figure 4.17(b)). For simplicity, only 5 horizontal clearance ratios have been displayed, ranging from 0.2872 (parent value) to 0.4. It is interesting to note that, in fact, the lower horizontal clearance ratios generate a quite inferior number of possible solutions.

As stated before, the minimization of total resistance seems incompatible with the seakeeping performance. The same applies to the minimization of construction costs. In order to reduce them, the smaller the horizontal clearance the better (less material, less reinforcements are needed). Therefore, and considering the main goal of this optimization, no efforts have been put into minimizing total resistance. Bearing this in mind, the method for selecting the optimum model began by identifying the minimum RMS_{az} value within the whole family of possible solutions (Figures 4.17(b) and 4.17(d)). It is important to note that there is no dependency on horizontal clearance in this case, which becomes particularly clear in Figures 4.17(b) and 4.17(d). This minimum value is $RMS_{az} = 2.320$ m/s^2 and has been designated as the optimum region. In fact, this refers to model 150, which Figures 4.13 and 4.14 already suggested as a possibly optimum solution. Then, motion sickness was evaluated. Figures 4.17(b) and 4.17(c) show that in order to minimize motion sickness, model 150 with $S/LWL = 0.4$ would have to be selected. However, considering both the additional construction costs and the effective gains in terms of MSI (the differences are of the order of 0.01% for different horizontal clearance ratios), it seems that the option with minimum horizontal clearance is the most appropriate solution, which leads us to model 150 with $S/LWL = 0.298$.

4.7 Overview of model 150

The main characteristics of the parent model and the optimized hull form (model 150) are presented in Table 4.3. Figure 4.18 shows the geometry of the latter, which can be compared with Figure 4.18 that corresponds to the parent hull. Given that the heave and pitch RAOs of both models will be presented in the next chapter, it is important to recall here that for the seakeeping analyses it was assumed that the position of the longitudinal centre of gravity is located at the same vertical plane as the longitudinal centre of buoyancy. For the case of the parent model and model 150, the differences in terms of *LCG* can be seen in Table 4.3. As stated earlier, this decision was a result of the lack of information regarding weight distributions at early stages of the preliminary design. Nevertheless, as pointed out by Kukner and Sarioz (1995), variations of the position of *LCG* should not significantly affect the characteristics of the seakeeping performance.

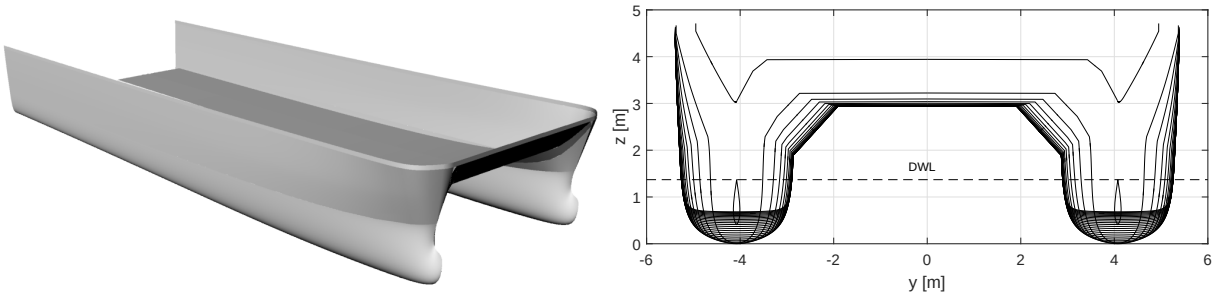

(a) Rendered model in Rhinoceros

(b) Hull body lines

Figure 4.18: Overview of model 150

Table 4.3: Main characteristics of the parent hull vs model 150

	Parent model	Model 150
V service [kn]	25 (F_n = 0.77)	25 (F_n = 0.77)
V maximum [kn]	30	30
t voyage, 50 km [min.]	65	65
LOA [m]	30	28.819
LPP [m]	28.389	28.388
LWL [m]	28.386	28.387
BWL, demi-hull [m]	2.361	2.361
Horizontal clearance (S) [m]	8.152	8.459
S/LWL	0.287	0.298
BOA [m]	10.771	11.079
Deck area [m^2]	319.579	318.61
D [m]	4.624	4.471
T (DWL) [m]	1.41	1.37
Δ [t]	112.600	112.513
KB [m]	0.868	0.883
KG [m]	1.5	1.5
LCB = LCG [m]	-0.926	0.399
C_b [-]	0.581	0.598
C_p [-]	0.776	0.798
C_{wp} [-]	0.816	0.914
C_m [-]	0.749	0.750
RMS_{az} at $x = 28.5$ m ($\approx$ *LWL*) [m/s^2]	2.644	2.320
Average MSI at passenger area [%]	9.603	8.267
Passenger area [m^2], [% of deck area]	50.73, 16	50, 16
Length of passenger area [m]	6.06	5.76
Free area aft [% of deck area]	10	11
Free area fwd. [% of deck area]	69	65
Total hull resistance [kN]	76.114	75.968

As explained in Chapter 4.3.1, the method of Lackenby allows the generation of hull variations so that the main dimentions of the parent model with respect to the underwater hull form are preserved. As it can be observed in Table 4.3, *LWL* and *BWL* (demi-hull) have been maintained with errors which are considered non significant. The displacement exhibits a higher discrepancy between models but it can be seen as constant as well, within acceptable limits (e.g. it is expressed in tons). The design draft *DWL* followed the variation of *LCB* and C_b in order to keep the parent displacement. Regarding the overall dimensions, as predicted in Chapter 4.3.2.1, both *BOA* and *LOA* changed with the Lackenby transformation. In terms of the specified parameters, *LCB* moved forward, increasing by 10%*LWL* reaching the limiting boundary (see Figure 4.12(a)). C_b increased by only 3%. In reality, given the relationships between them, all shape coefficients increased, as expected. The waterplane coefficient C_{wp} in particular, raised by 12%, which is quite significant. An exception for the midship coefficient C_m is worth mentioning which was maintained, as it is the ratio between block and prismatic coefficients. Finally, in terms of the figures of merit, improvements have been obtained. RMS_{az} decreased by 12.3%, although the motion sickness index at the passenger area only decreased by 1.3% (absolute difference in this case). Additionally, the selected resistance criteria associated with the optimization of the horizontal clearance, which went from S/LWL =0.287 to 0.298, ending up affecting the overall breadth of the catamaran, allowed to save 0.14 kN in terms of resistant force. Given this results, one might argue if it really is worth to increase the deck width by 30 cm in order to save so little in terms of resistance. In order to answer this question, a long term economical assessment in terms of fuel consumption would be required. In any case, given the imposed constraints, this solution is considered optimum.

4.7.1 Comparison of heave and pitch motions between the parent model and model 150

Figure 4.19 compares the body lines of the parent hull and of model 150. One of the things that immediately pops up is that the optimum vessel is ”bulgier” at the forward part, as a result of an increased *LCB*. In addition, it seems that the bulbous bow lost much of its original purpose, which perhaps becomes clearer in Figure 4.18(a). In fact, for model 150 it may be argued that a better option would be to completely remove it and use, instead, a regular shaped bow or even more sophisticated solutions such as an axe-bow or an inverted bow-type configuration. The high speeds at which the vessel operate also seem to suggest that. In any case, the optimization procedure presented here did not include such considerations because the generated models were product of an automated transformation. Despite this, it is important to mention that by properly discretizing different bow shapes, it could be possible to evaluate them using PDStrip, which seems to be a way of further optimizing model 150.

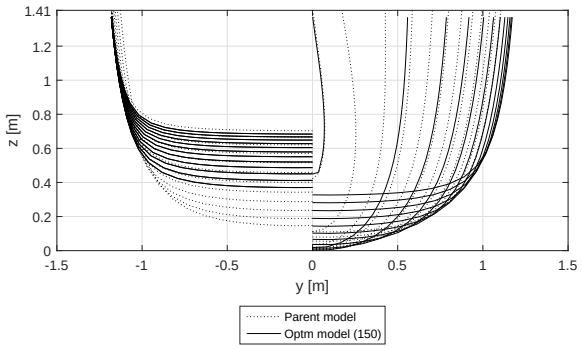

Figure 4.19: Underwater demi-hull body lines

Bellow, Figures 4.20(a)-4.20(d) compare heave and pitch motions of the parent model with model 150, namely heave and pitch amplitudes (both measured at $LPP/2$ according to PDStrip) and the absolute vertical displacement and acceleration at $x = 28.5$ m ($\approx$ *LWL*). Given the results, the influence of the shape coefficients seems clear. Despite this, it is not possible to attribute the differences to one single cause. In any case, the conclusions presented next attempt to establish relations between variations on those coefficients and the resulting vessel motions, being most of the times in agreement with the conclusions of other authors. Yet, caution is advised when extrapolating such relations to cases that are not covered within the limited scope of the work presented here.

To begin with, all figures confirm the conclusions of Chapter 4.5.2 that heave/pitch motions decrease with model 150. Kukner and Sarioz (1995) and Blok and Beukelman (1984) point out that by increasing BWL/DWL, improvements are obtained in heave and pitch RAOs, which goes along with the results (see Figure 4.20(a)-4.20(b)) given that *BWL* is constant in both models and *DWL* is smaller in model 150. Furthermore, Kukner and Sarioz (1995) suggests that increasing C_b reduces both heave and pitch motions. Although this apparently verifies, the results presented in Chapter 4.5.2 showed that its contribution is less influential than moving *LCB* forward, at least in terms of RMS response accelerations. In any case, given that C_b increased only by 3% with respect to the parent model and that all vertical

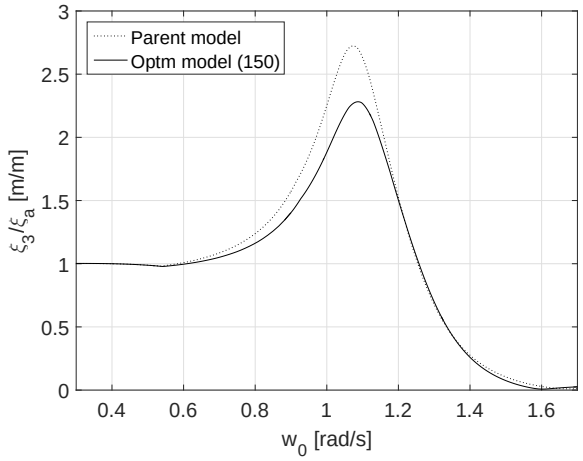

(a) Heave RAO divided by the wave amplitude as function of the wave frequency

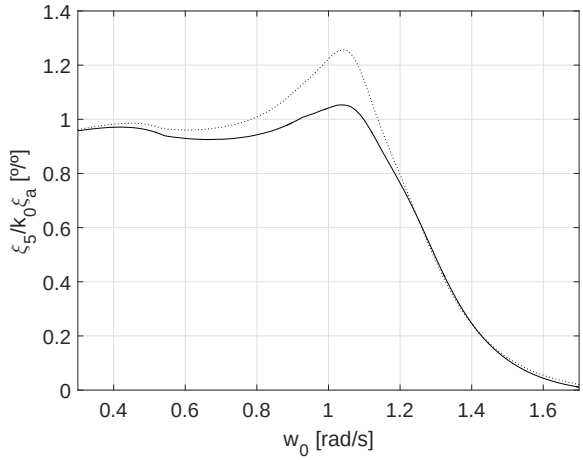

(b) Pitch RAO divided by the wave amplitude as function of the wave frequency

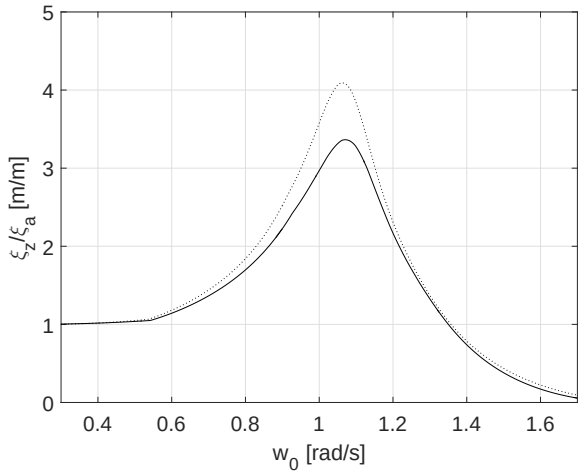

(c) Vertical absolute displacement RAOs divided by the wave amplitude as function of the wave frequency at $x = 28.5$ m ($\approx$ *LWL*)

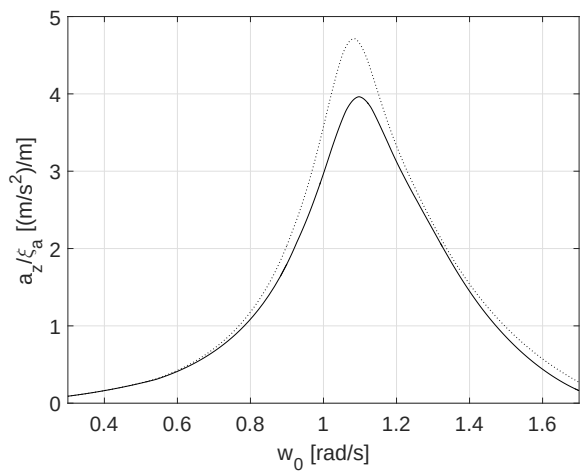

(d) Vertical absolute acceleration RAO divided by the wave amplitude as function of the wave frequency at $x = 28.5$ m ($\approx$ *LWL*)

Figure 4.20: Comparison of vertical motions at V_s = 25 knots between the parent model and model 150

motions (Figures 4.20(a)-4.20(d)) and responses (Figures 4.21(a)-4.21(b)) improved significantly, one could extrapolate that they are indeed more sensitive to variations of *LCB* (that raised by 10%). In reality the conclusions regarding *LCB* go against Kukner and Sarioz (1995) which suggested that decreasing *LCB* is beneficial for pitch motions and negligible for heave. Again, as a result of the applied parametric transformation of Lackenby, it is important to mention that a wide number of parameters have been varied an thus, attributing causes to a single one might be a risk. In fact, the remaining hull form parameters, particularly C_{wp} that increased 12% with respect to the parent model, are known to affect motions significantly.

As expected, PDStrip allowed for a proper definition of the motions around the resonance frequency, ω_r, which is vital in order to draw consistent conclusions. For this purpose, Tables 4.5 and 4.4 present discretized results at the captured resonance frequencies of the global hydrodynamic coefficients of the coupled heave/pitch motion equation for heave and pitch, respectively. The work of Blok and Beukelman (1984) will be used here to verify the established effects of C_{wp} and *BWL*/*DWL* ratio on the hydrodynamic

coefficients as well as the results in terms of heave and pitch motions.

Table 4.4: Comparison of the global coefficients of the coupled heave/pitch motion equation (3.4) at the heave resonance frequency at V = 25 knots with differences relative to the parent model

	ω_r $[rad/s]$	$\Delta + A_{33}$ $[t]$	B_{33} $[t/s]$	C_{33} $[t/s^2]$	A_{35} $[t.m]$	B_{35} $[t.m/s]$	C_{35} $[t.m/s^2]$	$\lvert F_3^E \rvert$ $[kN]$	Φ_3 $[^\circ]$
Parent	1.073	26.858	94.036	549.867	-152.345	993.936	1203.85	324.146	4.929
Model 150	1.087	34.019	104.004	614.687	-197.611	1027.327	679.776	313.829	13.639
Rel. difference	+1.3%	+26.7%	+10.6%	+11.8%	-29.7%	+3.4%	-43.5%	-3.2%	+176.7%
	ω_r $[rad/s]$	A_{53} $[t.m]$	B_{53} $[t.m/s]$	C_{53} $[t.m/s^2]$	$I_5 + A_{55}$ $[t.m^2]$	B_{55} $[t.m^2/s]$	C_{55} $[t.m^2/s^2]$	$\lvert F_5^E \rvert$ $[kN.m]$	Φ_5 $[^\circ]$
Parent	1.073	133.469	220.173	1187.31	639.601	9164.941	31854.822	2641.352	-71.605
Model 150	1.087	118.566	72.955	664.165	1253.655	10074.646	37189.596	3216.483	-73.534
Rel. difference	+1.3%	-11.2%	-66.9%	-44.1%	+96.0%	+9.9%	+16.7%	+21.8%	-2.7%

Table 4.5: Comparison of the global coefficients of the coupled heave/pitch motion equation (3.4) at the pitch resonance frequency at V = 25 knots with differences relative to the parent model

	ω_r $[rad/s]$	$\Delta + A_{33}$ $[t]$	B_{33} $[t/s]$	C_{33} $[t/s^2]$	A_{35} $[t.m]$	B_{35} $[t.m/s]$	C_{35} $[t.m/s^2]$	$\lvert F_3^E \rvert$ $[kN]$	Φ_3 $[^\circ]$
Parent	1.041	25.691	95.699	549.867	-186.884	972.617	1203.85	340.903	5.063
Model 150	1.036	32.360	108.251	614.687	-257.033	991.684	679.776	347.985	13.014
Rel. difference	-0.5%	+26.0%	+13.1%	+11.8%	-37.5%	+2.0%	-43.5%	+2.1%	+157.0%
	ω_r $[rad/s]$	A_{53} $[t.m]$	B_{53} $[t.m/s]$	C_{53} $[t.m/s^2]$	$I_5 + A_{55}$ $[t.m^2]$	B_{55} $[t.m^2/s]$	C_{55} $[t.m^2/s^2]$	$\lvert F_5^E \rvert$ $[kN.m]$	Φ_5 $[^\circ]$
Parent	1.041	139.309	216.317	1187.31	473.797	9282.499	31854.822	2593.611	-71.116
Model 150	1.036	135.689	60.060	664.165	1023.580	10460.630	37189.596	3142.425	-74.310
Rel. difference	-0.5%	-2.6%	-72.2%	-44.1%	+116.0%	+12.7%	+16.7%	+21.2%	-4.5%

Figure 4.20(a) indicates that at the resonance frequency (wavelengths of about 1.8-1.9*LWL*), model 150 experiences heaving amplitudes 16.5% smaller than the parent model. A decrease of the same order is observed for pitch at wavelengths of about 2*LWL* (Figure 4.20(b)). According to Blok and Beukelman (1984), the heave exciting force is proportional to the waterplane area and, consequently, to C_{wp}. However, although C_{wp} increased by 12% with respect to the parent model, Table 4.4 shows that F_3^E decreased by 3.2% at the resonance frequency. Given these results, it is here postulated that the inclusion of transom corrections for the calculation of the heave diffraction force, which increase the exciting force for vessels with larger wetted transom areas as is the case of the parent model due to a higher draft for the same breadth, could be the cause for this inconsistency. This effect becomes particularly significant at high Froude numbers as it can be observed, for instance, in Table B.7 of Appendix B that presents some of the numerical results obtained during the first part of this dissertation (Chapter 3). In

fact, a simple verification showed that, despite representing a small difference, the heave exciting force at the resonance frequency is 0.5% higher for model 150 than for the parent model if transom terms are neglected. Therefore, considering vessels with transom sterns, one could hypothesize that a higher C_{wp} is related with a larger exciting force at the heave resonance frequency if the ship has a higher transom area (inversely proportional to *BWL*/*DWL*). Regarding pitch motions, the same relationship with C_{wp} has been observed, although in this case the heave exciting force goes as predicted by Blok and Beukelman (1984) at the pitch resonance frequency (Table 4.5). Also dependent on C_{wp} are the restoring coefficients. C_{33} is directly proportional to the waterplane area while C_{55} is directly proportional to the longitudinal metacentric height for the same displacement. Model 150, with higher C_{wp} and *GML* (+26% difference), presents higher values for both in Tables 4.4 and 4.5 when compared to the parent model. Regarding C_{35} and C_{53}, these coefficients depend on the first area moment of the waterplane. C_{53} additionally includes a transom term correction that does not affect results significantly (refer to equation (3.23)). In any case, these values seem incorrect since they do not follow the increase in waterplane area from the parent model to model 150. This has to do with the method followed by the code developers to perform the integration along the waterplane area $-\rho g \int xBdx$ that considers a reference frame centred in *LPP*/2 [11], resulting in quite different coefficients. Nevertheless, this detail does not affect the final motion results. Furthermore, the first area moment of the waterplane is, as expected, greater for model 150 and thus, the effective values of the restoring coefficients C_{35} and C_{53} are in reality higher. Higher restoring coefficients contribute to smaller amplitudes as they translate the stiffness of the mass-spring-damper system. As for added mass, Blok and Beukelman (1984) states that it is proportional to *BWL*/*DWL* ratio. Thus, for a smaller draft at the same breadth, *BWL*/*DWL* is higher and so it is the added mass, which verifies for A_{33} and A_{55} in Tables 4.4-4.5. In any case, although added masses influence vertical amplitudes, the direct effect is hard to assess given the results presented here. Finally, the damping coefficient is proportional to C_{wp} [15], being expected that the model with the largest waterplane area have the highest damping. Tables 4.4-4.5 indicates good agreement with this prediction in terms of B_{33}, B_{35} and B_{55}. As a result, it can be observed that model 150 experiences motions with lower amplitudes, particularly at the resonance frequencies.

In terms of absolute vertical displacements and accelerations at $x = 28.5$ m ($\approx$ *LWL*) from Figures 4.20(c)-4.20(d), the observed trends for heave and pitch can be here applied as well, which seems reasonable considering that they are essentially a product of the combined vertical motions, behaving linearly with respect to the wave amplitude [15]. In fact, this joint contribution is easy to identify, particularly in the plot of ξ_z/ξ_a, as it resembles quite well the heave and pitch curves. Also, both figures indicate that the resonance frequencies (combined) were kept. Model 150 allowed improvements of about 18% in terms of vertical displacements at the resonance peak. Regarding accelerations, the effect of a frequency squared term can be clearly observed and a decrease of about 11% is experienced in model 150 at the resonance frequency.

All in all, it can be observed that model 150, with larger waterplane area, higher *BWL*/*DWL* ratio and a forward positioning of *LCB* (C_b has a weaker impact on heave and pitch motions), experiences lower

vertical amplitudes, which is particularly significant at the resonance peaks. Overall, neglecting a few deviations, added mass is proportional to *BWL*/*DWL* ratio, while the restoring coefficients and damping increase with the waterplane area, which effectively decreases vertical amplitudes. Also, it has been verified that the heave exciting force, although proportional to the waterplane area as well, is affected by large wetted transom areas. In any case, given the joint influence of such parameters on the coupled heave and pitch motions, a more detailed study is required in order to refine the conclusions.

Finally, Figures 4.21(a)-4.21(b) present the same comparison between the parent model and model 150 in terms of vertical responses at $x = 28.5$ m ($\approx$ *LWL*) upon the most probable seastate the vessel will have to face. Here the results are presented in terms of the encounter frequency, since analysing the moving reference frame is useful when handling the response spectrum. As expected, the improvements obtained with model 150 in terms of vertical motions and accelerations translate into better seakeeping performances upon the specified seaway. Note that the root mean square of the response spectrum of Figure 4.21(b) corresponds in reality to $RMS_{az} = 2.320$ m/s^2, the value that led to the selection of model 150 as optimum hull (refer to Figures 4.17 and 4.13).

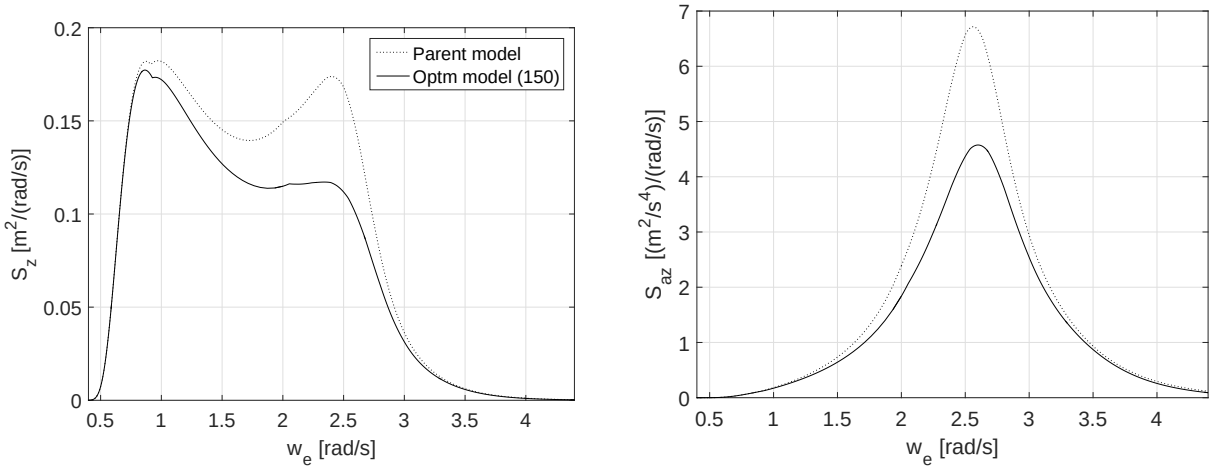

(a) Absolute vertical displacement responses as function of the encounter frequency

(b) Absolute vertical acceleration responses as function of the encounter frequency

Figure 4.21: Comparison of vertical responses at $x = 28.5$ m ($\approx$ *LWL*) considering the most probable seastate ($H_{1/3}$ = 1-2 m, T_p = 11-13 s, prob = 14.51%) at V$_s$ = 25 knots between the parent model and model 150

4.7.2 Effects of the seatate on RMS vertical acceleration responses and motion sickness for model 150

Here, the effects of the sestates on RMS vertical acceleration responses and motion sickness incidence will be assessed for model 150. Figure 4.22(a) shows the distribution of RMS vertical accelerations along the deck considering the most probable range of significant wave heights, $H_{1/3} = 1 - 2$ meters, for different peak periods. Note that the most probable seastate in terms of T_p ranges between 11 and 13 seconds. Results indicate that the minimum RMS values tend to gravitate towards the centre

of gravity while the maximum is experienced at the vessel extremities, particularly at the bow area, as expected. In Chapter 4.2, the analysis of the variance of the wave spectrum of Figure 4.6 allowed to conclude that, overall, it tended to increase as wave periods lengthened. However, Figure 4.22(a) reveals a different trend. In fact, for the same significant wave height, larger acceleration responses are obtained with wave periods that generate variance peaks nearest to the resonance frequency of the vertical motions. Bearing this in mind, by comparing the wave spectrum of Figure 4.6 with the vertical absolute accelerations of Figure 4.20(d), it is easy to understand why $T_p = 5 - 7$ produce the highest RMS acceleration values and $T_p > 17$ the lowest. This conclusion becomes even clearer in Figure 4.22(b), additionally showing that this is true regardless of the considered range of wave heights. Figure 4.22(b) presents the RMS_{az} values evaluated at $x = 28.5$ m ($\approx$ *LWL*) for all possible seastates, i.e., each combination of significant wave heights and peak periods. For $H_{1/3} = 1 - 2$ m, the values of RMS accerations as function of peak period, correspond to the values of the curves of Figure 4.22(a) in that position. Furthermore, $RMS_{az} = 2.320$ m/s^2 ($H_{1/3}$ = 1-2 m, T_p = 11-13 s) corresponds the value that led to the selection of model 150 as optimum hull (refer to Figures 4.17 and 4.13).

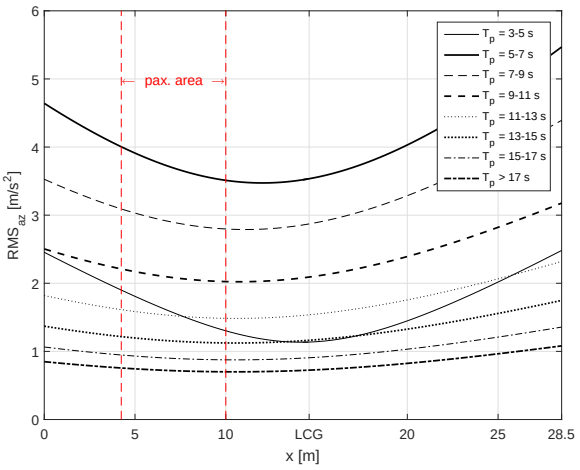

(a) RMS_{az} deck distribution considering the most probable significant wave heights ($H_{1/3}$ = 1-2 m, prob = 48.81%). Position of passenger area optimized for the most probable seastate ($H_{1/3}$ = 1-2 m, T_p = 11-13 s, prob = 14.51%)

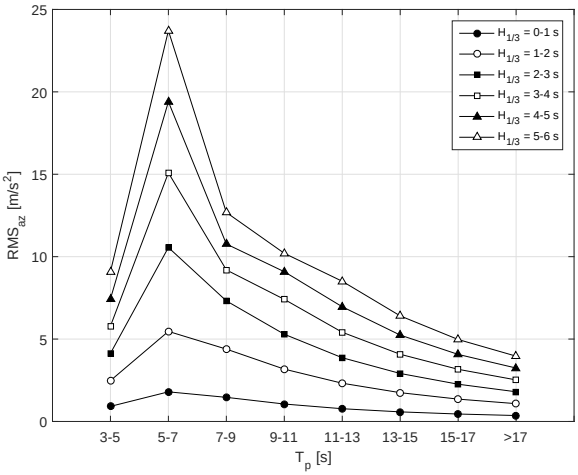

(b) RMS_{az} at $x = 28.5$ m ($\approx$ *LWL*) for all possible sestates

Figure 4.22: Seastate effects on RMS vertical acceleration responses (V$_s$ = 25 knots)

Another interesting discussion relates with the final location of the passenger area which, in Figures 4.22(a), 4.23(a), 4.23(c) and 4.23(d), has been marked in red. Note that all figures presented next refer to the optimum horizontal clearance ratio of $S/LWL = 0.298$. As stated in Chapter 4.3.2.2, the passenger area has been positioned in order to minimize the distribution of incidence of motion sickness along its length (by averaging the results) considering the most probabe sea state ($H_{1/3}$ = 1-2 m, T_p = 11-13 s). Figure 4.22(a) shows the optimized location of the passenger area. It begins 4.24 meters forward of the aft end of the ship (exceeding the minimum distance of 2 meters) and extends for 5.76 meters with a width of 8.68 meters. The total area sums up to 50 square meters which also exceeds, by a small margin, the area estimated in Figure 4.10 of 48.24 square meters. This deviation is a result of the distance between remote locations imposed along the deck that did not allow the exact value to be

used.

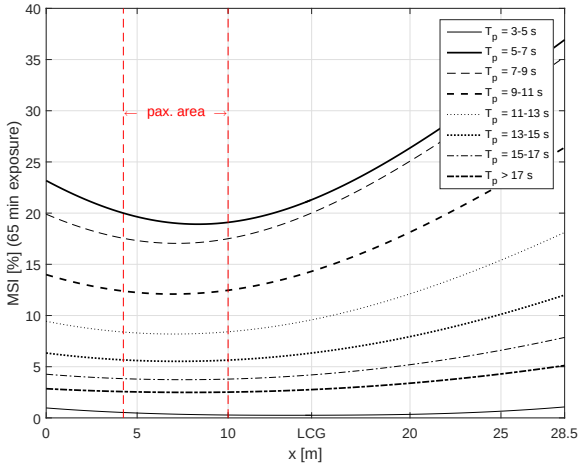

(a) MSI deck distribution for different peak period ranges considering the most probable significant wave heights ($H_{1/3}$ = 1-2 m, prob = 48.81%). Position of passenger area optimized for the most probable seastate ($H_{1/3}$ = 1-2 m, T_p = 11-13 s, prob = 14.51%)

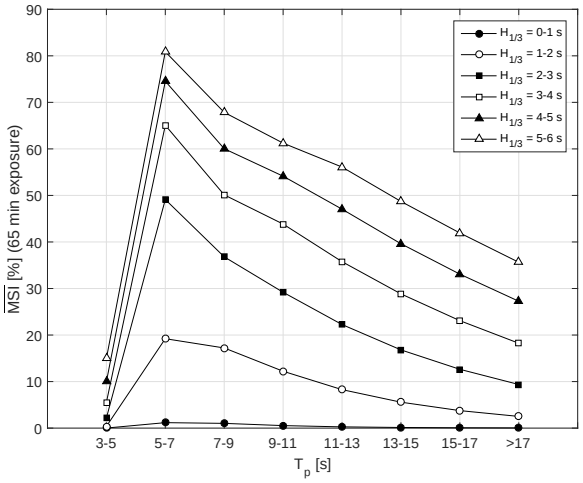

(b) Average MSI at the passenger area for all possible seastates

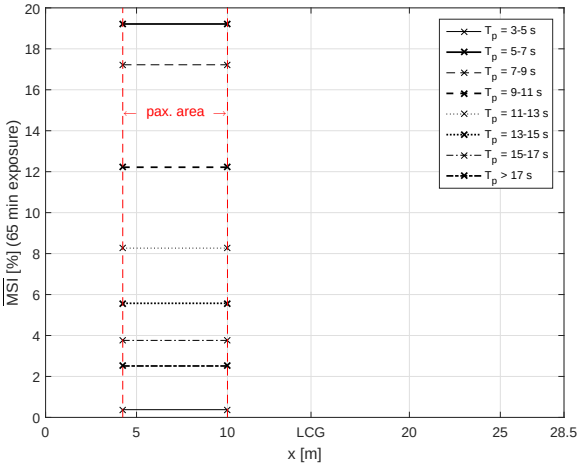

(c) Position of passenger area when optimized for the most probable seastate ($H_{1/3}$ = 1-2 m, T_p = 11-13 s, prob = 14.51%) and resulting average MSI for different peak period ranges considering the most probable significant wave heights ($H_{1/3}$ = 1-2 m, prob = 48.81%)

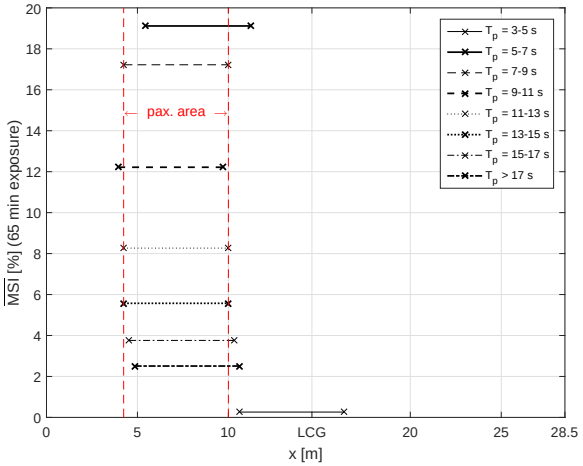

(d) Position of passenger area when optimized for each seastate individually and resulting average MSI for different peak period ranges considering the most probable significant wave heights ($H_{1/3}$ = 1-2 m, prob = 48.81%)

Figure 4.23: Seastate effects on motion sickness incidence considering the optimum horizontal clearance ratio of $S/LWL = 0.298$ (V_s = 25 knots)

Note that the length of the passenger area is a function of the horizontal clearance, upon the constraints set in Figure 4.9. A few considerations regarding this dependency will be presented in the next chapter. In any case, it can be verified that the passenger area occupies about 16% of the total deck area, which leaves enough free space for the remaining areas of the superstructure, if necessary, and to transport cargo on deck (about 11% aft and 65% forward). The apparently missing area of about 8% correspond

to the laterals of the passenger area which, in this case will probably correspond to the laterals of the superstructure. Furthermore, it is interesting to note in Figure 4.22(a) that the optimized location of the passenger area does not coincide with the minimum region of RMS accerations, near the centre of gravity. Figure 4.23(a), on the other hand, confirms the method used to optimize the position of the passenger area. Here, the MSI distribution along the deck is shown, considering the most probable significant wave height range, $H_{1/3} = 1 - 2$ meters, for different peak periods. For T_p = 11-13 seconds, the passenger area indeed captures the minimum MSI values. Given this discrepancy with respect to RMS accelerations, this could raise questions about whether using the incidence of motion sickness is truly the best approach to optimize comfort and welfare on board. However, as discussed in Chapter 4.5.2, the MSI model considers the fact that humans are capable of withstanding severe accelerations as long as the frequency is high enough. Results showed that moving the passenger area to an aft position increases the average frequencies, which generates lower motion sickness incidences, even though accelerations are more adverse. Finally, as a mere exercise, Figures 4.23(c) and 4.23(d) attempt to demonstrate the effects of optimizing the position of the passenger area with respect to the most probable seastate. Both present results for $H_{1/3}$ = 1-2 m. Figure 4.23(c) shows the incidences of motion sickness for different peak periods within the passenger area, which has been optimize with respect to the most probable seastate. Figure 4.23(d), on the other hand, displays the ideal passenger area position for each peak period range and the obtained MSI values. As it can be observed, although some seastates would require a significant shift in the positioning of the passenger area in order to minimize the average motion sickness, the outcome of that change is negligible. Therefore, optimizing for the most probable sea state was a good principle. Note that for $T_p = 11 - 13$ seconds, the position in Figures 4.23(c) and 4.23(d) is maintained, as expected.

4.7.3 Effects of horizontal clearance on motion sickness, resistance and stability for model 150

In this chapter, an assessment of the effects different horizontal clearances have on motion sickness, resistance and stability of model 150 will be carried out. First, the motion sickness for different peak periods within the passenger area is presented in Figure 4.24. It shows the exact same results as Figure 4.23(c) but considers a larger horizontal clearance ratio ($S/LWL = 0.4$). Again, it refers to the range of wave heights between 1 and 2 meters and the positioning of the passenger area (marked in red) favours the most probable seastate. The intent here was to demonstrate an obvious decrease in length of the passenger area for larger horizontal clearances as a result of the constraints imposed in Chapter 4.3.2.2. As a matter of fact, those constraints result in a relationship between length and horizontal clearance that can be seen in Figure 4.25. In the perspective of what has been said before, it is further added that, most of the times, it is not possible to impose the exact length needed to attain the total area for passengers due to the distance between remote locations on deck. As a result, the effective curve showed in Figure 4.25 would actually have to move about 20 cm up for all horizontal clearances. In any case, a comparison of Figures 4.24 and 4.23(c) shows that, although the effectiveness in minimizing

motion sickness at the passenger area decreases as the horizontal clearance increase, the difference

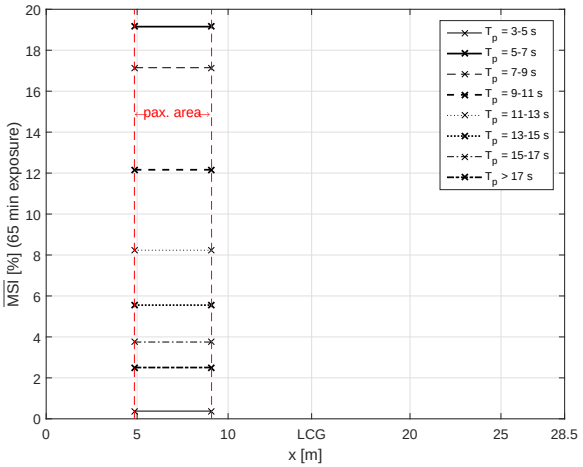

Figure 4.24: Position of passenger area when optimized for the most probable seastate ($H_{1/3}$ = 1-2 m, T_p = 11-13 s, prob = 14.51%) and resulting average MSI for different peak period ranges considering the most probable significant wave heights ($H_{1/3}$ = 1-2 m, prob = 48.81%). Results for $S/LWL = 0.4$ and V_s = 25 knots

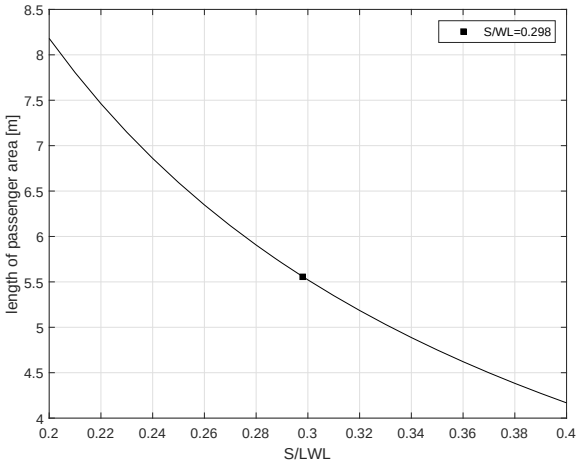

Figure 4.25: Estimate length of passenger area as function of the horizontal clearance (V_s = 25 knots)

Regarding total hull resistance, Figure 4.26 shows the relation between R_T and horizontal clearance. As expected, a decrease of total resistance is achieved by increasing S/LWL due to a less predominant influence of the interference effect between demi-hulls. Also, results indicate that for the specific case of model 150, a horizontal clearance ratio of $S/LWL = 0.298$ is the minimum in order to comply with the criteria that imposes a minimum resistance of 76.114 kN while, at the same time, providing the minimum RMS acceleration value of 2.320 m/s^2 at $x = 28.5$ m ($\approx$ *LWL*). When compared to the parent model, the gain obtained in terms of resistance only represents consuming less 1.88 kW of effective power at 25 knots. Again, such a small resistance improvement for an increase in deck of 30 cm could lead to the conclusion that other solutions would be more economically viable. However, at the absence of an economical study, model 150 with $S/LWL = 0.298$ is the best solution for the constraints imposed in this dissertation. Finally, a few results regarding stability analysis are shown in Figures 4.27 and 4.28. As stated before, only the parent horizontal clearance has been considered in these calculations. To assess the effects of different horizontal clearances would have required individual modelling of all generated hull forms. In any case, a horizontal clearance ratio of $S/LWL = 0.287$ provides good transverse stability performances and did not limit the number of possible solutions. Figure 4.27 shows that the maximum GZ is achieved at an heeling angle of 16°. In order to asses the effect of using different horizontal clearances in the stability analyses, Figure 4.28 from Birmingham (2004) has been included here. It presents a set of GZ curves indicating that as the horizontal clearance increases, transverse stability improves but the angle at which the maximum GZ value occurs becomes smaller, which seems to

suggest that maintaining a S/LWL ratio close to 0.287 was a safe approach. It is expected that with a horizontal clearance ratio of $S/LWL = 0.298$, no significant changes are verified in the GZ curve.

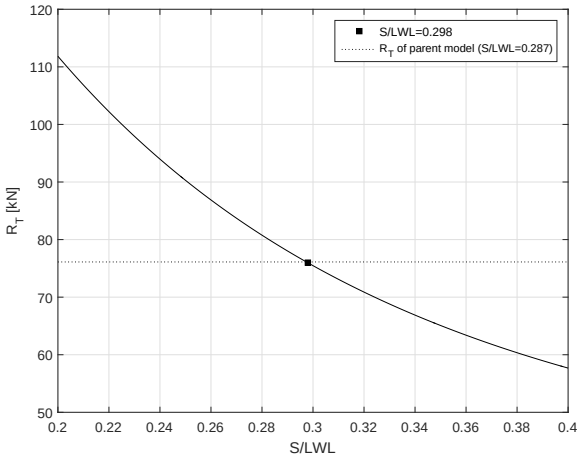

Figure 4.26: Total hull resistance as function of the horizontal clearance (V_s = 25 knots)

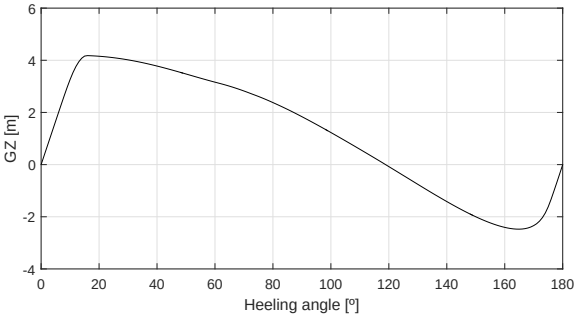

Figure 4.27: GZ curve for model 150 with the parent horizontal clearance ($S/LWL = 0.287$)

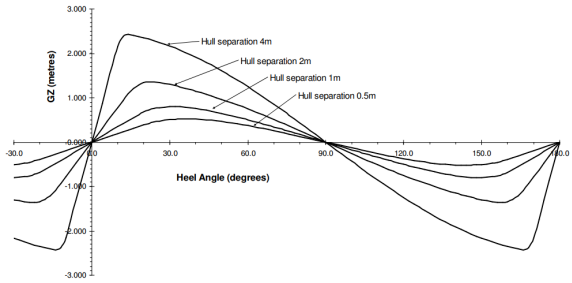

Figure 4.28: The effect on the GZ curve of a simplified catamaran (hulls of square crossection 1 m by 1m, floating at half depth) as the horizontal clearance is varied (source: [14])

4.7.4 Operability assessment of model 150 based on seakeeping criteria

In the final chapter of this dissertation, an operability analysis of the optimum model is carried out. The operability assessment considers human comfort criteria, being vital in the design of passenger vessels in particular. Such studies have been performed by several researchers, including Guedes Soares et al. (1995), Fonseca and Guedes Soares (2002b), Gasparotti and Rusu (2013) or Tezdogan et al. (2014). Guedes Soares et al. (1995) suggested that, due to linearity assumptions, the wave spectrum could be represented as the product of the wave spectrum in terms of the unitary significant wave height, $S_{\zeta 1}(\omega_e)$,

and the square of the significant wave height $H_{1/3}$.

$$S_\zeta\left(\omega_e, H_{1/3}, T_p\right) = H_{1/3}^2 S_{\zeta 1}\left(\omega_e, T_p\right) \tag{4.27}$$

Using the previous result, equation (4.8) for the vertical response of the vessel at a remote location (x, y, z) can be rewritten as follows:

$$S_z\left(x, \omega_e, H_{1/3}, T_p\right) = \left|\xi_z\left(x, \omega_e\right)\right|^2 H_{1/3}^2 S_{\zeta 1}\left(\omega_e, T_p\right) \tag{4.28}$$

Furthermore, recalling the definition for the spectral moment associated with the vertical acceleration response m_{4z} set in equation (4.11), we can resort to the last result to establish a relation to the normalized spectral moment and, consequently, root mean squared accelerations:

$$m_{4z} = H_{1/3}^2 m_{4z,1} \Rightarrow RMS_{a_z} = H_{1/3} RMS_{a_z,1} \tag{4.29}$$

Finally, given a seakeeping criterion defined in terms of RMS accelerations, $RMS_{a_z,\textit{criteria}}$, the limiting significant wave height as function of the period (for this dissertation the peak period T_p is being considered) is given by equation (4.30).

$$H_{1/3}^{\lim}\left(T_p\right) = \frac{RMS_{a_z,\textit{criteria}}}{RMS_{a_z,1}} \tag{4.30}$$

In terms of limiting criteria, the HSC code [73] defines in *Chapter 4 Accommodation and Escape Measures, 4.3 Design acceleration levels, 4.3.7* that "limiting sea states for operation of the craft shall be given in normal operation condition and in the worst intended conditions, at 90% of maximum speed and at reduced speed as necessary Furthermore, the worst intended conditions are defined in *Chapter 1 General Comments and Requirements, 1.4 Definitions, 1.4.61* as "the specified environmental conditions within which the intentional operation of the craft is provided for in the certification of the craft". For this operability assessment, 25 knots (service speed) and 27 knots (90% of the maximum speed of 30 knots) have been the considered vessel speeds. In *Chapter 4 Accommodation and Escape Measures, 4.3 Design acceleration levels, 4.3.1* of the HSC code [73], it is stated that "for passenger craft, superimposed vertical accelerations above 1.0 g at longitudinal centre of gravity shall be avoided". Under a conservative perspective, although in Chapter 4.1 of this dissertation the catamaran has been defined as cargo craft, this requirement will be imposed nonetheless. In fact, if this value of acceleration is achieved, the degradation of passenger safety is at stake, being considered a Level 3 Hazardous Effect (defined in the terms of *Table 1, Annex 3 Use of Probability Concept* of the HSC code [73]). Furthermore, the IMO Guidelines [74] (*5 Sea state limitations - significant wave height, 5.6 Safe handling limitations, 5.6.9*) refer that these vertical accelerations should be interpreted not as RMS values but as the mean of the 1% highest accelerations, $az_{1/100}$. Hoffman and Karst (1975) studies the properties of Rayleigh distribution and derives a formula to compute the average of the 1/nth highest amplitudes, which leads us to the following equation:

$$az_{1/n} = \left[n\sqrt{2} \left[\frac{\sqrt{\ln n}}{n} + \sqrt{\pi} \left(\frac{1}{2} - erf\sqrt{2\ln n} \right) \right] \right] RMS_{a_z} \tag{4.31}$$

In addition, as an attempt to further assess the limit operating conditions, the author resorted to the DNV GL rules for the classification of high speed crafts ([40]). Again, in *Section 3 Structures, C3.3 Design Acceleration, C3.3.1 Vertical acceleration at LCG*, the rules state that the design vertical acceleration at the centre of gravity corresponds to the mean 1% highest accelerations and are not to be taken less than:

$$a_{CG} = 0.36 \times 0.75 \times \frac{V}{\sqrt{LWL}} \tag{4.32}$$

, where a_{CG} is expressed in [g] and V in knots. The coefficients come from the fact that the catamaran operates as a supply vessel within 50 nautical miles off the coast. Further ahead in the same section, DNV GL defines the longitudinal distribution of vertical acceleration along the hull, a_v, as function of the distribution factor k_v:

$$a_v = k_v \times a_{CG} \tag{4.33}$$

$$\begin{aligned} k_v &= 1 \quad \textit{for} \quad x \leq LCG \\ &= 2 - \frac{1 - \frac{x}{LWL}}{1 - \frac{LCG}{LWL}} \quad \textit{for} \quad x > LCG \end{aligned} \tag{4.34}$$

Therefore, two limiting criteria have been established here. The first comes from the HSC code, associated with the maximum superimposed vertical accelerations at the centre of gravity of 1 g. The second criteria has been derived from DNV GL and relates with the longitudinal distribution of vertical accelerations, equation (4.33). In both cases, the accelerations refer to average 1% highest values and thus, equation (4.31) has been used to re-write (4.30) in order to obtain the limiting significant wave heights.

$$H_{1/3}^{\lim}(T_p) = \frac{1}{\left[az_{1/100,1}\left(x = LCG\right) \right] / g} \tag{4.35}$$

$$H_{1/3}^{\lim}(T_p) = \frac{a_v}{\left[az_{1/100,1} \right] / g} \tag{4.36}$$

In addition, in *Section 3 Structures, C3.3 Design Acceleration, C3.3.3 Assessment of limit operating conditions*, the DNV GL rules [40] impose direct limitations on the maximum allowed significant wave heights which shall not be greater than (4.37) and (4.38).

$$H_{sm} = 5\frac{a_{CG}}{V}\frac{LWL^{1.5}}{6 + 0.14LWL} \tag{4.37}$$

, where vertical acceleration aCG is defined in equation (4.32), but need not to be taken less than 1 g.

$$H_s = \frac{10.9 \times a_{CG} \times K_{cat} \times K_H}{F_H^2} \tag{4.38}$$

$$K_{cat} = 1 + \frac{B_{cl} - H_{sm}}{LWL} \geq 1.0$$
$$= 1.0 \quad \textit{for monohulls and trimarans} \tag{4.39}$$

$$K_F = \frac{3.23}{LWL}\left(2.43\sqrt{LWL} + V\right) \tag{4.40}$$

$$K_H = K^{0.35}\sqrt{\left(\frac{1}{K^2}\right)^2 + 1} \tag{4.41}$$

$$K = \frac{K_F}{K_T} \tag{4.42}$$

$$K_T = \sqrt{\frac{4.6A_{wp}}{\Delta}}\sqrt{\frac{x_{CG}}{LWL}} \tag{4.43}$$

, where, B_{cl} is the horizontal clearance (distance between the centrelines of the hulls of the catamaran), A_{wp} is the area of waterline and x_{CG} is the distance from aft perpendicular to *LCG*.

Given the previous limiting operating conditions by DNV GL, an upper bound for maximum allowed significant wave height has been imposed, corresponding to the minimum value between (H_{sm}, H_s).

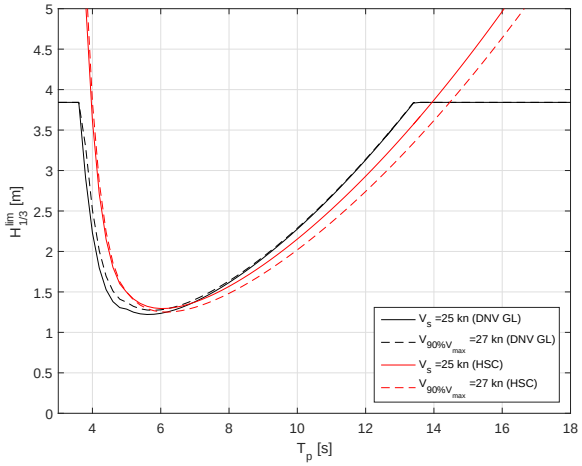

(a) Comparison of seakeeping criterion from DNV GL and HSC code for service speed and 90% of maximum speed

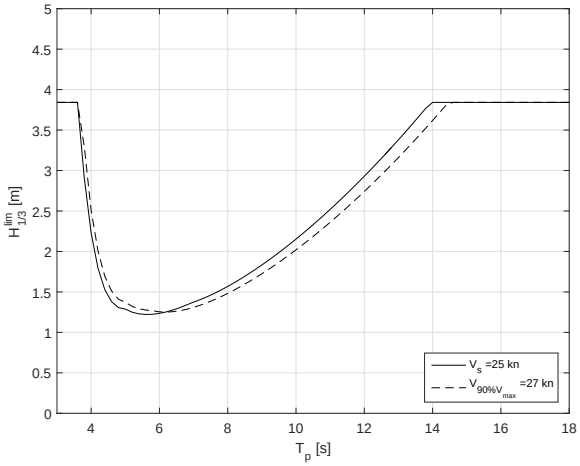

(b) Final limiting seastates for the operation of the fast crew supplier at service speed and 90% of maximum speed

Figure 4.29: Maximum allowed $H_{1/3}$ as function of the peak period based on criterion imposed by the classification societies

Finally, Fonseca and Guedes Soares (2002b) define the operability index as "the percentage of time during which the ship is operational". For that purpose, a scatter diagram can be used to sum up the probabilities of occurrence of the seastates upon which the catamaran is suited to operate according to Figure 4.29(b). However, the scatter diagram provided by the work of Costa et al. (2001), which presents wave data as function of ranges of significant wave height and peak period, does not present discretized enough data to allow for a reliable computation of the operability index. In any case, operability boundaries can be estimated based on the available data. From a conservative perspective, the fast crew supplier will be able to operate at the Alentejo basin only 52% of the time. In a more optimistic scenario, the author expects an operability index of 91%. Furthermore, it is likely that the effective operability is

much closer to the upper boundary. Also, a decrease in operability is expected at higher speeds, given the more strict limitations.

4.8 Summary

Throughout this chapter, the parent catamaran model provided by DAMEN Shipyards was optimized in terms of seakeeping performance to operate at 25 knots as a fast crew supplier used in the transport of 12 passengers to an offshore platform at the Alentejo basin, for which the work of Costa et al. (2001) was used to simulate the seastates at the location. MATLAB was used as main optimization engine. PDStrip, selected in Chapter 3 as the most suited strip theory code to predict heave and pitch motions of fast catamarans in head seas, was used as seakeeping tool. The RMS vertical acceleration responses at the bow and the Motion Sickness Incidence (MSI) for 65 minutes of exposure ([87], [34]) at the passenger area were selected as objective functions to minimize. Both were assessed considering the most probable seastate. In this regard, as an attempt to include a preliminary design of the general arrangement, the dimensions and position of the passenger area on deck were optimized in order to maintain the average motion sickness at a minimum level. Furthermore, stability criteria from the High Speed Craft (HSC) code [73] was applied, for which Maxsurf Stability was used, as well as a constrain on the maximum allowed total ship resistance. Regarding the latter, the wave resistance was computed by Maxsurf Resistance [8] with slender-body theory and the method of Jamaluddin et al. (2013) was used to calculate total resistance, including the hull interference components. Both criteria enabled a study of the effects of horizontal clearance, for which the range between $S/LWL = 0.2$ to 0.4 was used. Additionally, although the horizontal clearance has not been directly included into seakeeping calculations, it was taken into account when computing the average MSI at the passenger area. This has been accomplished by defining a relationship between the length of the passenger area and its width (the later being a function of the horizontal clearance), for a given minimum allowed area, estimated based on a database of similar vessels resorting to regression analysis.

In order to quickly generate a large number of hull variations from the parent model, the well known parametric transformation method of Lackenby was used to impose combinations of *LCB* and C_b, varied within the range of +-10%, while maintaining the main dimensions of the underwater hull geometry, namely, *LWL*, *BWL* and displacement. For this purpose, Maxsurf Modeler was used. Results showed that from the 224 models generated, about 15% were neglected due to an excessively distorted geometry. In fact, an assessment of the limits of variation of C_b and *LCB* revealed that, for this particular parent hull, the maximum allowed increase of C_b value is +6%.

The optimum hull form was obtained with an increase of C_b by +3%, shifting *LCB* forward by +10% and by increasing the horizontal clearance by about 30 cm. The resulting geometry also benefited from an increased waterplane area (+12% of C_{wp}) and a lower design draft (-2.8%). It has also been verified that the parametric transformation generated an overall shorter hull (less 1.18 meters). Also, the optimum model appeared to be ”bulgier” at the forward part when compared to the parent one, as a

result of the increased *LCB*. In addition, it has been verified that the bulbous bow lost much of its original purpose, having almost vanished. The best option would have been to completely remove it and use, instead, a regular shaped bow or even more sophisticated solutions such as an axe-bow or an inverted bow-type configuration. Such solutions are typical in high-speed crafts. In any case, the performed optimization procedure did not include such considerations since the generated models were product of an automated transformation and no effort was put into further improving local geometry.

It became clear that the influence of the hull shape coefficients on heave and pitch motions is high. Although it was not possible to attribute the differences to one single cause, relationships have been established between variations of those coefficients and the resulting vessel motions. Yet, caution is advised when extrapolating such relations to cases that are not covered within the limited scope of the work presented here.

Results showed higher restoring coefficients and damping coefficients for the optimum model when compared to the parent one, both having a direct effect on the amplitudes of heave and pitch motions since they reflect, respectively, the stiffness and the damping of the equivalent mass-spring-damper system. In fact, at the resonance frequency (wavelengths of about 1.8-1.9*LWL*), the optimum model experienced heaving amplitudes 16.5% smaller than the parent one. A decrease of the same order was observed for pitch at wavelengths of about 2*LWL*. The forces associated with those coefficients are proportional to C_{wp} [15], which was in agreement with the presented results. Furthermore, by increasing BWL/DWL, improvements are obtained in the heave and pitch RAOs [81]. Again, since the optimum model presented a smaller *DWL* when compared to the parent one, the previous this relationship has also been verified. In any case, as stated before, given the large number of varied parameters, it is not possible to attribute the differences to single causes. The exciting force is proportional to C_{wp} [15]. However, when comparing the optimum with the parent model, results showed the opposite trend. This had to do with the inclusion of transom terms in the equations which decrease the exciting force for vessels with a large transom area. Given that the parent model had a smaller draft for the same value of *BWL*, its wetted transom area was higher, which cancelled the effects of the larger waterplane area of the optimum model on the exciting force. In terms of absolute vertical displacements and accelerations, considering that they are essentially a product of the combined heave and pitch motions, the same trends observed for heave and pitch motions applied. The optimum model experienced, at the resonance peak, vertical displacements 18% smaller, while in terms of accelerations the decrease was of about 11%.

As expected, the previous results allowed improvements in terms of the vessel responses on a seaway with the optimum model. With the purpose of assessing the effect of different combinations of *LCB* and C_b on RMS vertical acceleration responses, the whole range of generated models was analysed. Results showed that increasing *LCB* improves effectively the seakeeping performance, while the influence of C_b is much less significant, although decreasing it tend to improve RMS accelerations for low values of *LCB*. In this regard, the optimum model allowed decreasing RMS vertical acceleration responses at the bow by about 12% when compared to the parent model.

In terms of motion sickness, the improvements were more subtle. With the optimum model and by decreasing horizontal clearance by 30 cm, less 1.3% people experience motion sickness when compared to the parent model. The imposition of a fixed distance of 1.20 meters between the passenger area and the ship sides allowed larger horizontal clearance, i.e. wider passenger areas, to generate smaller incidences of motion sickness since, for the same area, the resulting smaller lengths capture more effectively the regions of lower MSI values. From this perspective, it could be possible to improve this result. However, it has been verified that the gains would not be significant. Also, it was taken into account that wider decks would imply higher building costs. The final position of the passenger area begins 4.24 meters forward of the aft end of the ship (exceeding the minimum imposed distance of 2 meters) and extends for 5.76 meters with a width of 8.68 meters, summing up to 50 square meters. This represents 16% of the total deck area, which leaves enough free space for cargo both in the aft part of the deck (11%), as in the forward part (65%). Again, this optimization considered the most probable seastate. Furthermore, the differences in terms of motion sickness were not significant when optimizing for other seastates, although considerable shifts in the position of the passenger area have been verified. Still with respect to motion sickness, an interesting phenomenon was observed. Improvements in terms of MSI were expected as the RMS vertical acceleration responses decrease. However, the influence of frequencies in the MSI model is quite significant and that linear tendency was only observed for average frequencies up to 0.16 Hertz. In fact, within the range of 0.35 to 0.37 Hertz (the average frequency range experienced by all models), if the decrease in accelerations between two models is not significant, the resulting decrease in frequency will lead to higher incidences of motion sickness. This is in agreement with the idea that humans are capable of tolerating higher accelerations at higher frequencies without experiencing the same tendency towards motion sickness [93]. This effect has been identified when studying the variation of C_b which, as stated before, is not very effective in improving seakeeping performance with respect to motions in the vertical plane. Furthermore, understanding this behaviour of the motion sickness model proposed by McCauley et al. (1976) was very useful when analysing the optimized position of the passenger area on deck. In fact, results for the distribution of RMS accelerations on deck revealed an expected concentration of the lower values around the centre of gravity. However, a correspondence with the region of lower motion sickness incidences was not verified, which led to a positioning of the passenger area aft of the centre of gravity where RMS accelerations are not minimum. Again, this shows the influence of frequencies in the MSI model that tend to attenuate the more intuitive effect of high accelerations.

Results showed that the interference effect between the hulls of the catamaran is indeed quite predominant from the point of view of hull resistance. Larger horizontal clearances decrease the interference effect and thus, lead to smaller total resistance coefficients. In any case, it has been showed that optimizing for hull resistance is incompatible with maximizing seakeeping performance. In order to use both as objective functions, it is necessary to find a compromise. Therefore, for this dissertation, the imposed resistance criterion was based on a maximum total hull resistance equal to the parent model with the original horizontal clearance. The minimum value that allowed obtaining the minimum acceleration responses while complying with this restriction was $S/LWL = 0.298$, corresponding to the already referred

decrease of 30 cm when compared to the parent horizontal clearance. These results allowed to slightly decrease hull resistance, representing consuming less 1.88 kW of effective power at 25 knots.

Regarding stability, in order to study different horizontal clearances, each generated model would have to be modelled individually, which was not feasible. Therefore, the author was forced to stick to the parent S value, with which all models satisfied the imposed criteria in terms of minimum heeling angle of maximum GZ and minimum area under GZ curve. It is further added that from the parent horizontal clearance ratio of $S/LWL = 0.287$ to the optimized one ($S/LWL = 0.298$), it is expected that no significant changes occur, although smaller horizontal clearances generally imply less transverse stability and an increase of the heeling angle at which the maximum GZ value occurs. With the parent horizontal clearance this angle corresponds to 16°.

Finally, an operability assessment of the optimized catamaran operating at two different speeds (service and 90% of maximum speed) was carried out based on limiting seakeeping criteria imposed by the High Speed Craft (HSC) code and DNV-GL in terms of the average 1% highest accelerations. Although the wave scatter diagram provided by Costa et al. (2001) did not present discretized enough data (probabilities of occurrence provided for ranges of significant wave heights and peak periods), estimates of the operability index were presented. From a quite conservative perspective, the fast crew supplier should be able to operate at the Alentejo basin only 52% of the time. In a more optimistic scenario, the author expects an operability index of 91%. Furthermore, it is likely that the effective operability is much closer to the upper boundary. Also, a decrease in operability is expected at higher speeds, given the more strict limitations imposed by the classification societies.

This page was intentionally left blank.

Chapter 5

Conclusions

As a result of the widespread development of high-speed crafts and its use to transport passengers, the amount of research on the assessment and optimization of the seakeeping behaviour is vast. In fact, the requirement to operate well at high speeds, often in adverse weather conditions, is critical for such vessels. Furthermore, the present demands of the industry, which commonly resort to catamarans for this purpose, reinforce the relevance of the subject and suggests that much work is yet to be done.

A typical application of catamarans is as fast crew supply vessels, quite commonly found in the offshore industry. From this perspective, the work of Carvalho (2016), who conceptualized a potential deep offshore hydrocarbon field located 50 Km off the coast of Sines, at the Alentejo Basin, Portugal, laid the ideal foundation for a solid case study to be developed for this dissertation.

With this regard, a parent catamaran model kindly provided by DAMEN Shipyards was optimized in terms of seakeeping performance to operate at 25 knots as a fast crew supplier used in the transport of 12 passengers to an offshore platform at the Alentejo basin, for which the work of Costa et al. (2001) was used to simulate the seastates at the location.

Despite the development of powerful, state of the art, methods to predict the seakeeping behaviour, namely CFD solvers, the fact that the chosen tool was to be embedded into an optimization procedure was an important limitation. Strip theories, even considering their limited range of applications (slow speeds, slender hulls, small motion amplitudes, inviscid fluid assumptions), continue to be a meaningful research topic due to the low computational power required and the fast calculations provided. They are particularly useful within academic contexts and during early design stages. With respect to the type of motions to study, considering the higher transverse stability of double-hulled vessels, it seemed reasonable to assume that the most critical situations come from heave and pitch motions upon head seas. Therefore, these were the main focus.

5.1 Achievements

For the purpose of selecting a strip-theory code to be used in the optimization procedure, a benchmarking study was carried out, a work that comprised the entire first part of this dissertation. Three software packages were considered, namely, PDStrip, a public-domain code developed by Söding and Bertram (2009), Fonseca, an in-house code developed at CENTEC (Centre for Marine Technology and Ocean Engineering) in Técnico Lisboa (IST) (linear version of Fonseca and Guedes Soares, 1998) and the commercially available software Maxsurf, for which the module Motions [7] was used. Despite a few non-linear considerations by PDStrip, all the codes are linear and the computations are carried out in the frequency domain, following in a general sense the commonly cited work of Salvesen et al. (1970). PDStrip, includes the additional contributions of a longitudinal force associated with surging motion and a non-linear transverse drag force. Furthermore, Fonseca neglects the contribution of transom terms while the remaining two allow their inclusion. PDStrip additionally has into account the contribution of transom terms into the longitudinal Froude-Krylov force and the restoring coefficient C_{53}. Their numerical predictions were compared with model tests of a catamaran [63] and the fast mono-hull Model 5 [15]. The goal was to assess not only the accuracy in computing heave and pitch motions of catamarans but their capacity to do it at high speeds. It is important to note that none of these codes included phenomenon that are at the origin of the hydrodynamic interaction between demi-hulls. However, these are less noticeable if motions are restricted to heave and pitch upon head seas, as was the case and thus, an assumption about negligible hull interaction was exploited. The following conclusions were drawn:

1. It has been shown that with increasing vessel speed, the accuracy in predicting heave and pitch motions with strip theory decreases, a well-known limitation of such theories and a general principle that must be taken into account.

2. For the higher Froude numbers ($F_n = 0.6, 1.14$), heave and pitch response peaks were generally overestimated. Also, it was visible that the inclusion of transom terms damped the system, being generally beneficial for predicting heave and pitch motions, i.e., PDStrip and Maxsurf Motions with transom terms performed better.

3. For $F_n = 0, 0.2, 0.4, 0.57$, not using transom terms was a better option, for which Fonseca seemed to be the most suited choice. PDStrip, without transom terms, also performed reasonably well.

4. The order of magnitude of the differences between numerical and experimental results for the case of the fast mono-hull and the catamaran seemed to indicate that all the studied codes performed better with the fast mono-hull. This was an expected result since these methods neglect phenomenon associated with hull interaction. In any case, PDStrip with transom terms suggested reasonably good predictions with heaving/pitching catamarans being capable of determining the resonance peak, both in terms of frequency and amplitude, with sufficient accuracy, particularly at higher speeds.

5. PDStrip allowed a large number of ship sections and offset points for geometry discretization, which improves accuracy during seakeeping computations, as well as a large number of wave-

lengths within a wide range to be used for motion results, being advantageous for a proper definition of the complete frequency spectrum.

6. From the perspective of embedding the code into an optimization procedure where a minimum level of automation is required, PDStrip can be conveniently compiled into an executable file with separate input text files. Finally, as an open source Fortran code, it is possible to edit and improve PDStrip if necessary, a useful characteristic bearing future work in mind. In any case, it is important to stress out the total unintelligibility of the output files of PDStrip, as well as the difficulties presented when looking into the source code. This aspect of PDStrip have already been mentioned by authors like Palladino et al. (2006) who faced the same type of problems. On top of that, the code had to be modified so that the needed results were displayed. In summary, working with PDStrip proved to be extremely laborious.

Throughout the second half of the work, PDStrip was used as seakeeping tool to optimize the DAMEN catamaran. MATLAB was used as the engine of the optimization procedure. The RMS vertical acceleration responses at the bow and the Motion Sickness Incidence (MSI) for 65 minutes of exposure [87] at the passenger area were selected as objective functions to minimize. Both were assessed considering the most probable seastate. In this regard, as an attempt to include a preliminary design of the general arrangement, the dimensions and position of the passenger area on deck were optimized in order to maintain the average motion sickness at a minimum level. Furthermore, stability criteria from the High Speed Craft (HSC) code [73] was applied, as well as a constraint on the maximum allowed total hull resistance equal to the parent model (with the parent horizontal clearance). Regarding the latter, the wave resistance was computed with slender-body theory and the empirical method of Jamaluddin et al. (2013) was used to calculate total resistance, including the hull interference components. The effects of horizontal clearance ratios between 0.2 and 0.4 were studied with respect to resistance, stability and motion sickness incidence. In order to quickly generate a large number of hull variations from the parent model, the well known parametric transformation method of Lackenby was used to impose combinations of *LCB* and C_b, varied within the range of +-10%, while maintaining the main dimensions of the underwater hull geometry, namely, *LWL*, *BWL* and displacement. For this purpose, Maxsurf Modeler was used. The main conclusions of this work are shown bellow.

1. Results showed that increasing *LCB* decreases effectively the RMS vertical acceleration responses at the bow, while the influence of C_b is much less significant, although decreasing it tend to improve the seakeeping performance for low values of *LCB*. In this regard, the optimum model allowed decreasing RMS accelerations by about 12% when compared to the parent model.

2. In terms of motion sickness, the improvements were more subtle. With the optimum model, less 1.3% people experience motion sickness when compared to the parent model. The impact of frequencies on the MSI model has been confirmed, which revealed that humans are capable of withstanding higher acceleration levels with low incidences of motion sickness if the experienced frequency is high enough.

3. The hull form that allowed to capture the minimum RMS accelerations at the bow within the whole family of possible solutions was obtained with an increase of C_b by +3%, shifting *LCB* forward by +10% and by increasing the horizontal clearance by about 30 cm. The resulting geometry also benefited from an increased waterplane area (+12% of C_{wp}) and a lower design draft (-2.8%). It has also been verified that the parametric transformation generated an overall shorter hull (less 1.18 meters).

4. Results suggested that heave and pitch motions benefit directly from an increase of C_{wp} and BWL/DWL since they associated with the stiffness and damping of the equivalent mass-spring-damper system. At the resonance frequency (wavelengths of about 1.8-1.9*LWL*), the optimum model experienced heaving amplitudes 16.5% smaller than the parent one. A decrease of the same order was observed for pitch at wavelengths of about 2*LWL*. Consequently, absolute vertical displacements and accelerations at the remote locations and the vessel responses upon the specified seaway improved as well.

5. The final position of the passenger area was set at 4.24 meters forward of the aft end of the ship (exceeding the minimum imposed distance of 2 meters) extending for 5.76 meters with a width of 8.68 meters, which sums up to 50 square meters. This represents 16% of the total deck area, which leaves enough free space for cargo both in the aft part of the deck (11%), as in the forward part (65%). Results showed that different horizontal clearances position the passenger area in different locations without significantly affecting the incidence of motion sickness. The same applies to the optimization of the passenger area considering other seastates rather than the most probable.

6. Regarding resistance, larger horizontal clearances decrease the interference effect and thus, lead to smaller total resistance forces. The minimum value that allowed obtaining the minimum acceleration responses while maintaining the total resistance of the parent model was $S/LWL = 0.298$, corresponding to the already referred decrease of 30 cm when compared to the parent horizontal clearance. These results allowed a decrease in consumption of less 1.88 kW of effective power at 25 knots.

7. With respect to stability, only the parent horizontal clearance was evaluated, with which all models satisfied the criteria imposed by the classification societies. Given the small difference to the parent horizontal clearance, it is expected that no significant changes occur, although smaller horizontal clearances generally imply less transverse stability and an increase of the heeling angle at which the maximum GZ value occurs.

8. Finally, an operability assessment of the optimized catamaran operating at two different speeds was carried out based on limiting seakeeping criteria imposed by the High Speed Craft (HSC) code and DNV-GL in terms of the average 1% highest accelerations. Although the wave scatter diagram provided by Costa et al. (2001) did not present discretized enough data (probabilities of occurrence provided for ranges of significant wave height and peak periods), estimates of the

operability index were presented. From a quite conservative perspective, the fast crew supplier should be able to operate at the Alentejo basin only 52% of the time. In a more optimistic scenario, the author expects an operability index of 91%. Furthermore, it is likely that the effective operability is much closer to the upper boundary. Also, a decrease in operability is expected at higher speeds, given the more strict limitations imposed by the classification societies.

5.2 Future Work

With respect to the first part of this dissertation, i.e., benchmarking study of strip theory codes, the following aspects stand as suggestions for future work:

1. A detailed analysis of the mathematical causes for the divergences between the motion predictions of each code by comparing the global hydrodynamic coefficients individually and evaluating the results based on the different formulations. In fact, part of this work has already been done (refer to Appendix A.2 and B.2) but the scope of the work of this dissertation and the limited amount of time to accomplish it forced the author to put it on hold.

2. With respect to PDStrip, it could be interesting to assess the actual influence of the additional contributions of the longitudinal force associated with surging motion and the transverse drag force on heave and pitch motions. Furthermore, given the impenetrable nature of the output files it seems clear that the code needs improvement.

3. In order to assess the influence of viscous damping in heave and pitch motions of catamarans, a direct comparison between possible viscous and potential contributions could be performed in the future. The conclusion from such study could lead to improvements in the predictions of catamaran motions with strip-methods.

4. Given the difficulty in finding publicly available data from model testing of high speed catamarans, particularly with variable horizontal clearance ratios S/LWL, the author concludes that this is an under developed research topic that is worth investing in.

Regarding the optimization procedure presented in the second part, a few suggestions are also worth mentioning:

1. Assess the seakeeping behaviour of the catamaran considering a larger range of wave headings in other to approach the problem in a more realistic way. This would imply using or developing a numerical tool that considers the interaction effect between the demi-hulls.

2. Generate hull variations by imposing combinations of *LCB* and C_{wp}, rather than C_b which does not affect the seakeeping behavior significantly. In any case, the matrix type distribution of those parameters is still advised since it allows studying seakeeping trends of the variation of only one parameter.

3. Develop a method to parametrically vary the hull shape coefficients while keeping the remaining ones constant, particularly the ones that effectively affect seakeeping performance like *LCB*, C_{wp} and BWL/BW, so that the conclusions presented in this dissertation can be further refined. This would imply selecting parameters that do not depend on each other.

4. Optimize the seakeeping behaviour of the catamaran resorting to an alternative procedure. This could be achieved by using, for instance, genetic algorithms which are based on the idea of natural selection and find optimum solutions more effectively.

5. Include into the optimization procedure a module for economical evaluation of the designs to support the decision making process or even to impose design constraints. This would have been helpful for this dissertation when evaluating the hull resistance and motion sickness, both functions of the horizontal clearance, against the construction costs.

6. Find an alternative method to perform stability analyses with variable horizontal clearance ratios S/LWL.

7. Find an alternative software for geometry handling and parametric transformation, rather than Maxsurf Modeler. Even though no comments have been made regarding this topic, this dissertation shed some light into the very limited capabilities of Maxusrf Modeler in terms of exporting the geometries within an automated procedure (via VBAs). This problem was solved resorting to the system command of Windows which allowed to remotely reach the user interface and perform the needed routines. However this increased running time considerably.

8. Optimize the position of the passenger area together with the whole superstructure, which would imply a previous study regarding the needed infrastructures.

9. Obtain discretized wave data relative to the seaway in which the vessel will operate, rather than have it as ranges of significant wave heights and peak periods. This allows a more accurate prediction of the operability index. Furthermore, it would be interesting if seasonal data were available.

10. Given that the bulbous bow of model 150 lost much of its original purpose, it would have been interesting to re-model the geometry in that region and study the effects that different solutions have on seakeeping performance, e.g, using a regular shaped bow, an axe-bow or an inverted bow-type configuration. A detailed description of the bow cross sections would probably allow an evaluation with PDStrip.

Bibliography

[1] Ang, J. H., Goh, C., and Li, Y. (2015). Hull form design optimisation for improved efficiency and hydrodynamic performance of 'ship-shaped' offshore vessels. In *International Conference on Computer Applications in Shipbuilding (ICCAS) 2015*, Bremen, Germany. Royal Institution of Naval Architects, RINA.

[2] Arribas, F. P. and Fernandez, J. A. C. (2006). Strip theories applied to the vertical motions of high speed crafts. *Ocean Engineering*, 33(8):1214–1229.

[3] Augener, P. H. and Krüger, S. (2014). Computation of drift forces for dynamic positioning within the very early design stage of offshore wind farm installation vessels. In *Proceedings of the ASME 2014, 33rd International Conference on Ocean, Offshore and Arctic Engineering*, San Francisco, California, USA. American Society of Mechanical Engineers.

[4] Bagheri, L., Ghassemi, H., and Dehghanian, A. (2014). Optimizing the seakeeping performance of ship hull forms using genetic algorithm. *The International Journal on Marine Navigation and Safety of Sea Transportation (TransNav)*, 8(1):49–57.

[5] Bai, K. J. and Yeung, R. W. (1974). Numerical solutions to free-surface flow problems. In *Proceedings of the 10th Symposium on Naval Hydrodynamics*, pages 609–647, Cambridge, Massachusetts, USA.

[6] Beck, R. F. and Allan, R. (1991). Time-domain analysis for predicting ship motions. In *Symposium on the Dynamics of Marine Vehicles and Structures in Waves*, pages 49–65, Brunel University, Uxbridge, U.K. Royal Institution of Naval Architects, RINA.

[7] Bentley Systems, Incorporated (2013a). *Maxsurf Motions, Windows Version 20, User Manual*. Bentley Systems, Incorporated.

[8] Bentley Systems, Incorporated (2013b). *Maxsurf Resistance, Windows Version 20, User Manual*. Bentley Systems, Incorporated.

[9] Bentley Systems, Incorporated (2016a). *Maxsurf Modeler, Windows Version 21, User Manual*. Bentley Systems, Incorporated.

[10] Bentley Systems, Incorporated (2016b). *Maxsurf Stability, Windows Version 21, User Manual*. Bentley Systems, Incorporated.

[11] Bertram, V. (2000). *Practical Ship Hydrodynamics*. Butterworth Heinemann. ISBN: 0 7506 4851 1.

[12] Bertram, V. and Söding, H. (1991). A panel method for ship motions. In *Proceedings of the 6th International Workshop on Water Waves and Floating Bodies*, Woods Hole, Massachusetts, USA.

[13] Biliotti, I., Brizzolara, S., Viviani, M., Vernengo, G., Ruscelli, D., Galliussi, M., Guadalupi, D., and Manfredini, A. (2011). Automatic parametric hull form optimization of fast naval vessels. In *Proceedings of the 11th International Conference on Fast Sea Transportation, FAST2011*, pages 294–301, Honolulu, Hawaii, USA.

[14] Birmingham, R. (2004). Design for stability and for instability - finding the right balance for small craft. *The international HISWA Symposium on yacht design and yacht construction*.

[15] Blok, J. J. and Beukelman, W. (1984). The high-speed displacement ship systematic series hull forms - seakeeping characteristics. *Transactions of the Society of Naval Architects and Marine Engineers, SNAME*, 92:125–150.

[16] Bordogna, G. (2013). The aero-hydrodynamic characteristics of yachts sailing upwind in waves. Master's thesis, TU Delft, Delft University of Technology.

[17] Bossak, M. A. (1998). Simulation based design. *Journal of Materials Processing Technology*, 76(1):8–11.

[18] Brizzolara, S. (2003). Parametric optimisation of SWATH hull forms by systematic use of CFD methods. In *Proceedings of the 13th International Offshore and Polar Engineering Conference*, number I-03-381, Honolulu, Hawaii, USA. International Society of Offshore and Polar Engineering (ISOPE).

[19] Brizzolara, S. (2004). Parametric optimization of swat-hull forms by a viscous-inviscid free surface method driven by a differential evolution algorithm. In *Proceedings of the 25th Symposium on Naval Hydrodynamics*, volume 5, pages 47–64, St. John's, Newfoundland and Labrador, Canada.

[20] Brizzolara, S., Bonfiglio, L., and de Medeiros, J. S. (2013). Influence of viscous effects on numerical prediction of motions of SWATH vessels in waves. *Ocean Systems Engineering*, 3(3):219–236.

[21] Cabrita-Mendes, A. (2015). Mais de metade do mar português tem potencial petrolífero. `http://www.jornaldenegocios.pt/mercados/materias-primas/petroleo/detalhe/mais-de-metade-do-mar-portugues-tem-potencial-petrolifero`.

[22] Campana, E. F., Peri, D., Tahara, Y., and Stern, F. (2006). Shape optimization in ship hydrodynamics using computational fluid dynamics. *Computer methods in applied mechanics and engineering*, 196(1):634–651.

[23] Carrica, P. M., Wilson, R. V., and Stern, F. (2006). Unsteady rans simulation of the ship forward diffraction problem. *Computers and Fluids*, 35(5):545–570.

[24] Carrica, P. M., Wilson, R. V., and Stern, F. (2007). Ship motions using single-phase level set with dynamic overset grids. *Computers and Fluids*, 36(9):1415–1433.

[25] Carvalho, A. (2016). Análise do modelo de desenvolvimento de campos de hidrocarbonetos aplicado à bacia do alentejo. Master's thesis, Universidade de Aveiro.

[26] Castiglione, T., Stern, F., Bova, S., and Kandasamy, M. (2011). Numerical investigation of the seakeeping behavior of a catamaran advancing in regular head waves. *Ocean Engineering*, 38(16):1806–1822.

[27] Centeno, R., Fonseca, N., and Guedes Soares, C. (2000). Prediction of motions of catamarans accounting for viscous effects. *International shipbuilding Progress (ISP)*, 47(451):303–323.

[28] Centeno, R. and Guedes Soares, C. (1999). Ship motion analysis of a catamaran series. In *Proceedings of the 5th International Symposium on High Speed Marine Vehicles*, number V5, pages V5.1–V5.13, Capri, Italy.

[29] Centeno, R., Varyani, K. S., and Guedes Soares, C. (2001). Experimental study on the influence of hull spacing on hard-chine catamaran motions. *Journal of Ship Research*, 45(3):216–227.

[30] Cepowski, T. (2010). Influence analysis of changes of design parameters of passenger-car ferries on their selected sea-keeping qualities. *Polish Maritime Research*, 17(1):25–32.

[31] Cepowski, T. (2012). The prediction of the motion sickness incidence index at the initial design stage. *Zeszyty Naukowe/Akademia Morska w Szczecinie*, 103(31):45–48.

[32] Chan, H. S. (1993). Prediction of motion and wave loads of twin-hull ships. *Marine Structures*, 6(1):75–102.

[33] Chapman, R. B. (1980). Time-domain method for computing forces and moments acting on three dimensional surface-piercing ship hulls with forward speed. Technical Report SAI-462-80-560-LJ, Science Applications, Inc, La Jolla, California, USA.

[34] Colwell, J. L. (1989). Human factors in the naval environment: a review of motion sickness and biodynamic problems. Technical Report DREA-TM-89-220, Defence Research Establishment Atlantic,, Dartmouth, Nova Scotia, Canada.

[35] Costa, M., Silva, R., and Vitorino, J. a. (2001). Contribuição para o estudo do clima de agitação marítima na costa portuguesa. In *2^{a} Jornadas Portuguesas de Engenharia Costeira e Portuária*, number 20, Sines, Portugal.

[36] Cummins, W. E. (1962). The impulse response function and ship motions. *Schiffstechnik*, 47(9):101–109.

[37] Datta, R., Fonseca, N., and Guedes Soares, C. (2013). Analysis of the forward speed effects on the radiation forces on a fast ferry. *Ocean Engineering*, 60:136–148.

[38] Datta, R., Rodrigues, J. M., and Guedes Soares, C. (2011). Study of the motions of fishing vessels by a time domain panel method. *Ocean Engineering*, 38:782–792.

[39] Davis, M. R. and Holloway, D. S. (2003). The influence of hull form on the motions of high speed vessels in head seas. *Ocean Engineering*, 30(16):2091–2115.

[40] DNV-GL (2012). *Rules for Classification and Construction, I Ship Technology, 3 Special Craft, 1 High Speed Craft*. DNV GL, 2012 edition.

[41] Dubrovsky, V. A. (2014). Application and development of multi-hulls. *Journal of Ocean, Mechanical and Aerospace*, 6:1–7.

[42] Dudson, E. and Rambech, H. J. (2003). Optimisation of the catamaran hull to minimise motions and maximise operability. In *Proceedings of the 7th International Conference on Fast Sea Transportation, FAST2003*, number P2003-7, Ischia, Italy.

[43] ENMC (2015). Mapa de concessões em portugal continental. `http://www.enmc.pt/`. Entidade Nacional para o Mercado de Combustíveis (ENMC).

[44] Faltinsen, O., Zhao, R., and Umeda, N. (1991). Numerical predictions of ship motions at high forward speed. *Philosophical Transactions: Physical Sciences and Engineering*, 334(1634):241–252.

[45] Finkelstein, A. B. (1957). The initial value problem for transient water waves. *Communications on Pure and Applied Mathematics*, 10(4):511–522.

[46] Fonseca, N. (2009). Apontamentos de dinâmica e hidrodinâmica do navio.

[47] Fonseca, N. and Guedes Soares, C. (1994). Time domain analysis of vertical ship motions. In *Marine, Offshore and Ice Technology*, pages 224–243, Southampton, UK. Computational Mechanics Publications.

[48] Fonseca, N. and Guedes Soares, C. (1998). Time-domain analysis of large-amplitude vertical ship motions and wave loads. *Journal of Ship Research*, 42(2):39–153.

[49] Fonseca, N. and Guedes Soares, C. (2002a). Comparison of numerical and experimental results of nonlinear wave-induced vertical ship motions and loads. *Journal of Marine Science and Technology*, 6(4):193–204.

[50] Fonseca, N. and Guedes Soares, C. (2002b). Sensitivity of the expected ships availability to different seakeeping criteria. In *Proceedings of 21st International Conference on Offshore Mechanics and Artic Engineering (OMAE'02)*, pages 595–603, Oslo, Norway.

[51] Fonseca, N. and Guedes Soares, C. (2004a). Experimental investigation of the nonlinear effects on the statistics of vertical motions and loads of a containership in irregular waves. *Journal of Ship Research*, 48(2):148–167.

[52] Fonseca, N. and Guedes Soares, C. (2004b). Experimental investigation of the nonlinear effects on the vertical motions and loads of a containership in regular waves. *Journal of Ship Research*, 48(2):118–147.

[53] Fonseca, N. and Guedes Soares, C. (2004c). Validation of a time-domain strip method to calculate the motions and loads on a fast monohull. *Applied Ocean Research*, 26(6):256–273.

[54] Fonseca, N. and Guedes Soares, C. (2005). Comparison between experimental and numerical results of the nonlinear vertical ship motions and loads on a containership in regular waves. *International Shipbuilding Progress*, 52(1):57–89.

[55] Fonseca, N. and Santos, C. (2008). *Manual do programa de cálculo do comportamento de navios no mar (em preparação)*. Secção Autónoma de Engenharia Naval, Instituto Superior Técnico.

[56] Frank, W. (1967). Oscillation of cylinders in or below the free surface of deep fluids. Technical Report 2375, Naval Ship Research and Development Centre, Washington DC, USA.

[57] Gasparotti, C. and Rusu, L. (2013). Seakeeping performance assessment for a containership in a specific sea area. *Mechanical Testing and Diagnosis*, 3(1):38–48.

[58] Ghassemi, H., Majdfar, S., and Gill, V. (2015). Calculations of the heave and pitch rao's for three different ship's hull forms. *Journal of Ocean, Mechanical and Aerospace - Science and Engineering*, 22:1–8.

[59] Gourlay, T., von Graefe, A., Shigunov, V., and Lataire, E. (2015). Comparison of aqwa, gl rankine, moses, octopus, pdstrip and wamit with model test results for cargo ship wave-induced motions in shallow water. In *Proceedings of the ASME 2015, 34th International Conference on Ocean, Offshore and Arctic Engineering*, St. John's, Newfoundland, Canada. American Society of Mechanical Engineers.

[60] Grigoropoulos, G. J. (2004). Hull form optimization for hydrodynamic performance. *Marine Technology*, 41(4):167–182.

[61] Grigoropoulos, G. J. and Chalkias, D. S. (2010). Hull-form optimization in calm and rough water. *Computer-Aided Design*, 42(11):977–984.

[62] Guedes Soares, C., Fonseca, N., and Centeno, R. (1995). Seakeeping performance of fishing vessels in the portuguese economic zone. In *Proceedings of the International Conference on Seakeeping and Weather*, pages 1–10, London, England.

[63] Guedes Soares, C., Fonseca, N., Santos, P., and Maron, A. (1999). Model tests of the motions of a catamaran hull in waves. In *Proceedings of the International Conference on Hydrodynamics of High-Speed Craft*, pages 1–10, London, UK. Royal Institution of Naval Architects (RINA).

[64] Guo, Z., Ma, Q., and Hu, X. (2016). Seakeeping analysis of a wave-piercing catamaran using urans-based method. *International Journal of Offshore and Polar Engineering*, 26(1):48–56.

[65] Guo, Z., Ma, Q., and Lin, Z. (2014). A comparison of seakeeping predictions for wave-piercing catamarans using stf and urans methods. In *Proceedings of the 24th International Ocean and Polar Engineering Conference*, number I-14-420, pages 746–752, Busan, Korea. International Society of Offshore and Polar Engineering (ISOPE).

[66] Hadler, J. B., Lee, C. M., Birmingham, J. T., and Jones, H. D. (1974). Ocean catamaran seakeeping design based on the experiences of usns hayes. In *Proceedings of the SNAME Annual Meeting*, pages 126–161, New York, USA.

[67] Hearn, G. E., Hills, W., and Sarioz, K. (1990). Making seakeeping analysis work for the designer: a new practical approach. this paper only serves as note of relevant research during its time. i could not find the actual article. In *Proceedings of the 19th Scientific and Methodological Seminar on Ship Hydrodynamics, SSMH 90*, Varna, Bugaria.

[68] Hearn, G. E., Hills, W., and Sarioz, K. (1991). A hydrodynamic design methodology for conceptual ship design. In *Proceedings of the 7th International Conference on Computer Applications in the Automation of Shipyard Operation and Ship Design, ICCAS 1991*, pages 113–129, Rio de Janeiro, Brazil.

[69] Hearn, G. E., Hills, W., and Sarioz, K. (1992). Practical seakeeping for design: a ship shape approach. In *Transactions of the Royal Institution of Naval Architects, RINA 134*, volume 134, pages 215–235.

[70] Hermundstad, O. A., Aarsnes, J. V., and Moan, T. (1999). Linear hydroelastic analysis of high-speed catamarans and monohulls. *Journal of Ship Research*, 43(1):48–63.

[71] Hoffman, D. and Karst, O. J. (1975). The theory of the rayleigh distribution and some of its applications. *Journal of Ship Research*, 19(3):12–191.

[72] Holloway, D. S. and Davis, M. R. (2006). Ship motion computations using a high froude number time domain trip theory. *Journal of Ship Research*, 50(1):15–30.

[73] IMO (2008). *International code of safety for high-speed craft (2000)*. IMO, Maritime Safety Committee (MSC), MSIS 34 (2008) edition.

[74] IMO (2009). *Guidelines for uniform operating limitations of high-speed craft*. IMO, Maritime Safety Committee (MSC), MSC.1/circ.1329 edition.

[75] Insel, M. and Molland, A. F. (1992). An investigation into the resistance components of high speed displacement catamarans. In *Transactions of the Royal Institution of Naval Architects, RINA 134*, volume 134, pages 1–20.

[76] Jacobs, W. R. (1958). The analytical calculation of ship bending moments in regular waves. *Journal of Ship Research*, 2(1):20–29.

[77] Jamaluddin, A., Utama, I. K. A. P., Widodo, B., and Molland, A. F. (2013). Experimental and numerical study of the resistance component interactions of catamarans. *Journal of Engineering for the Maritime Environment*, 227(1):51–60.

[78] Kapsenberg, G. K. (2005). Finding the hull form for given seakeeping characteristics. Technical report, MARIN, Wageningen, Netherlands.

[79] Korvin-Kroukovsky, B. V. and Jacobs, W. R. (1957). Pitching and heaving motions of a ship in regular waves. In *Transactions of the Society of Naval Architects and Marine Engineers, SNAME*, volume 65, pages 590–632.

[80] Kring, D. C. (1994). *Time domain ship motions by a three-dimensional Rankine panel metho*. Phd thesis, Massachusetts Institute of Technology, Massachusetts, USA.

[81] Kukner, A. and Sarioz, K. (1995). High speed hull form optimisation for seakeeping. *Advances in Engineering Software*, 22(3):179–189.

[82] Lee, C. M. and Curphey, R. M. (1977). Prediction of motion, stability, and wave load of small-waterplane-area, twin-hull ships. *Transactions of the Society of Naval Architects and Marine Engineers, SNAME*, 85:94–130.

[83] Lee, C. M., Jones, H. D., and M, C. R. (1973). Prediction of motion and hydrodynamic loads of catamarans. *Marine Technology*, 10(4):392–405.

[84] Maisonneuve, J. J., Harries, S., Marzi, J., Raven, H. C., Viviani, U., and Piippo, H. (2003). Towards optimal design of ship hull shapes. In *Proceedings of the 8th International Marine Design Conference, IMDC 2003*, pages 31–42, Athens, Greece.

[85] Marón, A., Ponce, J., Fonseca, N., and Guedes Soares, C. (2004). Experimental investigation of a fast monohull in forced harmonic motions. *Applied Ocean Research*, 26(6):241–255.

[86] Martins, J. M. (2015). Conferência: Pesquisa de petróleo em portugal. Entidade Nacional para o Mercado de Combustíveis (ENMC). Fundação Calouste Gulbenkian, Lisboa, Portugal.

[87] McCauley, M. E., Royal, J. W., Wylie, C. D., O'Hanlon, J. F., and Mackie, R. R. (1976). Motion sickness incidence: exploratory studies of habituation, pitch and roll, and the refinement of a mathematical model. Technical Report 1733-2, Office of Naval Research, Department of the Navy, Goleta, California, USA.

[88] Moraes, H. B., Vasconcellos, J. M., and Almeida, P. M. (2007). Multiple criteria optimization applied to high speed catamaran preliminary design. *Ocean Engineering*, 34(1):133–147.

[89] Moreno, C. A. S. (1993). *Interferência hidrodinâmica no comportamento em ondas*. PhD thesis, Instituto Alberto Luiz Coimbra de Pós-Graduação e Pesquisa de Engenharia, Universidade Federal do Rio de Janeiro (COPPE/UFRJ), Rio de Janeiro, Brasil.

[90] Mousaviraad, S. M., Carrica, P. M., and Stern, F. (2010). Development and validation of harmonic wave group single-run procedure for rao with comparison to regular wave and transient wave group procedures using urans. *Ocean Engineering*, 37(8):653–666.

[91] Nowacki, H. and Papanikolaou, A. (1990). Konzeptentwurf und hydrodynamische optimierung fur eine SWATH passagier/auto fahre fur den mittelmeerraum. In *Proceedings of the STG-Sommertagung*, Luzern, Switzerland.

[92] Ogilvie, T. F. and Tuck, E. O. (1969). A rational strip theory of ship motions: Part i. Technical Report 013, Department Naval Architecture and Marine Engineering, College of Engineering, The University of Michigan, USA, Ann Arbor, Michigan, USA.

[93] O'Hanlon, J. F. and McCauley, M. E. (1973). Motion sickness incidence as a function of the frequency and acceleration of vertical sinusoidal motion. Technical Report 1733-1, Office of Naval Research, Department of the Navy, Goleta, California, USA.

[94] Ohkusu, M. and Takaki, M. (1971). On the motion of twin hull ship in waves. *Journal of the Society of Naval Architects of Japan*, 1971(129):29–40.

[95] Palladino, F., Bouscasse, B., Lugni, C., and Bertram, V. (2006). Validation of ship motion functions of pdstrip for some standard test cases. In *9th Numerical Towing Tank Symposium*, Le Croisic, France.

[96] Papanikolaou, A. (1990). Hydrodynamic and technoeconomical optimization of a high-speed SWATH passenger/car ferry. *Tecnica Italiana*, 55(1):23–35.

[97] Papanikolaou, A., Kaklis, P., Koskinas, C., and Spanos, D. (1996). Hydrodynamic optimization of fast displacement catamarans. In *Proceedings of the 21st International Symposium on Naval Hydrodynamics (ONR 96)*, pages 697–714, Trondheim, Norway.

[98] Papanikolaou, A., Zaraphonitis, G., and Androulakakis, M. (1991). Preliminary design of a high-speed SWATH passenger/car ferry. *Marine technology*, 28(3):129–141.

[99] Pierson, W. J. and St Denis, M. (1953). On the motion of ships in confused seas. *Transactions of the Society of Naval Architects and Marine Engineers, SNAME*, 61:280–332.

[100] Piscopo, V. and Scamardella, A. (2015). The overall motion sickness incidence applied to catamarans. *International Journal of Naval Architecture and Ocean Engineering (IJNAOE)*, 7(4):655–669.

[101] Purvin, S. (2003). Hydrodynamic design of high speed catamaran vessels. Master's thesis, Massachusetts Institute of Technology.

[102] Rajendran, S., Fonseca, N., and Guedes Soares, C. (2015). Simplified body non linear time domain calculation of vertical ship motions and wave loads in large amplitude waves. *Ocean Engineering*, 107:157–177.

[103] Rajendran, S., Fonseca, N., and Guedes Soares, C. (2016). Prediction of vertical responses of a container ship in abnormal waves. *Ocean Engineering*, 119:165–180.

[104] Rollings, S. E. (2003). Seakeeping analysis of small displacement high-speed vessels. Postgraduate Thesis. Naval Postgraduate School, Monterey, California.

[105] Sahoo, P. K., Mason, S., and Tuite, A. (2008). Practical evaluation of resistance of high-speed catamaran hull forms - part ii. *Ships and Offshore Structures*, 3(3):239–245.

[106] Sahoo, P. K., Salas, M., and Schwetz, A. (2007). Practical evaluation of resistance of high-speed catamaran hull forms - part i. *Ships and Offshore Structures*, 2(4):307–324.

[107] Salio, M. P., Taddei, F., Gualeni, P., Guagnano, A., and Perra, F. (2013). Ship performance and sea state condition: an assessment methodology integrated in an early design stage tool. In *Proceedings of tthe 10th International Conference on Maritime Systems and Technologies, MAST 2013*, Gdansk, Poland.

[108] Salvesen, N., Kerczek, C. H. V., Scragg, C. A., Cressy, C. P., and Melnhold, M. J. (1985). Hydronumeric design of SWATH ships. *Transactions of the Society of Naval Architects and Marine Engineers, SNAME*, 93:325–346.

[109] Salvesen, N., Tuck, E. O., and Faltinsen, O. (1970). Ship motions and sea loads. In *Transactions of the Society of Naval Architects and Marine Engineers, SNAME*, volume 78, pages 250–287.

[110] Sarioz, K. (1993). *A hydrodynamic hull form design methodology for concept and preliminary design stage*. PhD thesis, University of Newcastle, Newcastle Upon Tyne, United Kingdom.

[111] Sariöz, K. and Narli, E. (2005). Effect of criteria on seakeeping performance assessment. *Ocean Engineering*, 32(10):1161–1173.

[112] Sato, Y., Miyata, H., and Sato, T. (1999). CFD simulation of 3-dimensional motion of a ship in waves: application to an advancing ship in regular head waves. *Journal of Marine Science and Technology*, 4(3):108–116.

[113] Scamardella, A. and Piscopo, V. (2014). Passenger ship seakeeping optimization by the overall motion sickness incidence. *Ocean Engineering*, 76:86–97.

[114] Schellin, T. E. and Rathje, H. (1995). A panel method applied to hydrodynamic analysis of twinhull ships. In *Proceedings of the 3rd International Conference on Fast Sea Transportation, FAST '95*, volume 2, pages 905–916, Lubeck-Travemunde, Germany. Schiffbautechnische Gesellschaft, Germany.

[115] Schoop-Zipfel, J. (2017). *Efficient simulation of ship maneuvers in waves*. PhD thesis, Schriftenreihe Schiffbau der Technischen Universität Hamburg, Hamburg, Germany.

[116] Schoop-Zipfel, J. and Abdel-Maksoud, M. (2011). A numerical model to determine ship manoeuvring motion in regular waves. In Eça, L., nate, E. O., García, J., Kvamsdal, T., and Bergan, P., editors, *4th International Conference on Computational Methods in Marine Engineering, MARINE 2011*, Lisbon, Portugal. Springer.

[117] Söding, H. (1969). Eine modifikation der streifenmethode. *Schiffstechnik*, 16:15–18.

[118] Söding, H. (1993). A method for accurate force calculations in potential flow. *Ship Technology Research*, 40(4):176–189.

[119] Söding, H. and Bertram, V. (2009). Program PDSTRIP: public domain strip method. https://sourceforge.net/projects/pdstrip/.

[120] Söding, H., von Graefe, A., el Moctar, O., and Shigunov, V. (2012). Rankine source method for seakeeping predictions. In *Proceedings of the ASME 2012, 31st International Conference on Ocean, Offshore and Arctic Engineering*, pages 449–460, Rio de Janeiro, Brazil. American Society of Mechanical Engineers.

[121] Stoker, J. J. (1957). *Water waves: the mathematical theory with applications*. Interscience Publishers, New York.

[122] Sun, H., Jiang, Y., Zhuang, J., and Zou, J. (2015). Numerical simulation of the longitudinal movement of a SSB catamaran in regular waves. In *2015 International Conference on Materials Engineering and Information Technology Applications (MEITA 2015)*, pages 530–535, Guilin, China. Atlantis Press.

[123] Tezdogan, T., Incecik, A., and Turan, O. (2014). Operability assessment of high speed passenger ships based on human comfort criteria. *Ocean Engineering*, 89(1):32–52.

[124] Triunfante Martins, P., Fonseca, N., and Guedes Soares, C. (2004). Comparação entre dados experimentais e numéricos do comportamento em ondas de um catamaran. In e V. Gonçalves de Brito, C. G. S., editor, *As Actividades Marítimas e a Engenharia*, pages 565–582. Edições Salamandra. ISBN: 972-689-229-5.

[125] Ursell, F. (1949). On the heaving motion of a circular cylinder on the surface of a fluid. *The Quarterly Journal of Mechanics and Applied Mathematics*, 2(2):218–231.

[126] Vernengo, G., Biliotti, I., Brizzolara, S., Viviani, M., Ruscelli, D., Galliussi, M., and Manfredini, A. (2009). Influence of form parameters selection on the hull surface shape control for hydrodynamic design. In *Proceedings of the 16th International Conference on Ship and Shipping Research, NAV 2009*, pages 40–49, Genova, Italy.

[127] Vernengo, G., Brizzolara, S., and Bruzzone, D. (2015). Resistance and seakeeping optimization of a fast multihull passenger ferry. *International Journal of Offshore and Polar Engineering*, 25(1):26–34.

[128] Vernengo, G. and Bruzzone, D. (2016). Resistance and seakeeping numerical performance analyses of a semi-small waterplane area twin hull at medium to high speeds. *Journal of Marine Science and Application*, 15(1):1–7.

[129] Watanabe, I. and Guedes Soares, C. (1999). Comparative study on the time-domain analysis of non-linear ship motions and loads. *Marine Structures*, 12(3):153–170.

[130] Wilson, R. V., Carrica, P. M., and Stern, F. (2006). Unsteady rans method for ship motions with application to roll for a surface combatant. *Computers and Fluids*, 35(5):501–524.

Appendix A

Comparison between numerical and experimental results - catamaran case

A.1 Frequency dependent errors

Table A.1: Comparison between numerical and experimental results for heave RAOs, Catamaran, $F_n = 0.000$

ω_0	$\zeta_3/\zeta_a[m/m]$	$\zeta_3/\zeta_a[m/m]$, absolute difference $[m/m]$				
$[rad/s]$	Experiment	Fonseca	MaxMotions w/o trans	MaxMotions w/ trans	PDStrip w/o trans	PDStrip w/ trans
0.599	0.751	0.929, 0.178	0.969, 0.219	0.969, 0.219	0.933, 0.182	0.936, 0.185
0.691	0.854	0.875, 0.021	0.927, 0.073	0.927, 0.073	0.883, 0.029	0.886, 0.032
0.846	0.718	0.730, 0.013	0.802, 0.084	0.802, 0.084	0.751, 0.033	0.751, 0.034
0.946	0.607	0.598, 0.008	0.677, 0.070	0.677, 0.070	0.631, 0.024	0.629, 0.023
1.012	0.523	0.497, 0.026	0.573, 0.050	0.573, 0.050	0.539, 0.017	0.536, 0.014
1.050	0.391	0.433, 0.042	0.507, 0.116	0.507, 0.116	0.482, 0.091	0.479, 0.088
1.093	0.319	0.360, 0.040	0.413, 0.093	0.413, 0.093	0.417, 0.098	0.412, 0.093
1.197	0.189	0.178, 0.011	0.216, 0.027	0.216, 0.027	0.261, 0.072	0.255, 0.066
1.262	0.122	0.073, 0.048	0.182, 0.061	0.182, 0.061	0.181, 0.059	0.175, 0.053
1.338	0.118	0.055, 0.063	0.155, 0.038	0.155, 0.038	0.127, 0.009	0.126, 0.008
1.693	0.059	0.108, 0.049	0.162, 0.103	0.162, 0.103	0.087, 0.028	0.083, 0.023

Table A.2: Comparison between numerical and experimental results for heave RAOs, Catamaran, $F_n = 0.200$

ω_0 $[rad/s]$	$\zeta_3/\zeta_a[m/m]$	$\zeta_3/\zeta_a[m/m]$, absolute difference $[m/m]$				
	Experiment	Fonseca	MaxMotions w/o trans	MaxMotions w/ trans	PDStrip w/o trans	PDStrip w/ trans
0.599	0.949	0.947, 0.002	1.015, 0.066	1.010, 0.060	0.942, 0.008	0.948, 0.001
0.757	0.878	0.856, 0.022	0.979, 0.101	0.969, 0.091	0.863, 0.015	0.870, 0.008
0.892	0.678	0.718, 0.040	0.908, 0.230	0.903, 0.225	0.760, 0.082	0.766, 0.088
1.012	0.553	0.544, 0.010	0.854, 0.301	0.862, 0.308	0.648, 0.095	0.655, 0.102
1.093	0.398	0.400, 0.002	0.891, 0.493	0.907, 0.509	0.574, 0.175	0.579, 0.181
1.197	0.144	0.207, 0.064	1.018, 0.874	1.034, 0.891	0.497, 0.353	0.497, 0.353
1.262	0.077	0.125, 0.048	0.716, 0.639	0.773, 0.696	0.466, 0.389	0.457, 0.380
1.431	0.411	0.250, 0.161	0.105, 0.306	0.117, 0.294	0.357, 0.053	0.321, 0.090
1.693	0.128	0.181, 0.053	0.060, 0.069	0.067, 0.062	0.219, 0.091	0.233, 0.105

Table A.3: Comparison between numerical and experimental results for heave RAOs, Catamaran, $F_n = 0.400$

ω_0 $[rad/s]$	$\zeta_3/\zeta_a[m/m]$	$\zeta_3/\zeta_a[m/m]$, absolute difference $[m/m]$				
	Experiment	Fonseca	MaxMotions w/o trans	MaxMotions w/ trans	PDStrip w/o trans	PDStrip w/ trans
0.599	0.988	0.972, 0.016	1.077, 0.089	1.072, 0.084	0.959, 0.029	0.979, 0.009
0.757	0.925	0.913, 0.012	1.166, 0.241	1.167, 0.242	0.924, 0.001	0.957, 0.032
0.846	0.842	0.860, 0.018	1.338, 0.496	1.334, 0.493	0.916, 0.074	0.951, 0.109
0.946	0.674	0.792, 0.117	2.074, 1.400	1.925, 1.251	0.945, 0.270	0.969, 0.294
1.012	0.586	0.756, 0.170	2.417, 1.831	2.332, 1.746	1.018, 0.432	1.011, 0.425
1.093	0.949	0.774, 0.175	1.933, 0.984	2.042, 1.093	1.226, 0.277	1.123, 0.174
1.197	1.265	0.924, 0.341	0.447, 0.818	0.568, 0.697	1.636, 0.371	1.327, 0.062
1.338	0.288	0.177, 0.112	0.037, 0.252	0.056, 0.232	0.483, 0.195	0.494, 0.205
1.431	0.029	0.092, 0.063	0.048, 0.018	0.058, 0.029	0.109, 0.079	0.106, 0.077
1.545	0.069	0.098, 0.028	0.044, 0.025	0.053, 0.016	0.086, 0.016	0.108, 0.039

Table A.4: Comparison between numerical and experimental results for heave RAOs, Catamaran, $F_n = 0.600$

ω_0 $[rad/s]$	$\zeta_3/\zeta_a[m/m]$ Experiment	$\zeta_3/\zeta_a[m/m]$, absolute difference $[m/m]$				
		Fonseca	MaxMotions w/o trans	MaxMotions w/ trans	PDStrip w/o trans	PDStrip w/ trans
0.599	1.017	1.008, 0.009	1.170, 0.153	1.167, 0.150	0.988, 0.029	1.031, 0.015
0.757	0.977	1.019, 0.042	1.604, 0.627	1.567, 0.590	1.045, 0.068	1.103, 0.126
0.846	0.943	1.060, 0.117	2.674, 1.731	2.369, 1.427	1.181, 0.239	1.208, 0.265
0.892	1.098	1.114, 0.016	3.562, 2.464	3.031, 1.933	1.328, 0.230	1.302, 0.204
0.946	1.614	1.243, 0.370	3.529, 1.916	3.165, 1.552	1.642, 0.029	1.476, 0.138
1.012	2.010	1.577, 0.433	1.446, 0.564	1.827, 0.182	2.351, 0.341	1.815, 0.194
1.050	2.014	1.895, 0.119	0.873, 1.141	1.129, 0.884	2.756, 0.743	2.056, 0.043
1.093	1.619	2.165, 0.546	0.520, 1.099	0.670, 0.949	2.519, 0.900	2.180, 0.561
1.197	0.549	0.639, 0.090	0.140, 0.408	0.181, 0.368	0.817, 0.268	0.986, 0.437
1.338	0.038	0.014, 0.024	0.009, 0.028	0.019, 0.018	0.140, 0.102	0.119, 0.081
1.693	0.020	0.011, 0.009	0.006, 0.014	0.010, 0.010	0.028, 0.008	0.026, 0.006

Table A.5: Comparison between numerical and experimental results for pitch RAOs, Catamaran, $F_n = 0.000$

ω_0 $[rad/s]$	$\zeta_5/k_0\zeta_a[^\circ/^\circ]$ Experiment	$\zeta_5/k_0\zeta_a[^\circ/^\circ]$, absolute difference $[^\circ/^\circ]$				
		Fonseca	MaxMotions w/o trans	MaxMotions w/ trans	PDStrip w/o trans	PDStrip w/ trans
0.599	1.098	0.967, 0.132	1.017, 0.081	1.017, 0.081	0.981, 0.118	0.954, 0.144
0.691	0.958	0.936, 0.022	1.003, 0.045	1.003, 0.045	0.951, 0.007	0.925, 0.033
0.846	0.887	0.849, 0.038	0.950, 0.063	0.950, 0.063	0.864, 0.023	0.840, 0.047
0.946	0.805	0.764, 0.041	0.887, 0.082	0.887, 0.082	0.779, 0.026	0.758, 0.047
1.012	0.722	0.695, 0.027	0.829, 0.107	0.829, 0.107	0.710, 0.013	0.691, 0.031
1.050	0.625	0.650, 0.025	0.791, 0.165	0.791, 0.165	0.664, 0.039	0.648, 0.022
1.093	0.520	0.596, 0.076	0.742, 0.221	0.742, 0.221	0.610, 0.090	0.595, 0.075
1.197	0.405	0.452, 0.047	0.598, 0.193	0.598, 0.193	0.464, 0.059	0.454, 0.049
1.262	0.335	0.357, 0.022	0.487, 0.152	0.487, 0.152	0.367, 0.032	0.360, 0.025
1.338	0.231	0.246, 0.015	0.343, 0.112	0.343, 0.112	0.253, 0.022	0.250, 0.019
1.693	0.009	0.082, 0.073	0.112, 0.103	0.112, 0.103	0.085, 0.076	0.082, 0.073

Table A.6: Comparison between numerical and experimental results for pitch RAOs, Catamaran, $F_n = 0.200$

ω_0 $[rad/s]$	$\zeta_5/k_0\zeta_a[^\circ/^\circ]$	$\zeta_5/k_0\zeta_a[^\circ/^\circ]$, absolute difference $[^\circ/^\circ]$				
	Experiment	Fonseca	MaxMotions w/o trans	MaxMotions w/ trans	PDStrip w/o trans	PDStrip w/ trans
0.599	1.049	1.011, 0.038	1.091, 0.043	1.078, 0.030	1.009, 0.040	0.985, 0.063
0.757	0.937	0.991, 0.054	1.167, 0.230	1.128, 0.192	0.976, 0.039	0.948, 0.011
0.892	0.809	0.942, 0.133	1.257, 0.448	1.177, 0.368	0.918, 0.109	0.883, 0.074
1.012	0.819	0.862, 0.043	1.359, 0.540	1.221, 0.402	0.837, 0.018	0.793, 0.026
1.093	0.767	0.784, 0.017	1.417, 0.650	1.237, 0.470	0.763, 0.003	0.711, 0.055
1.197	0.686	0.653, 0.034	1.257, 0.570	1.114, 0.427	0.643, 0.043	0.582, 0.104
1.262	0.625	0.551, 0.074	0.865, 0.241	0.813, 0.188	0.553, 0.072	0.487, 0.138
1.431	0.414	0.206, 0.208	0.113, 0.301	0.123, 0.291	0.245, 0.169	0.189, 0.225
1.693	0.081	0.090, 0.009	0.028, 0.053	0.033, 0.048	0.074, 0.007	0.091, 0.010

Table A.7: Comparison between numerical and experimental results for pitch RAOs, Catamaran, $F_n = 0.400$

ω_0 $[rad/s]$	$\zeta_5/k_0\zeta_a[^\circ/^\circ]$	$\zeta_5/k_0\zeta_a[^\circ/^\circ]$, absolute difference $[^\circ/^\circ]$				
	Experiment	Fonseca	MaxMotions w/o trans	MaxMotions w/ trans	PDStrip w/o trans	PDStrip w/ trans
0.599	1.053	1.068, 0.015	1.196, 0.143	1.120, 0.067	1.040, 0.013	1.010, 0.043
0.757	1.071	1.102, 0.031	1.446, 0.375	1.267, 0.196	1.049, 0.022	0.991, 0.080
0.846	1.153	1.116, 0.037	1.684, 0.531	1.408, 0.255	1.055, 0.098	0.974, 0.180
0.946	1.256	1.126, 0.130	2.082, 0.826	1.647, 0.392	1.068, 0.188	0.948, 0.307
1.012	1.269	1.127, 0.142	2.138, 0.869	1.687, 0.417	1.085, 0.184	0.929, 0.341
1.093	1.136	1.111, 0.025	1.399, 0.263	1.263, 0.127	1.114, 0.022	0.897, 0.239
1.197	0.881	0.999, 0.118	0.438, 0.443	0.483, 0.398	1.076, 0.195	0.815, 0.066
1.197	0.888	0.999, 0.111	0.438, 0.450	0.483, 0.405	1.076, 0.188	0.815, 0.073
1.197	0.830	0.999, 0.168	0.438, 0.393	0.483, 0.348	1.076, 0.245	0.815, 0.016
1.338	0.341	0.321, 0.020	0.105, 0.236	0.119, 0.222	0.362, 0.021	0.350, 0.009
1.431	0.110	0.066, 0.044	0.029, 0.080	0.035, 0.075	0.123, 0.013	0.098, 0.012
1.545	0.013	0.016, 0.004	0.006, 0.006	0.011, 0.002	0.015, 0.002	0.011, 0.002

Table A.8: Comparison between numerical and experimental results for pitch RAOs, Catamaran, $F_n = 0.600$

ω_0 $[rad/s]$	$\zeta_5/k_0\zeta_a[^\circ/^\circ]$	$\zeta_5/k_0\zeta_a[^\circ/^\circ]$, absolute difference $[^\circ/^\circ]$				
	Experiment	Fonseca	MaxMotions w/o trans	MaxMotions w/ trans	PDStrip w/o trans	PDStrip w/ trans
0.599	1.203	1.122, 0.081	1.317, 0.114	1.138, 0.066	1.078, 0.125	1.018, 0.186
0.757	1.320	1.212, 0.108	1.773, 0.453	1.403, 0.083	1.150, 0.170	1.023, 0.297
0.846	1.456	1.286, 0.170	2.461, 1.005	1.738, 0.282	1.240, 0.216	1.043, 0.413
0.892	1.572	1.333, 0.239	2.879, 1.307	1.918, 0.346	1.314, 0.258	1.060, 0.512
0.946	1.514	1.399, 0.115	2.679, 1.165	1.868, 0.354	1.439, 0.075	1.090, 0.424
1.012	1.201	1.507, 0.306	1.093, 0.108	1.114, 0.087	1.640, 0.439	1.140, 0.061
1.050	1.045	1.611, 0.565	0.704, 0.341	0.767, 0.278	1.659, 0.614	1.167, 0.121
1.093	0.882	1.688, 0.806	0.465, 0.418	0.523, 0.359	1.335, 0.453	1.139, 0.257
1.197	0.440	0.585, 0.145	0.184, 0.256	0.212, 0.228	0.497, 0.057	0.589, 0.150
1.338	0.109	0.096, 0.013	0.044, 0.065	0.054, 0.056	0.144, 0.034	0.134, 0.025
1.693	0.011	0.008, 0.003	0.004, 0.007	0.007, 0.004	0.010, 0.001	0.013, 0.002

A.2 Coefficients of the coupled heave/pitch motion equation

Table A.9: Numerical results for the coefficients of the first coupled heave/pitch motion equation (3.4), Catamaran, $F_n = 0.000$

ω_0 $[rad/s]$	Code	$\Delta + A_{33}$ $[t]$	B_{33} $[t/s]$	C_{33} $[t/s^2]$	A_{35} $[t.m]$	B_{35} $[t.m/s]$	C^*_{35} $[t.m/s^2]$	$\lvert F^E_3 \rvert$ $[kN]$	Φ $[^\circ]$
	Fonseca	176.9	107.4	908.9	382.6	218.0	491.3	760.7	176.6
	MaxMotions w/o trans	176.5	106.2	907.6	355.9	213.6	489.4	760.9	3.3
0.599	MaxMotions w/ trans	176.5	106.2	907.6	355.9	213.6	489.4	760.9	3.3
	PDStrip w/o trans	177.0	107.3	908.5	983.6	589.7	3559.5	761.1	-3.7
	PDStrip w/ trans	177.0	107.2	908.5	983.6	588.0	3559.5	761.1	-3.7
	Fonseca	157.2	117.8	908.9	343.5	237.2	491.3	701.0	175.8
	MaxMotions w/o trans	158.6	116.8	907.6	304.6	235.9	489.4	700.6	4.1
0.691	MaxMotions w/ trans	158.6	116.8	907.6	304.6	235.9	489.4	700.6	4.1
	PDStrip w/o trans	157.4	118.2	908.5	878.3	650.6	3559.5	701.7	-5.2
	PDStrip w/ trans	157.4	118.1	908.5	878.3	649.0	3559.5	701.6	-5.2
	Fonseca	131.1	131.7	908.9	292.8	262.2	491.3	565.0	174.5
	MaxMotions w/o trans	134.9	130.6	907.6	241.6	262.0	489.4	564.6	5.3
0.846	MaxMotions w/ trans	134.9	130.6	907.6	241.6	262.0	489.4	564.6	5.3
	PDStrip w/o trans	131.1	132.8	908.5	737.8	731.7	3559.5	566.2	-8.6
	PDStrip w/ trans	131.1	132.7	908.5	737.8	730.7	3559.5	566.2	-8.6
	Fonseca	117.8	138.4	908.9	267.6	274.1	491.3	454.5	174.1
	MaxMotions w/o trans	122.3	137.3	907.6	211.9	274.1	489.4	454.9	5.3
0.946	MaxMotions w/ trans	122.3	137.3	907.6	211.9	274.1	489.4	454.9	5.3
	PDStrip w/o trans	117.9	140.1	908.5	668.1	772.9	3559.5	456.1	-11.8
	PDStrip w/ trans	117.9	140.1	908.5	668.1	772.4	3559.5	456.1	-11.8
	Fonseca	110.3	142.0	908.9	253.5	280.3	491.3	374.7	174.3
	MaxMotions w/o trans	114.9	140.9	907.6	195.8	280.5	489.4	374.7	5.0
1.012	MaxMotions w/ trans	114.9	140.9	907.6	195.8	280.5	489.4	374.7	5.0
	PDStrip w/o trans	110.4	144.1	908.5	628.7	795.8	3559.5	376.5	-14.5
	PDStrip w/ trans	110.4	144.1	908.5	628.7	795.6	3559.5	376.5	-14.5
	Fonseca	106.2	143.8	908.9	246.1	283.4	491.3	326.3	174.7
	MaxMotions w/o trans	110.8	142.6	907.6	187.6	283.6	489.4	327.7	4.8
1.050	MaxMotions w/ trans	110.8	142.6	907.6	187.6	283.6	489.4	327.7	4.8
	PDStrip w/o trans	106.1	146.1	908.5	606.4	807.1	3559.5	328.3	-16.3
	PDStrip w/ trans	106.1	146.1	908.5	606.4	807.1	3559.5	328.3	-16.3
	Fonseca	102.0	145.5	908.9	238.3	286.5	491.3	271.4	175.5
	MaxMotions w/o trans	106.4	144.4	907.6	179.1	286.8	489.4	268.0	3.8
1.093	MaxMotions w/ trans	106.4	144.4	907.6	179.1	286.8	489.4	268.0	3.8
	PDStrip w/o trans	102.2	148.2	908.5	585.7	819.2	3559.5	273.5	-19.0
	PDStrip w/ trans	102.2	148.2	908.5	585.7	819.3	3559.5	273.5	-19.0
	Fonseca	92.9	148.8	908.9	221.7	292.1	491.3	141.9	-158.9
	MaxMotions w/o trans	96.8	147.7	907.6	162.3	292.7	489.4	143.4	-2.6
1.197	MaxMotions w/ trans	96.8	147.7	907.6	162.3	292.7	489.4	143.4	-2.6
	PDStrip w/o trans	92.9	152.0	908.5	537.3	840.4	3559.5	144.0	-29.7
	PDStrip w/ trans	92.9	152.0	908.5	537.3	840.5	3559.5	144.0	-29.7
	Fonseca	88.0	150.2	908.9	212.8	294.5	491.3	71.8	-163.8
	MaxMotions w/o trans	91.5	148.9	907.6	155.2	295.0	489.4	105.2	-32.4
1.262	MaxMotions w/ trans	91.5	148.9	907.6	155.2	295.0	489.4	105.2	-32.4
	PDStrip w/o trans	88.1	153.7	908.5	512.2	849.2	3559.5	74.1	-46.9
	PDStrip w/ trans	88.1	153.7	908.5	512.2	849.6	3559.5	74.2	-46.9
	Fonseca	82.9	151.1	908.9	203.6	296.2	491.3	38.4	-87.0
	MaxMotions w/o trans	85.7	150.0	907.6	148.4	297.1	489.4	71.6	-99.2
1.338	MaxMotions w/ trans	85.7	150.0	907.6	148.4	297.1	489.4	71.6	-99.2
	PDStrip w/o trans	82.7	154.7	908.5	484.3	854.4	3559.5	36.9	-125.7
	PDStrip w/ trans	82.7	154.8	908.5	484.3	854.8	3559.5	36.9	-125.7
	Fonseca	66.3	147.8	908.9	174.0	291.4	491.3	67.8	-7.9
	MaxMotions w/o trans	67.6	146.9	907.6	134.6	293.2	489.4	68.2	-24.9
1.693	MaxMotions w/ trans	67.6	146.9	907.6	134.6	293.2	489.4	68.2	-24.9
	PDStrip w/o trans	66.0	150.6	908.5	397.4	825.4	3559.5	66.9	131.2
	PDStrip w/ trans	66.0	150.6	908.5	397.4	825.4	3559.5	66.9	131.2

* Differences to PDStrip are consequence of the adopted reference frame to compute the component $-\rho g \int x B dx$

Table A.10: Numerical results for the coefficients of the second coupled heave/pitch motion equation (3.4), Catamaran, $F_n = 0.000$

ω_0 $[rad/s]$	Code	A_{53} $[t.m]$	B_{53} $[t.m/s]$	C^*_{53} $[t.m/s^2]$	$I_5 + A_{55}$ $[t.m^2]$	B_{55} $[t.m^2/s]$	C_{55} $[t.m^2/s^2]$	$\lvert F^E_5 \rvert$ $[kN.m]$	Φ $[^\circ]$
	Fonseca	382.578	218.0	491.3	17395.1	10427.0	101735.0	3150.5	-101.0
	MaxMotions w/o trans	355.9	213.6	489.4	17641.8	10332.7	101440.3	3140.0	-78.8
0.599	MaxMotions w/ trans	355.9	213.6	489.4	17641.8	10332.7	101440.3	3140.0	-78.8
	PDStrip w/o trans	983.6	589.7	3559.5	22022.2	13235.4	112726.7	4325.5	-50.2
	PDStrip w/ trans	983.6	588.0	3541.3	22022.2	13206.8	112726.7	4343.5	-50.1
	Fonseca	343.462	237.2	491.3	15490.3	11472.4	101735.0	3953.1	-100.7
	MaxMotions w/o trans	304.6	235.9	489.4	15934.8	11378.4	101440.3	3948.5	-79.2
0.691	MaxMotions w/ trans	304.6	235.9	489.4	15934.8	11378.4	101440.3	3948.5	-79.2
	PDStrip w/o trans	878.3	650.6	3559.5	19645.0	14640.2	112726.7	4840.7	-59.7
	PDStrip w/ trans	878.3	649.0	3541.3	19645.0	14612.7	112726.7	4858.6	-59.8
	Fonseca	292.808	262.2	491.3	12949.1	12900.1	101735.0	5117.6	-101.6
	MaxMotions w/o trans	241.6	262.0	489.4	13603.5	12787.2	101440.3	5126.2	-78.5
0.846	MaxMotions w/ trans	241.6	262.0	489.4	13603.5	12787.2	101440.3	5126.2	-78.5
	PDStrip w/o trans	737.8	731.7	3559.5	16435.6	16541.7	112726.7	5667.0	-73.0
	PDStrip w/ trans	737.8	730.7	3541.3	16435.6	16523.9	112726.7	5683.8	-73.0
	Fonseca	267.601	274.1	491.3	11644.3	13618.2	101735.0	5563.2	-102.6
	MaxMotions w/o trans	211.9	274.1	489.4	12378.7	13492.4	101440.3	5467.7	-77.6
0.946	MaxMotions w/ trans	211.9	274.1	489.4	12378.7	13492.4	101440.3	5467.7	-77.6
	PDStrip w/o trans	668.1	772.9	3559.5	14821.6	17517.3	112726.7	5969.8	-80.2
	PDStrip w/ trans	668.1	772.4	3541.3	14821.6	17506.6	112726.7	5984.3	-80.3
	Fonseca	253.539	280.3	491.3	10902.3	14008.9	101735.0	5653.5	-103.3
	MaxMotions w/o trans	195.8	280.5	489.4	11669.5	13882.0	101440.3	5586.9	-76.9
1.012	MaxMotions w/ trans	195.8	280.5	489.4	11669.5	13882.0	101440.3	5586.9	-76.9
	PDStrip w/o trans	628.7	795.8	3559.5	13904.8	18061.1	112726.7	5989.2	-84.6
	PDStrip w/ trans	628.7	795.6	3541.3	13904.8	18055.9	112726.7	6001.5	-84.8
	Fonseca	246.053	283.4	491.3	10502.9	14210.2	101735.0	5617.5	-103.7
	MaxMotions w/o trans	187.6	283.6	489.4	11284.6	14077.1	101440.3	5595.9	-76.6
1.050	MaxMotions w/ trans	187.6	283.6	489.4	11284.6	14077.1	101440.3	5595.9	-76.6
	PDStrip w/o trans	606.4	807.1	3559.5	13384.7	18331.1	112726.7	5917.1	-87.2
	PDStrip w/ trans	606.4	807.1	3541.3	13384.7	18328.6	112726.7	5927.8	-87.3
	Fonseca	238.275	286.5	491.3	10083.9	14413.4	101735.0	5494.2	-104.1
	MaxMotions w/o trans	179.1	286.8	489.4	10874.3	14279.9	101440.3	5471.4	-76.3
1.093	MaxMotions w/ trans	179.1	286.8	489.4	10874.3	14279.9	101440.3	5471.4	-76.3
	PDStrip w/o trans	585.7	819.2	3559.5	12896.5	18619.8	112726.7	5759.0	-90.2
	PDStrip w/ trans	585.7	819.3	3541.3	12896.5	18619.6	112726.7	5767.6	-90.4
	Fonseca	221.675	292.1	491.3	9176.7	14810.1	101735.0	4802.7	-104.8
	MaxMotions w/o trans	162.3	292.7	489.4	9972.7	14674.4	101440.3	4776.2	-75.7
1.197	MaxMotions w/ trans	162.3	292.7	489.4	9972.7	14674.4	101440.3	4776.2	-75.7
	PDStrip w/o trans	537.3	840.4	3559.5	11752.6	19139.9	112726.7	5002.2	-98.0
	PDStrip w/ trans	537.3	840.5	3541.3	11752.6	19141.6	112726.7	5004.5	-98.2
	Fonseca	212.815	294.5	491.3	8684.3	14990.7	101735.0	4111.8	-104.6
	MaxMotions w/o trans	155.2	295.0	489.4	9476.0	14853.9	101440.3	4080.0	-77.0
1.262	MaxMotions w/ trans	155.2	295.0	489.4	9476.0	14853.9	101440.3	4080.0	-77.0
	PDStrip w/o trans	512.2	849.2	3559.5	11153.6	19369.7	112726.7	4283.4	-103.7
	PDStrip w/ trans	512.2	849.6	3541.3	11153.6	19376.1	112726.7	4281.9	-104.0
	Fonseca	203.579	296.2	491.3	8164.6	15143.4	101735.0	3093.7	-103.2
	MaxMotions w/o trans	148.4	297.1	489.4	8936.4	15028.1	101440.3	2960.6	-80.0
1.338	MaxMotions w/ trans	148.4	297.1	489.4	8936.4	15028.1	101440.3	2960.6	-80.0
	PDStrip w/o trans	484.3	854.4	3559.5	10485.9	19525.2	112726.7	3247.2	-112.5
	PDStrip w/ trans	484.3	854.8	3541.3	10485.9	19532.4	112726.7	3241.2	-112.8
	Fonseca	173.984	291.4	491.3	6448.4	15105.8	101735.0	1295.1	46.1
	MaxMotions w/o trans	134.6	293.2	489.4	7049.5	14997.8	101440.3	972.0	147.5
1.693	MaxMotions w/ trans	134.6	293.2	489.4	7049.5	14997.8	101440.3	972.0	147.5
	PDStrip w/o trans	397.4	825.4	3559.5	8352.5	19149.3	112726.7	1438.7	84.9
	PDStrip w/ trans	397.4	825.4	3541.3	8352.5	19152.1	112726.7	1440.8	84.3

* Differences to PDStrip are consequence of the adopted reference frame to compute the component $-\rho g \int x B dx$

Table A.11: Numerical results for the coefficients of the first coupled heave/pitch motion equation (3.4), Catamaran, $F_n = 0.200$

ω_0 $[rad/s]$	Code	$\Delta + A_{33}$ $[t]$	B_{33} $[t/s]$	C_{33} $[t/s^2]$	A_{35} $[t.m]$	B_{35} $[t.m/s]$	C^*_{35} $[t.m/s^2]$	$\lvert F_3^E \rvert$ $[kN]$	Φ $[°]$
	Fonseca	146.7	123.4	908.9	-582.1	850.0	491.3	759.8	176.0
	MaxMotions w/o trans	149.1	122.4	907.6	-618.8	859.1	489.4	759.5	3.9
0.599	MaxMotions w/ trans	122.0	141.3	907.6	-1246.9	1090.2	489.4	775.6	3.9
	PDStrip w/o trans	146.8	124.0	908.5	-87.0	1285.7	3559.5	749.2	-2.4
	PDStrip w/ trans	119.8	142.7	908.5	-805.4	1578.0	3559.5	767.4	-2.4
	Fonseca	111.9	141.2	908.9	-327.0	738.6	491.3	650.1	174.2
	MaxMotions w/o trans	116.5	140.2	907.6	-379.6	757.5	489.4	649.3	5.5
0.757	MaxMotions w/ trans	98.8	154.8	907.6	-759.9	950.6	489.4	664.2	4.9
	PDStrip w/o trans	112.1	143.2	908.5	46.1	1253.3	3559.5	635.3	-3.9
	PDStrip w/ trans	94.4	157.5	908.5	-393.2	1491.5	3559.5	653.2	-4.7
	Fonseca	90.7	149.5	908.9	-191.2	665.8	491.3	519.0	173.3
	MaxMotions w/o trans	94.4	148.3	907.6	-246.8	681.4	489.4	519.6	6.2
0.892	MaxMotions w/ trans	81.8	160.3	907.6	-507.3	848.2	489.4	529.7	4.9
	PDStrip w/o trans	90.8	152.7	908.5	108.8	1223.3	3559.5	505.2	-5.8
	PDStrip w/ trans	78.2	164.4	908.5	-193.4	1424.6	3559.5	517.5	-7.6
	Fonseca	77.0	151.4	908.9	-106.7	613.1	491.3	376.7	173.6
	MaxMotions w/o trans	79.3	150.2	907.6	-155.4	623.3	489.4	379.1	6.0
1.012	MaxMotions w/ trans	69.9	160.8	907.6	-345.6	771.7	489.4	383.1	3.7
	PDStrip w/o trans	77.0	155.8	908.5	146.3	1189.9	3559.5	368.6	-8.4
	PDStrip w/ trans	67.6	165.6	908.5	-75.1	1364.8	3559.5	372.2	-11.6
	Fonseca	70.0	149.9	908.9	-62.1	582.0	491.3	271.8	175.1
	MaxMotions w/o trans	71.6	148.8	907.6	-104.2	589.8	489.4	274.8	4.4
1.093	MaxMotions w/ trans	63.8	158.2	907.6	-259.0	728.4	489.4	274.3	1.2
	PDStrip w/o trans	69.9	155.0	908.5	167.0	1160.5	3559.5	269.5	-11.2
	PDStrip w/ trans	62.2	163.8	908.5	-13.3	1320.6	3559.5	266.2	-15.7
	Fonseca	63.3	144.7	908.9	-15.7	546.7	491.3	139.6	-158.1
	MaxMotions w/o trans	64.2	143.9	907.6	-49.6	552.3	489.4	142.9	-2.4
1.197	MaxMotions w/ trans	58.2	152.3	907.6	-168.9	680.9	489.4	138.2	-8.1
	PDStrip w/o trans	63.0	150.5	908.5	190.4	1111.7	3559.5	144.3	-18.2
	PDStrip w/ trans	57.0	158.3	908.5	51.5	1256.6	3559.5	133.1	-25.7
	Fonseca	60.3	139.9	908.9	8.3	527.0	491.3	68.7	-160.6
	MaxMotions w/o trans	60.9	139.2	907.6	-20.8	531.4	489.4	63.3	-23.6
1.262	MaxMotions w/ trans	55.7	147.2	907.6	-122.4	655.5	489.4	62.7	-37.2
	PDStrip w/o trans	60.0	146.0	908.5	204.7	1075.3	3559.5	74.4	-30.0
	PDStrip w/ trans	54.8	153.2	908.5	86.4	1213.5	3559.5	61.5	-44.3
	Fonseca	56.2	122.6	908.9	58.2	482.1	491.3	83.8	-35.2
	MaxMotions w/o trans	56.1	122.1	907.6	39.6	484.9	489.4	80.5	-144.9
1.431	MaxMotions w/ trans	52.8	129.3	907.6	-27.2	601.9	489.4	93.3	-148.8
	PDStrip w/o trans	55.7	128.1	908.5	241.9	953.6	3559.5	69.7	-175.9
	PDStrip w/ trans	52.3	134.9	908.5	163.9	1088.1	3559.5	85.5	175.7
	Fonseca	57.6	87.8	908.9	110.8	427.8	491.3	61.2	-6.8
	MaxMotions w/o trans	56.9	88.2	907.6	103.1	430.9	489.4	60.7	-12.5
1.693	MaxMotions w/ trans	55.2	95.1	907.6	68.7	548.8	489.4	64.3	-22.8
	PDStrip w/o trans	57.0	93.7	908.5	300.3	787.7	3559.5	73.9	151.3
	PDStrip w/ trans	55.3	100.9	908.5	259.9	934.3	3559.5	68.4	136.1

* Differences to PDStrip are consequence of the adopted reference frame to compute the component $-\rho g \int xBdx$

Table A.12: Numerical results for the coefficients of the second coupled heave/pitch motion equation (3.4), Catamaran, $F_n = 0.200$

ω_0 $[rad/s]$	Code	A_{53} $[t.m]$	B_{53} $[t.m/s]$	C^*_{53} $[t.m/s^2]$	$I_5 + A_{55}$ $[t.m^2]$	B_{55} $[t.m^2/s]$	C_{55} $[t.m^2/s^2]$	$\lvert F^E_5 \rvert$ $[kN.m]$	Φ $[^\circ]$
	Fonseca	1227.802	-355.2	491.3	18886.1	15762.7	101735.0	3374.1	-94.0
	MaxMotions w/o trans	1175.8	-365.4	489.4	19486.8	15621.9	101440.3	3357.7	-85.8
0.599	MaxMotions w/ trans	686.0	-23.3	489.4	8111.4	19813.0	101440.3	3365.4	-80.8
	PDStrip w/o trans	821.8	682.7	3559.5	13352.9	18757.7	112726.7	4217.8	-49.0
	PDStrip w/ trans	1138.8	483.1	3541.3	7165.1	25378.1	112726.7	4420.5	-52.3
	Fonseca	840.037	-180.5	491.3	12959.1	16323.7	101735.0	4650.7	-96.4
	MaxMotions w/o trans	778.0	-199.2	489.4	13797.7	16178.3	101440.3	4624.2	-83.4
0.757	MaxMotions w/ trans	458.3	66.4	489.4	6912.0	19670.9	101440.3	4769.7	-80.2
	PDStrip w/o trans	637.5	793.1	3559.5	10834.1	20599.5	112726.7	5033.8	-63.5
	PDStrip w/ trans	837.8	643.7	3541.3	6399.2	25511.0	112726.7	5378.0	-66.8
	Fonseca	626.461	-79.2	491.3	9972.4	16576.4	101735.0	5465.5	-99.0
	MaxMotions w/o trans	564.7	-93.8	489.4	10808.8	16412.8	101440.3	5412.5	-81.0
0.892	MaxMotions w/ trans	337.3	124.6	489.4	6093.0	19445.5	101440.3	5657.4	-79.3
	PDStrip w/o trans	526.3	850.4	3559.5	9163.6	21542.4	112726.7	5606.7	-72.8
	PDStrip w/ trans	662.7	730.5	3541.3	5859.2	25408.2	112726.7	6028.5	-76.5
	Fonseca	492.840	-19.5	491.3	8191.0	16482.8	101735.0	5715.7	-101.2
	MaxMotions w/o trans	439.8	-27.8	489.4	8942.7	16351.6	101440.3	5656.1	-79.0
1.012	MaxMotions w/ trans	270.0	159.2	489.4	5497.7	19029.3	101440.3	5937.6	-78.6
	PDStrip w/o trans	454.7	873.7	3559.5	8036.0	21855.0	112726.7	5749.1	-79.6
	PDStrip w/ trans	551.3	770.8	3541.3	5497.1	25005.0	112726.7	6167.9	-84.0
	Fonseca	423.173	7.2	491.3	7299.8	16225.9	101735.0	5527.9	-102.4
	MaxMotions w/o trans	377.7	2.1	489.4	7966.2	16087.5	101440.3	5485.0	-77.9
1.093	MaxMotions w/ trans	238.1	172.4	489.4	5162.6	18597.2	101440.3	5758.2	-78.5
	PDStrip w/o trans	417.9	873.4	3559.5	7446.5	21749.5	112726.7	5547.1	-84.0
	PDStrip w/ trans	493.6	778.1	3541.3	5327.4	24502.8	112726.7	5911.3	-89.1
	Fonseca	352.520	26.9	491.3	6445.1	15654.7	101735.0	4789.4	-103.4
	MaxMotions w/o trans	316.3	25.0	489.4	6990.1	15529.4	101440.3	4773.3	-77.2
1.197	MaxMotions w/ trans	207.7	178.2	489.4	4829.5	17859.4	101440.3	4990.1	-79.0
	PDStrip w/o trans	381.8	853.0	3559.5	6870.1	21204.6	112726.7	4864.2	-89.9
	PDStrip w/ trans	436.2	763.8	3541.3	5196.7	23543.8	112726.7	5094.7	-96.3
	Fonseca	317.404	31.6	491.3	6052.2	15166.8	101735.0	4062.2	-103.3
	MaxMotions w/o trans	286.5	31.3	489.4	6518.8	15051.4	101440.3	4061.5	-77.5
1.262	MaxMotions w/ trans	193.7	176.1	489.4	4678.2	17297.7	101440.3	4224.2	-80.1
	PDStrip w/o trans	365.8	829.0	3559.5	6624.7	20639.3	112726.7	4203.6	-94.3
	PDStrip w/ trans	409.6	742.0	3541.3	5181.1	22778.8	112726.7	4324.7	-101.7
	Fonseca	250.530	20.6	491.3	5431.6	13477.5	101735.0	1587.1	-95.3
	MaxMotions w/o trans	231.2	24.2	489.4	5708.5	13393.8	101440.3	1556.1	-88.9
1.431	MaxMotions w/ trans	170.1	154.9	489.4	4504.8	15512.2	101440.3	1561.9	-98.8
	PDStrip w/o trans	342.4	724.9	3559.5	6318.3	18323.4	112726.7	1926.1	-114.8
	PDStrip w/ trans	365.8	644.7	3541.3	5341.2	20214.6	112726.7	1788.4	-128.0
	Fonseca	196.986	-45.0	491.3	5310.0	10086.8	101735.0	1247.1	53.7
	MaxMotions w/o trans	189.7	-36.7	489.4	5369.8	10081.1	101440.3	1213.5	125.7
1.693	MaxMotions w/ trans	158.9	88.2	489.4	4743.9	12214.8	101440.3	1408.0	123.6
	PDStrip w/o trans	346.3	553.6	3559.5	6563.9	14532.4	112726.7	1364.1	100.4
	PDStrip w/ trans	353.0	473.3	3541.3	6053.3	16422.2	112726.7	1540.5	84.2

* Differences to PDStrip are consequence of the adopted reference frame to compute the component $-\rho g \int x B dx$

Table A.13: Numerical results for the coefficients of the first coupled heave/pitch motion equation (3.4), Catamaran, $F_n = 0.400$

ω_0 $[rad/s]$	Code	$\Delta + A_{33}$ $[t]$	B_{33} $[t/s]$	C_{33} $[t/s^2]$	A_{35} $[t.m]$	B_{35} $[t.m/s]$	C_{35}^* $[t.m/s^2]$	$\lvert F_3^E \rvert$ $[kN]$	Φ $[°]$
	Fonseca	123.9	135.4	908.9	-1098.5	1286.6	491.3	760.0	175.5
	MaxMotions w/o trans	128.1	134.3	907.6	-1140.8	1320.8	489.4	759.0	4.4
0.599	MaxMotions w/ trans	86.7	166.5	907.6	-2219.6	1564.6	489.4	787.6	4.3
	PDStrip w/o trans	124.0	136.7	908.5	-690.3	1774.4	3559.5	737.7	-1.1
	PDStrip w/ trans	82.5	168.5	908.5	-1905.2	2119.7	3559.5	774.1	-1.0
	Fonseca	89.8	149.7	908.9	-587.6	1031.5	491.3	651.5	173.8
	MaxMotions w/o trans	93.4	148.5	907.6	-640.1	1061.7	489.4	651.1	5.9
0.757	MaxMotions w/ trans	68.7	172.4	907.6	-1216.1	1291.5	489.4	675.9	4.8
	PDStrip w/o trans	89.9	153.2	908.5	-300.5	1596.3	3559.5	622.3	-1.2
	PDStrip w/ trans	65.2	176.2	908.5	-955.7	1892.9	3559.5	657.3	-2.9
	Fonseca	76.7	151.3	908.9	-401.9	926.6	491.3	568.3	173.3
	MaxMotions w/o trans	78.9	150.2	907.6	-448.1	945.8	489.4	569.1	6.4
0.846	MaxMotions w/ trans	60.3	171.0	907.6	-865.7	1165.5	489.4	588.7	4.6
	PDStrip w/o trans	76.7	156.2	908.5	-160.3	1512.8	3559.5	541.4	-1.3
	PDStrip w/ trans	58.0	175.5	908.5	-636.7	1782.6	3559.5	569.2	-4.4
	Fonseca	66.2	147.7	908.9	-247.8	835.4	491.3	455.6	173.4
	MaxMotions w/o trans	67.5	146.8	907.6	-284.2	846.9	489.4	457.5	6.3
0.946	MaxMotions w/ trans	53.9	164.5	907.6	-580.4	1057.4	489.4	469.5	3.5
	PDStrip w/o trans	65.9	154.1	908.5	-43.0	1426.7	3559.5	438.5	-1.6
	PDStrip w/ trans	52.3	170.0	908.5	-380.0	1669.0	3559.5	452.8	-6.6
	Fonseca	61.5	142.3	908.9	-169.4	788.4	491.3	372.6	174.1
	MaxMotions w/o trans	62.3	141.5	907.6	-199.6	796.3	489.4	375.0	5.6
1.012	MaxMotions w/ trans	51.3	157.9	907.6	-437.4	1003.2	489.4	382.0	2.0
	PDStrip w/o trans	61.1	150.1	908.5	19.1	1376.2	3559.5	365.9	-2.1
	PDStrip w/ trans	50.1	164.1	908.5	-250.5	1603.7	3559.5	368.7	-8.6
	Fonseca	57.8	132.6	908.9	-90.8	742.3	491.3	263.9	176.3
	MaxMotions w/o trans	58.0	132.0	907.6	-114.0	746.8	489.4	266.6	3.4
1.093	MaxMotions w/ trans	49.6	147.1	907.6	-295.5	951.9	489.4	267.9	-1.5
	PDStrip w/o trans	57.3	142.0	908.5	85.2	1312.8	3559.5	271.9	-3.3
	PDStrip w/ trans	48.8	154.0	908.5	-119.1	1524.7	3559.5	259.7	-12.2
	Fonseca	55.8	116.5	908.9	-13.3	700.1	491.3	128.0	-175.6
	MaxMotions w/o trans	55.6	116.1	907.6	-28.9	701.5	489.4	130.2	-5.1
1.197	MaxMotions w/ trans	49.6	130.3	907.6	-157.2	909.4	489.4	127.5	-14.6
	PDStrip w/o trans	55.3	125.9	908.5	160.2	1211.8	3559.5	150.3	-7.4
	PDStrip w/ trans	49.3	136.9	908.5	16.1	1423.4	3559.5	122.1	-21.3
	Fonseca	55.8	116.5	908.9	-13.3	700.1	491.3	128.0	-175.6
	MaxMotions w/o trans	55.6	116.1	907.6	-28.9	701.5	489.4	130.2	-5.1
1.197	MaxMotions w/ trans	49.6	130.3	907.6	-157.2	909.4	489.4	127.5	-14.6
	PDStrip w/o trans	55.3	125.9	908.5	160.2	1211.8	3559.5	150.3	-7.4
	PDStrip w/ trans	49.3	136.9	908.5	16.1	1423.4	3559.5	122.1	-21.3
	Fonseca	55.8	116.5	908.9	-13.3	700.1	491.3	128.0	-175.6
	MaxMotions w/o trans	55.6	116.1	907.6	-28.9	701.5	489.4	130.2	-5.1
1.197	MaxMotions w/ trans	49.6	130.3	907.6	-157.2	909.4	489.4	127.5	-14.6
	PDStrip w/o trans	55.3	125.9	908.5	160.2	1211.8	3559.5	150.3	-7.4
	PDStrip w/ trans	49.3	136.9	908.5	16.1	1423.4	3559.5	122.1	-21.3
	Fonseca	57.2	90.9	908.9	60.8	666.8	491.3	43.0	-62.0
	MaxMotions w/o trans	56.6	91.2	907.6	52.2	667.2	489.4	39.7	-114.3
1.338	MaxMotions w/ trans	52.9	105.0	907.6	-27.7	887.1	489.4	58.1	-122.1
	PDStrip w/o trans	56.5	98.2	908.5	244.2	1059.3	3559.5	23.1	-78.3
	PDStrip w/ trans	52.9	111.3	908.5	152.5	1316.8	3559.5	40.9	-158.4
	Fonseca	59.6	73.8	908.9	95.1	654.7	491.3	86.6	-28.8
	MaxMotions w/o trans	58.9	74.8	907.6	89.8	656.9	489.4	85.9	-151.5
1.431	MaxMotions w/ trans	56.3	88.8	907.6	31.2	888.4	489.4	105.2	-152.5
	PDStrip w/o trans	59.0	80.7	908.5	288.8	969.6	3559.5	65.4	-165.7
	PDStrip w/ trans	56.4	94.9	908.5	221.0	1253.2	3559.5	96.0	173.8
	Fonseca	62.8	50.6	908.9	126.8	630.8	491.3	95.5	-20.7
	MaxMotions w/o trans	62.8	56.4	907.6	123.4	653.7	489.4	94.6	-161.8
1.545	MaxMotions w/ trans	61.1	70.9	907.6	83.5	901.9	489.4	112.8	-165.7
	PDStrip w/o trans	62.9	61.9	908.5	334.3	901.3	3559.5	105.3	-178.2
	PDStrip w/ trans	61.2	76.7	908.5	288.2	1206.3	3559.5	116.8	161.5

[*] Differences to PDStrip are consequence of the adopted reference frame to compute the component $-\rho g \int xBdx$

Table A.14: Numerical results for the coefficients of the second coupled heave/pitch motion equation (3.4), Catamaran, $F_n = 0.400$

ω_0 $[rad/s]$	Code	A_{53} $[t.m]$	B_{53} $[t.m/s]$	C_{53}^{*} $[t.m/s^2]$	I_5+A_{55} $[t.m^2]$	B_{55} $[t.m^2/s]$	C_{55} $[t.m^2/s^2]$	$\lvert F_5^E \rvert$ $[kN.m]$	Φ $[°]$
	Fonseca	1656.693	-749.0	491.3	22600.7	24610.5	101735.0	3553.2	-89.0
	MaxMotions w/o trans	1591.5	-783.6	489.4	23646.3	24392.7	101440.3	3534.6	-90.6
0.599	MaxMotions w/ trans	840.8	-199.4	489.4	4113.1	28804.5	101440.3	3539.4	-82.3
	PDStrip w/o trans	700.4	755.8	3559.5	7883.2	22848.0	112726.7	4111.9	-47.7
	PDStrip w/ trans	1177.5	423.2	3541.3	-539.3	35808.7	112726.7	4503.7	-54.3
	Fonseca	1019.722	-444.1	491.3	12826.1	21530.3	101735.0	4760.2	-93.4
	MaxMotions w/o trans	955.4	-473.2	489.4	13782.8	21338.7	101440.3	4719.7	-86.4
0.757	MaxMotions w/ trans	507.9	-40.3	489.4	3353.5	25501.2	101440.3	4964.4	-81.1
	PDStrip w/o trans	521.8	857.6	3559.5	6779.2	23810.7	112726.7	4859.0	-61.1
	PDStrip w/ trans	789.6	618.8	3541.3	909.2	32548.2	112726.7	5523.8	-67.8
	Fonseca	786.840	-333.1	491.3	1Fonseca4.4	20138.2	101735.0	5319.3	-95.8
	MaxMotions w/o trans	731.9	-350.4	489.4	10805.8	19963.8	101440.3	5269.9	-84.1
0.846	MaxMotions w/ trans	395.0	22.1	489.4	3248.0	23940.9	101440.3	5622.6	-80.5
	PDStrip w/o trans	452.9	883.1	3559.5	6255.1	23882.9	112726.7	5243.3	-66.6
	PDStrip w/ trans	644.1	676.3	3541.3	1625.0	30924.6	112726.7	6016.9	-73.8
	Fonseca	595.344	-252.7	491.3	7989.2	18564.0	101735.0	5702.9	-98.2
	MaxMotions w/o trans	553.3	-261.1	489.4	8615.6	18413.8	101440.3	5653.9	-81.9
0.946	MaxMotions w/ trans	307.8	61.0	489.4	3251.7	22226.2	101440.3	6078.5	-80.1
	PDStrip w/o trans	396.9	885.5	3559.5	5812.4	23508.7	112726.7	5519.3	-71.4
	PDStrip w/ trans	524.8	698.0	3541.3	2330.1	29040.5	112726.7	6333.0	-79.7
	Fonseca	499.769	-222.5	491.3	7108.9	17460.9	101735.0	5742.9	-99.4
	MaxMotions w/o trans	465.5	-226.6	489.4	7622.2	17327.2	101440.3	5694.9	-80.8
1.012	MaxMotions w/ trans	266.3	69.6	489.4	3315.3	21072.1	101440.3	6129.3	-80.0
	PDStrip w/o trans	372.0	874.1	3559.5	5648.8	23033.9	112726.7	5563.4	-74.1
	PDStrip w/ trans	468.7	689.9	3541.3	2791.1	27774.1	112726.7	6338.1	-83.4
	Fonseca	406.651	-207.1	491.3	6364.9	15982.5	101735.0	5509.1	-100.6
	MaxMotions w/o trans	380.9	-207.1	489.4	6742.8	15872.2	101440.3	5491.2	-79.7
1.093	MaxMotions w/ trans	227.8	68.4	489.4	3456.2	19586.3	101440.3	5910.1	-80.2
	PDStrip w/o trans	351.5	842.3	3559.5	5576.6	22118.8	112726.7	5418.1	-77.2
	PDStrip w/ trans	417.6	653.1	3541.3	3366.6	26043.2	112726.7	6061.9	-88.0
	Fonseca	319.814	-217.4	491.3	5834.6	13918.5	101735.0	4676.7	-101.3
	MaxMotions w/o trans	303.1	-212.1	489.4	6058.3	13841.3	101440.3	4675.7	-79.2
1.197	MaxMotions w/ trans	195.1	44.8	489.4	3735.7	17605.3	101440.3	5024.2	-81.2
	PDStrip w/o trans	340.1	757.4	3559.5	5718.2	20232.1	112726.7	4843.5	-81.5
	PDStrip w/ trans	378.2	563.7	3541.3	4148.1	23572.1	112726.7	5198.6	-94.6
	Fonseca	319.814	-217.4	491.3	5834.6	13918.5	101735.0	4676.7	-101.3
	MaxMotions w/o trans	303.1	-212.1	489.4	6058.3	13841.3	101440.3	4675.7	-79.2
1.197	MaxMotions w/ trans	195.1	44.8	489.4	3735.7	17605.3	101440.3	5024.2	-81.2
	PDStrip w/o trans	340.1	757.4	3559.5	5718.2	20232.1	112726.7	4843.5	-81.5
	PDStrip w/ trans	378.2	563.7	3541.3	4148.1	23572.1	112726.7	5198.6	-94.6
	Fonseca	319.814	-217.4	491.3	5834.6	13918.5	101735.0	4676.7	-101.3
	MaxMotions w/o trans	303.1	-212.1	489.4	6058.3	13841.3	101440.3	4675.7	-79.2
1.197	MaxMotions w/ trans	195.1	44.8	489.4	3735.7	17605.3	101440.3	5024.2	-81.2
	PDStrip w/o trans	340.1	757.4	3559.5	5718.2	20232.1	112726.7	4843.5	-81.5
	PDStrip w/ trans	378.2	563.7	3541.3	4148.1	23572.1	112726.7	5198.6	-94.6
	Fonseca	246.207	-272.7	491.3	5651.8	10967.8	101735.0	2738.0	-99.7
	MaxMotions w/o trans	238.2	-262.2	489.4	5722.2	10954.2	101440.3	2758.6	-80.8
1.338	MaxMotions w/ trans	172.4	-12.7	489.4	4271.4	14932.1	101440.3	2976.9	-86.5
	PDStrip w/o trans	344.2	594.9	3559.5	6189.7	16718.9	112726.7	3357.9	-89.7
	PDStrip w/ trans	359.4	418.0	3541.3	5208.2	20250.2	112726.7	3230.1	-107.1
	Fonseca	217.694	-325.0	491.3	5745.5	9064.0	101735.0	1275.2	-93.5
	MaxMotions w/o trans	214.1	-311.1	489.4	5742.4	9115.8	101440.3	1291.2	-87.2
1.431	MaxMotions w/ trans	167.1	-58.5	489.4	4681.7	13304.5	101440.3	1442.1	-100.4
	PDStrip w/o trans	355.9	484.7	3559.5	6613.1	14375.2	112726.7	2101.3	-100.4
	PDStrip w/ trans	362.6	304.9	3541.3	5913.5	18053.9	112726.7	1723.5	-124.7
	Fonseca	192.969	-401.0	491.3	5969.3	6718.4	101735.0	391.4	33.6
	MaxMotions w/o trans	197.1	-378.4	489.4	5942.6	7039.2	101440.3	439.3	89.2
1.545	MaxMotions w/ trans	166.7	-116.2	489.4	5220.6	11535.9	101440.3	747.8	96.8
	PDStrip w/o trans	374.7	384.6	3559.5	7157.7	12230.2	112726.7	805.7	-150.8
	PDStrip w/ trans	375.7	186.8	3541.3	6720.8	16006.0	112726.7	782.5	145.3

* Differences to PDStrip are consequence of the adopted reference frame to compute the component $-\rho g \int xBdx$

Table A.15: Numerical results for the coefficients of the first coupled heave/pitch motion equation (3.4), Catamaran, $F_n = 0.600$

ω_0 $[rad/s]$	Code	$\Delta + A_{33}$ $[t]$	B_{33} $[t/s]$	C_{33} $[t/s^2]$	A_{35} $[t.m]$	B_{35} $[t.m/s]$	C^*_{35} $[t.m/s^2]$	$\lvert F^E_3 \rvert$ $[kN]$	Φ $[^\circ]$
	Fonseca	106.4	143.7	908.9	-1364.7	1594.1	491.3	760.5	175.1
	MaxMotions w/o trans	110.9	142.6	907.6	-1409.9	1650.5	489.4	759.3	4.7
0.599	MaxMotions w/ trans	62.1	184.5	907.6	-2765.5	1808.5	489.4	797.6	4.5
	PDStrip w/o trans	106.3	145.8	908.5	-1026.6	2117.9	3559.5	726.7	0.1
	PDStrip w/ trans	57.4	186.9	908.5	-2538.9	2401.3	3559.5	780.9	0.2
	Fonseca	75.1	151.3	908.9	-664.3	1222.2	491.3	651.8	173.7
	MaxMotions w/o trans	77.2	150.0	907.6	-707.3	1248.7	489.4	652.1	6.1
0.757	MaxMotions w/ trans	50.4	180.5	907.6	-1363.6	1466.0	489.4	683.7	4.6
	PDStrip w/o trans	74.9	156.3	908.5	-438.5	1806.8	3559.5	610.7	1.6
	PDStrip w/ trans	48.1	184.7	908.5	-1176.1	2096.3	3559.5	661.7	-1.1
	Fonseca	64.7	146.3	908.9	-420.0	1086.1	491.3	566.2	173.5
	MaxMotions w/o trans	65.7	145.4	907.6	-453.3	1100.9	489.4	567.3	6.2
0.846	MaxMotions w/ trans	46.6	171.4	907.6	-904.6	1336.2	489.4	592.1	4.0
	PDStrip w/o trans	64.5	153.5	908.5	-230.5	1677.8	3559.5	532.5	2.7
	PDStrip w/ trans	45.3	176.9	908.5	-736.6	1960.6	3559.5	571.4	-2.2
	Fonseca	61.0	141.4	908.9	-322.3	1033.5	491.3	515.0	173.6
	MaxMotions w/o trans	61.7	140.6	907.6	-350.7	1043.7	489.4	516.6	6.1
0.892	MaxMotions w/ trans	45.7	164.9	907.6	-725.1	1287.5	489.4	537.5	3.4
	PDStrip w/o trans	60.7	149.9	908.5	-146.2	1621.0	3559.5	489.2	3.2
	PDStrip w/ trans	44.6	171.1	908.5	-564.3	1900.2	3559.5	518.9	-3.0
	Fonseca	58.0	133.6	908.9	-225.3	984.4	491.3	448.5	174.1
	MaxMotions w/o trans	58.3	133.0	907.6	-248.5	990.4	489.4	450.5	5.6
0.946	MaxMotions w/ trans	45.4	155.9	907.6	-549.6	1244.7	489.4	466.9	2.3
	PDStrip w/o trans	57.6	144.1	908.5	-60.6	1560.8	3559.5	435.5	3.9
	PDStrip w/ trans	44.6	163.1	908.5	-394.7	1839.7	3559.5	452.1	-3.9
	Fonseca	56.1	122.0	908.9	-130.7	942.3	491.3	361.4	175.2
	MaxMotions w/o trans	56.0	121.6	907.6	-148.2	944.2	489.4	363.6	4.5
1.012	MaxMotions w/ trans	46.0	143.2	907.6	-380.1	1212.5	489.4	374.9	0.3
	PDStrip w/o trans	55.7	135.4	908.5	26.2	1496.4	3559.5	367.4	4.7
	PDStrip w/ trans	45.6	153.2	908.5	-230.9	1796.6	3559.5	366.8	-5.4
	Fonseca	55.8	114.3	908.9	-84.7	925.3	491.3	308.1	176.2
	MaxMotions w/o trans	55.6	114.1	907.6	-99.3	925.4	489.4	310.5	3.5
1.050	MaxMotions w/ trans	46.9	135.2	907.6	-298.6	1203.3	489.4	319.2	-1.4
	PDStrip w/o trans	55.2	130.4	908.5	68.3	1476.3	3559.5	327.6	5.2
	PDStrip w/ trans	46.7	148.0	908.5	-152.6	1792.6	3559.5	316.1	-6.3
	Fonseca	56.0	105.2	908.9	-40.3	912.1	491.3	247.8	177.9
	MaxMotions w/o trans	55.5	105.1	907.6	-51.7	910.4	489.4	250.1	1.8
1.093	MaxMotions w/ trans	48.3	125.9	907.6	-219.8	1199.2	489.4	256.4	-4.3
	PDStrip w/o trans	55.4	123.6	908.5	113.2	1463.7	3559.5	281.7	5.0
	PDStrip w/ trans	48.2	142.4	908.5	-75.8	1809.3	3559.5	259.2	-8.0
	Fonseca	58.4	81.9	908.9	42.4	899.6	491.3	108.5	-172.3
	MaxMotions w/o trans	57.7	82.5	907.6	35.5	897.7	489.4	110.9	-7.9
1.197	MaxMotions w/ trans	53.1	103.3	907.6	-75.8	1217.1	489.4	115.2	-21.0
	PDStrip w/o trans	57.7	95.2	908.5	219.0	1329.1	3559.5	162.5	2.6
	PDStrip w/ trans	53.1	117.9	908.5	89.3	1744.3	3559.5	117.7	-16.1
	Fonseca	61.1	53.1	908.9	103.7	862.1	491.3	40.9	-46.3
	MaxMotions w/o trans	63.2	54.7	907.6	108.8	913.4	489.4	45.3	-138.1
1.338	MaxMotions w/ trans	60.8	76.5	907.6	44.4	1278.8	489.4	71.1	-131.9
	PDStrip w/o trans	63.3	61.8	908.5	317.8	1174.2	3559.5	22.8	-48.1
	PDStrip w/ trans	60.9	83.9	908.5	244.4	1620.3	3559.5	46.8	-172.0
	Fonseca	78.0	16.4	908.9	182.1	1009.4	491.3	28.9	-25.0
	MaxMotions w/o trans	76.6	15.3	907.6	180.2	989.6	489.4	29.7	-161.1
1.693	MaxMotions w/ trans	76.2	41.4	907.6	160.9	1456.5	489.4	55.7	169.7
	PDStrip w/o trans	76.7	20.3	908.5	437.0	1092.2	3559.5	104.0	176.2
	PDStrip w/ trans	76.2	46.4	908.5	415.7	1648.9	3559.5	70.9	142.9

* Differences to PDStrip are consequence of the adopted reference frame to compute the component $-\rho g \int x B dx$

Table A.16: Numerical results for the coefficients of the second coupled heave/pitch motion equation (3.4), Catamaran, $F_n = 0.600$

ω_0 $[rad/s]$	Code	A_{53} $[t.m]$	B_{53} $[t.m/s]$	C^*_{53} $[t.m/s^2]$	$I_5 + A_{55}$ $[t.m^2]$	B_{55} $[t.m^2/s]$	C_{55} $[t.m^2/s^2]$	$\lvert F^E_5 \rvert$ $[kN.m]$	Φ $[^\circ]$
	Fonseca	1857.340	-1027.5	491.3	25212.0	34056.7	101735.0	3697.4	-85.2
	MaxMotions w/o trans	1785.7	-1083.4	489.4	26615.0	33757.6	101440.3	3675.2	-94.2
0.599	MaxMotions w/ trans	900.6	-323.1	489.4	2070.3	36618.5	101440.3	3672.6	-83.4
	PDStrip w/o trans	607.1	808.4	3559.5	4343.5	25836.4	112726.7	4011.4	-46.5
	PDStrip w/ trans	1156.6	384.8	3541.3	-4923.0	44248.7	112726.7	4595.5	-56.3
	Fonseca	1043.731	-629.0	491.3	12598.3	25789.2	101735.0	4846.9	-91.2
	MaxMotions w/o trans	988.4	-653.4	489.4	13457.3	25575.5	101440.3	4801.3	-88.5
0.757	MaxMotions w/ trans	502.9	-105.7	489.4	1559.6	29510.7	101440.3	5108.8	-81.8
	PDStrip w/o trans	443.9	883.6	3559.5	4514.7	25658.3	112726.7	4693.7	-58.5
	PDStrip w/ trans	716.9	580.7	3541.3	-1624.8	37030.6	112726.7	5672.1	-68.8
	Fonseca	761.960	-507.7	491.3	9487.3	22291.9	101735.0	5390.3	-94.2
	MaxMotions w/o trans	721.0	-518.9	489.4	10108.3	22121.8	101440.3	5344.9	-85.8
0.846	MaxMotions w/ trans	374.7	-47.8	489.4	1937.8	26382.1	101440.3	5774.1	-81.2
	PDStrip w/o trans	389.5	883.6	3559.5	4580.0	25006.5	112726.7	5058.8	-63.0
	PDStrip w/ trans	566.6	608.2	3541.3	7.5	33740.7	112726.7	6184.4	-74.2
	Fonseca	650.802	-470.4	491.3	8450.4	20640.0	101735.0	5596.6	-95.4
	MaxMotions w/o trans	616.4	-476.5	489.4	8963.3	20486.8	101440.3	5554.6	-84.6
0.892	MaxMotions w/ trans	325.9	-35.5	489.4	2182.9	24901.9	101440.3	6024.3	-81.0
	PDStrip w/o trans	369.6	873.3	3559.5	4636.1	24504.2	112726.7	5212.9	-64.8
	PDStrip w/ trans	509.2	602.8	3541.3	758.6	32159.9	112726.7	6373.3	-76.7
	Fonseca	542.223	-446.0	491.3	7561.7	18752.6	101735.0	5744.9	-96.7
	MaxMotions w/o trans	515.1	-446.9	489.4	7957.4	18625.9	101440.3	5704.9	-83.5
0.946	MaxMotions w/ trans	279.7	-32.8	489.4	2504.6	23231.2	101440.3	6204.4	-80.9
	PDStrip w/o trans	353.2	851.1	3559.5	4757.3	23744.1	112726.7	5346.6	-66.5
	PDStrip w/ trans	456.2	580.5	3541.3	1595.4	30369.9	112726.7	6505.4	-79.5
	Fonseca	439.162	-441.5	491.3	6857.9	16548.7	101735.0	5753.3	-97.8
	MaxMotions w/o trans	419.3	-438.7	489.4	7127.2	16450.9	101440.3	5723.6	-82.4
1.012	MaxMotions w/ trans	237.9	-44.8	489.4	2927.3	21311.6	101440.3	6233.2	-80.9
	PDStrip w/o trans	342.3	810.5	3559.5	4989.6	22581.4	112726.7	5420.7	-68.3
	PDStrip w/ trans	411.4	548.2	3541.3	2521.1	28539.1	112726.7	6504.1	-82.7
	Fonseca	390.719	-449.8	491.3	6590.7	15289.7	101735.0	5654.4	-98.3
	MaxMotions w/o trans	374.8	-442.0	489.4	6794.1	15213.2	101440.3	5643.8	-82.0
1.050	MaxMotions w/ trans	219.5	-59.3	489.4	3184.9	20240.1	101440.3	6153.4	-81.0
	PDStrip w/o trans	339.5	795.6	3559.5	5123.4	22001.8	112726.7	5413.8	-69.1
	PDStrip w/ trans	392.6	537.5	3541.3	2997.6	27761.2	112726.7	6415.0	-84.4
	Fonseca	345.429	-467.5	491.3	6392.2	13910.9	101735.0	5443.0	-98.7
	MaxMotions w/o trans	333.4	-457.8	489.4	6523.0	13856.4	101440.3	5436.0	-81.6
1.093	MaxMotions w/ trans	203.5	-80.5	489.4	3479.5	19085.5	101440.3	5936.4	-81.3
	PDStrip w/o trans	339.6	781.0	3559.5	5310.0	21428.8	112726.7	5359.3	-70.0
	PDStrip w/ trans	378.5	532.3	3541.3	3513.4	27180.8	112726.7	6233.0	-86.3
	Fonseca	267.227	-538.7	491.3	6234.3	10733.4	101735.0	4470.8	-99.0
	MaxMotions w/o trans	261.9	-523.7	489.4	6251.6	10753.8	101440.3	4485.7	-81.3
1.197	MaxMotions w/ trans	179.0	-147.9	489.4	4235.5	16537.4	101440.3	4949.8	-82.6
	PDStrip w/o trans	349.6	618.1	3559.5	6044.4	18212.0	112726.7	4902.4	-73.0
	PDStrip w/ trans	364.7	378.8	3541.3	4892.3	24098.5	112726.7	5340.8	-92.2
	Fonseca	204.277	-642.5	491.3	6313.8	6678.4	101735.0	2379.1	-97.2
	MaxMotions w/o trans	213.4	-645.1	489.4	6383.4	7198.1	101440.3	2400.9	-82.4
1.338	MaxMotions w/ trans	169.9	-250.1	489.4	5216.7	13814.9	101440.3	2793.0	-88.6
	PDStrip w/o trans	376.9	393.8	3559.5	7078.5	13823.3	112726.7	3567.7	-79.5
	PDStrip w/ trans	377.8	89.4	3541.3	6556.5	19406.5	112726.7	3224.8	-104.3
	Fonseca	196.508	-914.2	491.3	7437.6	2349.5	101735.0	933.0	76.7
	MaxMotions w/o trans	193.6	-899.2	489.4	7296.6	2188.0	101440.3	960.0	103.0
1.693	MaxMotions w/ trans	185.8	-426.9	489.4	6946.8	10642.5	101440.3	1473.8	117.9
	PDStrip w/o trans	445.9	147.6	3559.5	8963.8	8890.6	112726.7	1503.1	129.1
	PDStrip w/ trans	443.3	-234.6	3541.3	8966.4	15459.7	112726.7	1752.7	82.3

* Differences to PDStrip are consequence of the adopted reference frame to compute the component $-\rho g \int x B dx$

This page was intentionally left blank.

Appendix B

Comparison between numerical and experimental results - Model5 case

B.1 Frequency dependent errors

Table B.1: Comparison between numerical and experimental results for heave RAOs, Model5, $F_n = 0.570$

ω_0 $[rad/s]$	$\zeta_3/\zeta_a[m/m]$	$\zeta_3/\zeta_a[m/m]$, absolute difference $[m/m]$				
	Experiment	Fonseca	MaxMotions w/o trans	MaxMotions w/ trans	PDStrip w/o trans	PDStrip w/ trans
0.675	0.939	1.044, 0.105	0.996, 0.057	0.989, 0.049	1.074, 0.135	1.103, 0.164
0.758	0.922	1.082, 0.160	1.003, 0.082	0.986, 0.064	1.211, 0.289	1.161, 0.240
0.797	0.950	1.106, 0.156	1.009, 0.060	0.983, 0.034	1.298, 0.349	1.194, 0.244
0.847	0.988	1.140, 0.152	1.018, 0.030	0.977, 0.010	1.415, 0.427	1.231, 0.244
0.892	1.067	1.168, 0.101	1.022, 0.045	0.964, 0.103	1.492, 0.424	1.255, 0.187
0.951	1.067	1.176, 0.109	1.004, 0.063	0.923, 0.145	1.461, 0.394	1.239, 0.172
1.042	0.780	0.937, 0.158	0.796, 0.016	0.736, 0.044	1.058, 0.279	1.001, 0.222
1.128	0.381	0.426, 0.044	0.376, 0.006	0.401, 0.020	0.592, 0.211	0.578, 0.197
1.265	0.049	0.068, 0.019	0.048, 0.001	0.033, 0.016	0.142, 0.093	0.114, 0.066

Table B.2: Comparison between numerical and experimental results for heave RAOs, Model5, $F_n = 1.140$

ω_0	$\zeta_3/\zeta_a[m/m]$	$\zeta_3/\zeta_a[m/m]$, absolute difference $[m/m]$				
$[rad/s]$	Experiment	Fonseca	MaxMotions w/o trans	MaxMotions w/ trans	PDStrip w/o trans	PDStrip w/ trans
0.680	1.274	1.396, 0.122	1.337, 0.063	1.169, 0.104	1.912, 0.639	1.166, 0.108
0.737	1.199	1.656, 0.456	1.555, 0.356	1.239, 0.040	1.827, 0.627	1.271, 0.072
0.770	1.092	1.886, 0.795	1.746, 0.654	1.274, 0.183	1.582, 0.490	1.313, 0.222
0.805	0.958	2.136, 1.178	1.958, 1.000	1.283, 0.325	1.284, 0.326	1.313, 0.356
0.838	0.824	2.131, 1.307	1.974, 1.150	1.245, 0.420	1.025, 0.200	1.252, 0.427
0.884	0.639	1.437, 0.798	1.387, 0.749	1.069, 0.430	0.744, 0.105	1.065, 0.426
0.951	0.420	0.646, 0.226	0.590, 0.170	0.673, 0.254	0.498, 0.079	0.720, 0.301
1.016	0.182	0.247, 0.065	0.251, 0.069	0.355, 0.173	0.361, 0.179	0.441, 0.259
1.132	0.093	0.057, 0.036	0.055, 0.038	0.082, 0.011	0.188, 0.095	0.159, 0.066
1.255	0.082	0.027, 0.055	0.024, 0.058	0.008, 0.074	0.060, 0.021	0.044, 0.037

Table B.3: Comparison between numerical and experimental results for pitch RAOs, Model5, $F_n = 0.570$

ω_0	$\zeta_5/k_0\zeta_a[°/°]$	$\zeta_5/k_0\zeta_a[°/°]$, absolute difference $[°/°]$				
$[rad/s]$	Experiment	Fonseca	MaxMotions w/o trans	MaxMotions w/ trans	PDStrip w/o trans	PDStrip w/ trans
0.765	1.012	0.993, 0.018	1.021, 0.010	0.837, 0.174	0.987, 0.025	0.827, 0.184
0.807	1.002	0.979, 0.023	1.007, 0.004	0.812, 0.191	0.981, 0.022	0.803, 0.199
0.843	0.969	0.965, 0.004	0.990, 0.021	0.785, 0.184	0.967, 0.002	0.779, 0.190
0.899	0.877	0.937, 0.060	0.956, 0.079	0.737, 0.140	0.915, 0.038	0.733, 0.144
0.954	0.743	0.891, 0.149	0.902, 0.159	0.676, 0.067	0.811, 0.068	0.673, 0.070
1.034	0.489	0.717, 0.228	0.724, 0.235	0.545, 0.056	0.594, 0.105	0.538, 0.049
1.129	0.251	0.342, 0.091	0.356, 0.105	0.324, 0.074	0.369, 0.119	0.329, 0.079
1.258	0.051	0.071, 0.020	0.073, 0.022	0.081, 0.030	0.157, 0.106	0.103, 0.052

Table B.4: Comparison between numerical and experimental results for pitch RAOs, Model5, $F_n = 1.140$

ω_0	$\zeta_5/k_0\zeta_a[°/°]$	$\zeta_5/k_0\zeta_a[°/°]$, absolute difference $[°/°]$				
$[rad/s]$	Experiment	Fonseca	MaxMotions w/o trans	MaxMotions w/ trans	PDStrip w/o trans	PDStrip w/ trans
0.671	0.803	1.177, 0.374	1.218, 0.414	0.791, 0.012	1.198, 0.395	0.728, 0.075
0.727	0.789	1.325, 0.535	1.361, 0.572	0.797, 0.008	0.997, 0.208	0.721, 0.068
0.759	0.765	1.464, 0.699	1.490, 0.726	0.799, 0.034	0.817, 0.053	0.712, 0.052
0.805	0.685	1.698, 1.012	1.709, 1.023	0.789, 0.104	0.585, 0.100	0.682, 0.004
0.839	0.636	1.678, 1.043	1.705, 1.069	0.758, 0.122	0.467, 0.169	0.639, 0.003
0.897	0.477	0.977, 0.500	1.036, 0.560	0.624, 0.147	0.339, 0.138	0.524, 0.047
0.952	0.332	0.510, 0.177	0.517, 0.185	0.442, 0.110	0.271, 0.061	0.399, 0.067
1.035	0.193	0.175, 0.018	0.186, 0.007	0.222, 0.029	0.214, 0.021	0.240, 0.047
1.273	0.034	0.013, 0.022	0.018, 0.017	0.013, 0.021	0.061, 0.026	0.027, 0.007

B.2 Coefficients of the coupled heave/pitch motion equation

Table B.5: Numerical results for the coefficients of the first coupled heave/pitch motion equation (3.4), Model5, $F_n = 0.570$

ω_0 $[rad/s]$	Code	$\Delta + A_{33}$ $[t]$	B_{33} $[t/s]$	C_{33} $[t/s^2]$	A_{35} $[t.m]$	B_{35} $[t.m/s]$	C^*_{35} $[t.m/s^2]$	$\lvert F^E_3 \rvert$ $[kN]$	Φ $[^\circ]$
	Fonseca	432.7	673.1	2266.8	-3011.2	8517.0	7113.1	1611.6	174.2
	MaxMotions w/o trans	432.7	674.4	2266.2	-3859.3	7243.8	2792.8	1615.0	10.9
0.675	MaxMotions w/ trans	287.5	848.2	2266.2	-8405.1	9203.9	2792.8	1767.4	8.6
	PDStrip w/o trans	435.2	683.3	2263.2	-2531.3	9503.0	9995.0	1497.8	12.1
	PDStrip w/ trans	292.5	855.1	2263.2	-7458.2	11992.0	9995.0	1714.4	7.5
	Fonseca	380.3	677.7	2266.8	-1705.1	7835.6	7113.1	1412.0	173.8
	MaxMotions w/o trans	380.1	679.6	2266.2	-2454.7	6556.9	2792.8	1415.5	12.6
0.758	MaxMotions w/ trans	275.4	835.7	2266.2	-5613.8	8636.0	2792.8	1542.9	8.6
	PDStrip w/o trans	381.9	691.5	2263.2	-1292.3	8853.6	9995.0	1340.7	16.5
	PDStrip w/ trans	279.2	844.8	2263.2	-4722.4	11401.1	9995.0	1503.5	8.2
	Fonseca	361.7	673.5	2266.8	-1228.8	7564.4	7113.1	1303.3	173.8
	MaxMotions w/o trans	361.4	676.3	2266.2	-1943.4	6295.7	2792.8	1307.0	13.3
0.797	MaxMotions w/ trans	271.4	825.6	2266.2	-4629.1	8417.7	2792.8	1419.4	8.4
	PDStrip w/o trans	362.7	689.4	2263.2	-843.0	8595.8	9995.0	1266.3	18.8
	PDStrip w/ trans	274.4	835.3	2263.2	-3755.4	11153.0	9995.0	1390.6	8.5
	Fonseca	343.0	662.9	2266.8	-720.9	7257.4	7113.1	1153.2	173.8
	MaxMotions w/o trans	342.5	666.5	2266.2	-1399.6	6011.9	2792.8	1156.9	14.2
0.847	MaxMotions w/ trans	268.0	809.1	2266.2	-3601.1	8181.8	2792.8	1248.4	7.9
	PDStrip w/o trans	343.4	682.0	2263.2	-362.4	8315.3	9995.0	1169.4	21.5
	PDStrip w/ trans	270.4	819.8	2263.2	-2743.1	10878.4	9995.0	1234.5	8.8
	Fonseca	329.7	648.1	2266.8	-325.6	7002.9	7113.1	1002.9	173.9
	MaxMotions w/o trans	329.1	652.8	2266.2	-978.3	5788.6	2792.8	1006.5	14.9
0.892	MaxMotions w/ trans	266.5	790.4	2266.2	-2818.5	7999.8	2792.8	1077.1	7.1
	PDStrip w/o trans	329.6	670.5	2263.2	13.4	8086.6	9995.0	1075.9	23.8
	PDStrip w/ trans	268.3	801.7	2263.2	-1970.5	10649.0	9995.0	1078.2	9.0
	Fonseca	317.5	622.9	2266.8	99.2	6710.6	7113.1	797.6	174.2
	MaxMotions w/o trans	316.7	628.9	2266.2	-528.9	5549.3	2792.8	800.8	15.8
0.951	MaxMotions w/ trans	266.6	761.7	2266.2	-1997.9	7812.4	2792.8	843.0	5.3
	PDStrip w/o trans	317.1	648.6	2263.2	425.3	7817.0	9995.0	947.2	26.4
	PDStrip w/ trans	268.1	773.6	2263.2	-1151.6	10388.2	9995.0	863.3	9.2
	Fonseca	307.5	572.0	2266.8	615.0	6320.2	7113.1	473.0	174.6
	MaxMotions w/o trans	306.8	581.3	2266.2	4.8	5269.8	2792.8	476.0	17.1
1.042	MaxMotions w/ trans	271.3	709.4	2266.2	-1041.3	7616.4	2792.8	475.6	-1.6
	PDStrip w/o trans	307.0	600.3	2263.2	940.2	7398.9	9995.0	715.0	28.4
	PDStrip w/ trans	272.4	720.4	2263.2	-179.5	10026.3	9995.0	509.5	9.2
	Fonseca	305.3	512.5	2266.8	985.5	5998.3	7113.1	194.8	175.4
	MaxMotions w/o trans	305.1	528.3	2266.2	376.1	5086.3	2792.8	197.8	17.8
1.128	MaxMotions w/ trans	279.6	654.6	2266.2	-390.6	7518.1	2792.8	181.7	-30.3
	PDStrip w/o trans	305.2	544.5	2263.2	1316.8	6993.6	9995.0	463.9	26.7
	PDStrip w/ trans	280.4	663.9	2263.2	498.2	9711.8	9995.0	184.4	10.3
	Fonseca	320.9	521.1	2266.8	1324.6	6031.9	7113.1	88.0	8.0
	MaxMotions w/o trans	312.7	437.2	2266.2	790.9	4908.8	2792.8	103.0	-150.2
1.265	MaxMotions w/ trans	297.6	564.2	2266.2	317.6	7490.4	2792.8	261.9	-141.3
	PDStrip w/o trans	312.5	450.3	2263.2	1761.5	6424.6	9995.0	93.0	-47.3
	PDStrip w/ trans	297.9	574.8	2263.2	1256.0	9364.6	9995.0	228.4	-175.8

[*] Differences to PDStrip are consequence of the adopted reference frame to compute the component $-\rho g \int xBdx$

Table B.6: Numerical results for the coefficients of the second coupled heave/pitch motion equation (3.4), Model5, $F_n = 0.570$

ω_0 $[rad/s]$	Code	A_{53} $[t.m]$	B_{53} $[t.m/s]$	C^*_{53} $[t.m/s^2]$	$I_5 + A_{55}$ $[t.m^2]$	B_{55} $[t.m^2/s]$	C_{55} $[t.m^2/s^2]$	$\lvert F^E_5 \rvert$ $[kN.m]$	Φ [°]
	Fonseca	5805.461	-1729.2	7113.1	87525.0	153354.3	370806.0	14893.6	-96.9
	MaxMotions w/o trans	5084.9	-3000.0	2792.8	81373.1	144888.4	351303.0	15097.8	-86.7
0.765	MaxMotions w/ trans	2856.5	375.8	2792.8	14249.3	190405.8	351303.0	17299.1	-76.7
	PDStrip w/o trans	2574.3	4030.8	9995.0	45435.2	149993.6	389307.6	13131.4	-49.2
	PDStrip w/ trans	3790.1	3068.2	9968.4	9438.9	228179.4	389307.6	17984.9	-68.2
	Fonseca	5152.260	-1530.2	7113.1	79401.6	145749.1	370806.0	15408.6	-97.1
	MaxMotions w/o trans	4470.8	-2786.0	2792.8	73435.3	137532.0	351303.0	15573.4	-84.7
0.807	MaxMotions w/ trans	2575.5	442.1	2792.8	17010.7	184029.9	351303.0	18135.9	-76.4
	PDStrip w/o trans	2469.7	4013.2	9995.0	45375.9	148782.5	389307.6	13738.7	-49.2
	PDStrip w/ trans	3487.4	3119.7	9968.4	14301.3	221410.9	389307.6	18732.4	-69.7
	Fonseca	4669.014	-1410.2	7113.1	73766.4	139509.7	370806.0	15712.4	-97.1
	MaxMotions w/o trans	4015.8	-2645.6	2792.8	67904.8	131557.7	351303.0	15851.1	-83.0
0.843	MaxMotions w/ trans	2369.0	474.6	2792.8	19244.3	178829.8	351303.0	18680.1	-76.1
	PDStrip w/o trans	2394.7	3983.3	9995.0	45338.8	147456.7	389307.6	14280.3	-48.9
	PDStrip w/ trans	3264.8	3131.2	9968.4	18091.2	215806.3	389307.6	19250.6	-70.8
	Fonseca	4063.696	-1313.5	7113.1	67183.2	130500.7	370806.0	15845.0	-97.2
	MaxMotions w/o trans	3445.5	-2506.2	2792.8	61421.4	123051.5	351303.0	15942.8	-80.5
0.899	MaxMotions w/ trans	2114.0	481.9	2792.8	22345.5	171425.9	351303.0	19066.6	-75.9
	PDStrip w/o trans	2308.9	3914.8	9995.0	45437.9	145093.7	389307.6	15089.2	-48.3
	PDStrip w/ trans	2992.1	3093.6	9968.4	23193.9	207873.9	389307.6	19720.1	-72.4
	Fonseca	3595.311	-1306.8	7113.1	62522.2	122025.8	370806.0	15508.2	-97.2
	MaxMotions w/o trans	3001.1	-2443.8	2792.8	56784.7	115161.6	351303.0	15583.6	-78.2
0.954	MaxMotions w/ trans	1919.9	446.8	2792.8	25112.4	164594.5	351303.0	18909.1	-75.7
	PDStrip w/o trans	2255.3	3808.7	9995.0	45836.4	142097.4	389307.6	15826.9	-47.5
	PDStrip w/ trans	2794.2	2995.3	9968.4	27689.9	200593.3	389307.6	19731.2	-73.9
	Fonseca	3081.802	-1427.4	7113.1	57985.5	109908.2	370806.0	14055.8	-97.4
	MaxMotions w/o trans	2508.7	-2466.7	2792.8	52272.3	104089.0	351303.0	14120.6	-74.5
1.034	MaxMotions w/ trans	1712.6	333.3	2792.8	28828.7	155131.7	351303.0	17477.7	-75.8
	PDStrip w/o trans	2215.4	3552.2	9995.0	46856.4	135698.4	389307.6	16536.2	-47.1
	PDStrip w/ trans	2592.6	2741.7	9968.4	33430.4	189902.7	389307.6	18729.6	-76.2
	Fonseca	2675.666	-1713.9	7113.1	55091.3	95992.5	370806.0	10978.7	-98.8
	MaxMotions w/o trans	2118.1	-2619.1	2792.8	49340.1	91752.9	351303.0	11049.6	-69.2
1.129	MaxMotions w/ trans	1562.1	135.4	2792.8	32672.7	144828.5	351303.0	14023.8	-76.6
	PDStrip w/o trans	2216.3	3136.2	9995.0	48590.8	125610.7	389307.6	16396.0	-48.1
	PDStrip w/ trans	2464.7	2316.0	9968.4	39227.6	177073.6	389307.6	15829.3	-79.5
	Fonseca	2507.828	-2086.0	7113.1	54287.1	84788.3	370806.0	5553.4	-114.1
	MaxMotions w/o trans	1800.4	-2962.7	2792.8	47852.9	75824.4	351303.0	5630.0	-52.7
1.258	MaxMotions w/ trans	1462.8	-193.8	2792.8	37272.0	131969.5	351303.0	7079.5	-81.9
	PDStrip w/o trans	2270.6	2508.7	9995.0	51433.1	110295.8	389307.6	13524.6	-55.0
	PDStrip w/ trans	2411.1	1684.7	9968.4	45805.9	161251.4	389307.6	9166.0	-87.1

* Differences to PDStrip are consequence of the adopted reference frame to compute the component $-\rho g \int xBdx$

Table B.7: Numerical results for the coefficients of the first coupled heave/pitch motion equation (3.4), Model5, $F_n = 1.140$

ω_0 $[rad/s]$	Code	$\Delta + A_{33}$ $[t]$	B_{33} $[t/s]$	C_{33} $[t/s^2]$	A_{35} $[t.m]$	B_{35} $[t.m/s]$	C^*_{35} $[t.m/s^2]$	$\lvert F^E_3 \rvert$ $[kN]$	Φ $[^\circ]$
	Fonseca	333.4	653.2	2266.8	-2803.0	11289.3	7113.1	1556.8	173.8
	MaxMotions w/o trans	332.9	657.5	2266.2	-3476.6	10056.4	2792.8	1560.3	11.4
0.680	MaxMotions w/ trans	200.6	935.6	2266.2	-8371.2	12783.7	2792.8	1793.3	8.4
	PDStrip w/o trans	333.2	706.9	2263.2	-2769.0	12673.8	9995.0	1407.6	0.4
	PDStrip w/ trans	203.8	958.5	2263.2	-7821.8	16095.7	9995.0	1671.3	-0.1
	Fonseca	316.5	620.0	2266.8	-1580.1	10678.6	7113.1	1394.9	173.8
	MaxMotions w/o trans	315.8	626.2	2266.2	-2223.6	9513.6	2792.8	1399.5	12.3
0.737	MaxMotions w/ trans	217.7	890.9	2266.2	-5829.6	12812.7	2792.8	1615.4	8.0
	PDStrip w/o trans	316.3	686.8	2263.2	-1552.0	12213.5	9995.0	1249.8	5.0
	PDStrip w/ trans	220.5	923.8	2263.2	-5259.3	16105.1	9995.0	1526.1	0.6
	Fonseca	310.6	595.1	2266.8	-1007.4	10398.2	7113.1	1286.8	173.8
	MaxMotions w/o trans	309.8	602.8	2266.2	-1641.3	9286.7	2792.8	1292.3	12.8
0.770	MaxMotions w/ trans	227.6	862.2	2266.2	-4673.8	12870.1	2792.8	1497.6	7.5
	PDStrip w/o trans	310.2	662.6	2263.2	-939.9	11927.5	9995.0	1161.7	8.6
	PDStrip w/ trans	230.0	901.2	2263.2	-4085.3	16144.5	9995.0	1432.1	1.3
	Fonseca	307.0	566.0	2266.8	-507.8	10159.1	7113.1	1166.6	173.7
	MaxMotions w/o trans	306.3	575.8	2266.2	-1136.9	9112.1	2792.8	1173.1	13.4
0.805	MaxMotions w/ trans	237.8	831.3	2266.2	-3685.3	12959.1	2792.8	1367.2	7.0
	PDStrip w/o trans	306.4	630.0	2263.2	-387.4	11618.0	9995.0	1079.9	13.3
	PDStrip w/ trans	239.7	874.9	2263.2	-3065.3	16189.2	9995.0	1328.8	2.1
	Fonseca	305.5	535.1	2266.8	-101.9	9968.2	7113.1	1044.9	173.6
	MaxMotions w/o trans	305.1	547.9	2266.2	-732.6	8994.4	2792.8	1053.0	14.1
0.838	MaxMotions w/ trans	247.5	801.2	2266.2	-2901.6	13069.1	2792.8	1236.0	6.2
	PDStrip w/o trans	305.1	596.2	2263.2	61.3	11348.5	9995.0	1015.8	18.5
	PDStrip w/ trans	249.2	847.8	2263.2	-2244.4	16239.8	9995.0	1223.8	3.2
	Fonseca	305.2	481.2	2266.8	393.9	9723.6	7113.1	863.5	173.4
	MaxMotions w/o trans	306.1	506.2	2266.2	-264.9	8894.1	2792.8	875.9	15.4
0.884	MaxMotions w/ trans	261.1	758.4	2266.2	-2003.4	13261.6	2792.8	1041.6	4.8
	PDStrip w/o trans	306.1	546.5	2263.2	583.0	11019.0	9995.0	955.3	26.8
	PDStrip w/ trans	262.5	804.3	2263.2	-1282.6	16280.4	9995.0	1064.4	5.1
	Fonseca	288.7	566.2	2266.8	521.0	9607.5	7113.1	695.4	165.6
	MaxMotions w/o trans	311.7	444.7	2266.2	241.0	8854.5	2792.8	619.5	18.9
0.951	MaxMotions w/ trans	280.3	698.4	2266.2	-1041.1	13594.5	2792.8	754.8	1.3
	PDStrip w/o trans	311.5	475.8	2263.2	1150.6	10655.9	9995.0	928.6	38.0
	PDStrip w/ trans	281.1	735.1	2263.2	-217.1	16281.3	9995.0	818.2	9.3
	Fonseca	326.0	391.2	2266.8	1226.7	9719.8	7113.1	372.4	158.7
	MaxMotions w/o trans	320.3	385.3	2266.2	600.7	8895.8	2792.8	386.1	27.1
1.016	MaxMotions w/ trans	298.3	643.1	2266.2	-361.8	13963.3	2792.8	479.4	-5.6
	PDStrip w/o trans	319.9	412.0	2263.2	1556.6	10431.5	9995.0	930.8	45.0
	PDStrip w/ trans	298.7	670.4	2263.2	544.3	16315.0	9995.0	567.4	17.1
	Fonseca	339.9	280.5	2266.8	1695.5	9543.6	7113.1	161.0	104.8
	MaxMotions w/o trans	338.4	291.1	2266.2	1009.5	9079.5	2792.8	142.5	84.0
1.132	MaxMotions w/ trans	326.7	559.3	2266.2	410.1	14636.7	2792.8	153.1	-73.2
	PDStrip w/o trans	337.4	312.8	2263.2	2041.7	10199.7	9995.0	721.2	42.1
	PDStrip w/ trans	326.4	575.8	2263.2	1426.8	16510.8	9995.0	155.0	65.2
	Fonseca	361.8	189.2	2266.8	1991.3	9712.8	7113.1	144.4	44.9
	MaxMotions w/o trans	356.7	211.0	2266.2	1254.4	9318.9	2792.8	136.3	148.1
1.255	MaxMotions w/ trans	350.8	490.8	2266.2	874.7	15275.6	2792.8	336.1	-140.9
	PDStrip w/o trans	355.9	229.3	2263.2	2359.3	10105.5	9995.0	242.8	-10.5
	PDStrip w/ trans	350.4	506.7	2263.2	1974.2	16912.8	9995.0	349.8	176.6

* Differences to PDStrip are consequence of the adopted reference frame to compute the component $-\rho g \int xBdx$

Table B.8: Numerical results for the coefficients of the second coupled heave/pitch motion equation (3.4), Model5, $F_n = 1.140$

ω_0 $[rad/s]$	Code	A_{53} $[t.m]$	B_{53} $[t.m/s]$	C^*_{53} $[t.m/s^2]$	$I_5 + A_{55}$ $[t.m^2]$	B_{55} $[t.m^2/s]$	C_{55} $[t.m^2/s^2]$	$\lvert F^E_5 \rvert$ $[kN.m]$	Φ $[^\circ]$
	Fonseca	6889.089	-5612.6	7113.1	118975.2	229754.0	370806.0	14366.1	-88.2
	MaxMotions w/o trans	6264.9	-6827.1	2792.8	113105.4	222494.5	351303.0	15083.9	-98.2
0.671	MaxMotions w/ trans	3240.1	-702.2	2792.8	928.9	279756.6	351303.0	16150.9	-78.5
	PDStrip w/o trans	2351.3	4246.7	9995.0	28135.6	179721.2	389307.6	11707.1	-61.4
	PDStrip w/ trans	3930.2	2524.9	9968.4	-15383.2	331799.6	389307.6	17076.6	-64.9
	Fonseca	5499.122	-5326.9	7113.1	98369.7	192561.2	370806.0	15278.4	-89.2
	MaxMotions w/o trans	4916.8	-6466.4	2792.8	92525.6	186167.3	351303.0	15841.4	-94.7
0.727	MaxMotions w/ trans	2661.4	-651.8	2792.8	9592.8	256136.0	351303.0	17703.4	-77.5
	PDStrip w/o trans	2262.6	4247.5	9995.0	32180.8	177080.8	389307.6	11723.6	-61.5
	PDStrip w/ trans	3392.9	2558.7	9968.4	-543.2	309916.8	389307.6	18341.3	-68.2
	Fonseca	4872.532	-5282.6	7113.1	90009.5	174291.8	370806.0	15691.2	-89.5
	MaxMotions w/o trans	4306.0	-6370.5	2792.8	84198.4	168483.7	351303.0	16180.6	-92.9
0.759	MaxMotions w/ trans	2404.2	-678.3	2792.8	14146.5	244671.8	351303.0	18465.3	-77.0
	PDStrip w/o trans	2232.1	4148.0	9995.0	34680.5	174086.2	389307.6	11712.0	-60.4
	PDStrip w/ trans	3160.7	2529.2	9968.4	6756.7	299598.1	389307.6	19024.7	-69.8
	Fonseca	4159.968	-5345.0	7113.1	81254.3	151503.3	370806.0	16050.3	-89.7
	MaxMotions w/o trans	3609.5	-6352.6	2792.8	75462.4	146671.1	351303.0	16458.3	-90.7
0.805	MaxMotions w/ trans	2118.4	-776.9	2792.8	19965.9	230652.8	351303.0	19306.8	-76.5
	PDStrip w/o trans	2211.9	3880.2	9995.0	38317.8	167854.6	389307.6	11740.4	-57.0
	PDStrip w/ trans	2910.4	2401.2	9968.4	15919.2	286829.7	389307.6	19901.7	-71.5
	Fonseca	3751.670	-5463.9	7113.1	76633.5	136942.0	370806.0	16090.9	-89.7
	MaxMotions w/o trans	3211.8	-6407.2	2792.8	70849.9	132982.8	351303.0	16456.8	-89.3
0.839	MaxMotions w/ trans	1961.2	-880.9	2792.8	23688.5	221980.1	351303.0	19697.2	-76.1
	PDStrip w/o trans	2211.6	3641.4	9995.0	40784.4	162609.8	389307.6	11878.0	-53.1
	PDStrip w/ trans	2781.8	2243.4	9968.4	21803.3	278639.8	389307.6	20442.0	-72.5
	Fonseca	3171.408	-5755.1	7113.1	70800.9	113551.0	370806.0	15620.8	-89.6
	MaxMotions w/o trans	2681.1	-6610.5	2792.8	65159.1	112343.2	351303.0	15944.0	-87.1
0.897	MaxMotions w/ trans	1762.7	-1108.1	2792.8	29338.1	209203.0	351303.0	19871.6	-75.6
	PDStrip w/o trans	2231.0	3193.8	9995.0	44619.0	152869.6	389307.6	12679.7	-43.8
	PDStrip w/ trans	2628.1	1823.2	9968.4	30759.2	264817.0	389307.6	21132.5	-73.7
	Fonseca	3171.309	-4993.0	7113.1	63288.9	119606.3	370806.0	14239.2	-90.0
	MaxMotions w/o trans	2326.4	-6888.6	2792.8	61699.1	95906.5	351303.0	14782.4	-85.2
0.952	MaxMotions w/ trans	1642.6	-1353.2	2792.8	33811.8	199406.6	351303.0	19368.3	-75.3
	PDStrip w/o trans	2268.8	2789.2	9995.0	47780.6	144022.7	389307.6	14495.3	-34.6
	PDStrip w/ trans	2553.4	1317.0	9968.4	37896.1	252797.0	389307.6	21399.0	-74.2
	Fonseca	2515.184	-6976.1	7113.1	63961.9	73898.4	370806.0	11495.6	-88.9
	MaxMotions w/o trans	1980.4	-7390.6	2792.8	58680.7	75553.2	351303.0	11764.3	-80.8
1.035	MaxMotions w/ trans	1545.0	-1735.1	2792.8	39241.5	187943.1	351303.0	17322.9	-74.9
	PDStrip w/o trans	2344.2	2243.9	9995.0	51876.9	131932.5	389307.6	19359.5	-25.6
	PDStrip w/ trans	2518.6	533.0	9968.4	46308.0	237578.1	389307.6	20924.6	-73.7
	Fonseca	1848.474	-9818.1	7113.1	57829.4	-7947.2	370806.0	4750.3	-189.3
	MaxMotions w/o trans	1623.8	-8776.5	2792.8	56680.8	38165.0	351303.0	4873.2	9.3
1.273	MaxMotions w/ trans	1506.6	-2635.7	2792.8	48866.6	169174.0	351303.0	4941.0	-84.1
	PDStrip w/o trans	2581.4	1049.4	9995.0	60650.8	104661.0	389307.6	20976.2	-40.9
	PDStrip w/ trans	2634.1	-1002.1	9968.4	60126.0	215693.7	389307.6	8944.6	-77.8

* Differences to PDStrip are consequence of the adopted reference frame to compute the component $-\rho g \int x B dx$